DOCTOR OF SCIENCES

Stability of non-coplanar extrasolar system

Volpi, Mara

Award date:
2019

Awarding institution:
University of Namur

UNIVERSITY OF NAMUR

FACULTY OF SCIENCE

NAXYS RESEARCH INSTITUTE
DEPARTMENT OF MATHEMATICS

Stability of non-coplanar extrasolar systems

Thesis presented by
Mara Volpi
for the title
of Doctor of Science

Composition of the Jury:

Christos EFTHYMIOPOULOS
Anne LEMAITRE (President of the Jury)
Anne-Sophie LIBERT (Advisor)
Ugo LOCATELLI
Marco SANSOTTERA

August 2019

Cover design: ©Presses universitaires de Namur

Rempart de la Vierge, 13
B-5000 Namur (Belgique)

Cover picture created with Universe Sandbox
http://universesandbox.com/

Printed in Belgium.

ISBN: 978-2-39029-074-2
Registration of copyright: D/2019/1881/25

University of Namur
Faculty of Science
rue de Bruxelles, 61, B-5000 Namur (Belgique)

Stability of non-coplanar extrasolar systems

by Mara Volpi

Abstract: Due to the limitations of the radial velocity method, our knowledge of the spatial configuration of the hundreds of exoplanetary systems discovered so far is limited. The aim of the present work is, through analytical study based on a secular Hamiltonian expansion and numerical explorations performed with a chaos detector, to provide constraints on the orbital inclinations and the mutual inclinations of several two-planet extrasolar systems, that ensure the long-term stability of the system. In the first part, for systems with low eccentricities, we rely on perturbation theory and apply a reverse KAM approach to determine the ranges of the mutual inclination that allow the convergence of the algorithm constructing the invariant tori. In the second part, for systems with moderate to high eccentricities, we find that long-term stable evolutions of non-coplanar configurations exist for all the selected systems, either at low mutual inclinations, or at high mutual inclinations preferentially if the system is in the Lidov-Kozai resonance. We also show how the relativistic effects influence the extent of the Lidov-Kozai resonant region for planetary systems with close-in planets.

Stabilité des systèmes extrasolaires non-coplanaires

par Mara Volpi

Résumé : Notre connaissance des configurations spatiales des centaines de systèmes extrasolaires détectés par la méthode des vitesses radiales est limitée. L'objectif de ce travail est de déterminer, au moyen d'une étude analytique de la dynamique séculaire dans un formalisme hamiltonien et d'explorations numériques réalisées avec un détecteur de chaos, des contraintes sur les inclinaisons des plans orbitaux et les inclinaisons mutuelles de ces systèmes qui assurent leur stabilité à long terme. Dans la première partie, pour des systèmes à faibles excentricités, nous avons recours à la théorie des perturbations et appliquons une approche de KAM inverse pour déterminer les intervalles d'inclinaisons mutuelles qui garantissent la convergence de l'algorithme de construction des tores invariants. Dans la seconde partie, pour des systèmes avec des excentricités plus élevées, nous montrons que des évolutions stables de configurations non-coplanaires existent, soit à faibles inclinaisons mutuelles, soit à fortes inclinaisons de préférence lorsque le système est en résonance de Lidov-Kozai. Nous montrons également comment les effets relativistes modifient l'étendue de la résonance de Lidov-Kozai pour des systèmes planétaires proches de l'étoile.

Ph.D. thesis in Mathematics
Date: 30/08/2019
naXys Research Institute, Department of Mathematics
Advisor: Anne-Sophie Libert

You know what a learning experience is?
A learning experience is one of those things that says,
"You know that thing you just did? Don't do that."

DOUGLAS ADAMS,
"The salmon of doubt"

Acknowledgements

I once read: "finishing a Ph.D. is like finishing a group project where your partner made a ton of mistakes at the beginning of the assignment. Except your partner is just you four years ago". How unnervingly true. Looking at the silver lining of that, it shows that I was given the chance to grow (scientifically and otherwise) during these last years. For this I have to deeply thank Anne-Sophie Libert. I owe her a huge amount of support and encouragement, of teaching and confidence, since even before I was technically one of her Ph.D. students.

My infinite gratitude goes to Ugo Locatelli. He was the one who introduced me to Celestial Mechanics and coding, when I was still a Master student. He has selflessly been part of the help to get the Ph.D. studentship in Namur and kept following me from afar. Working with him is always enriching, from both a scientific and personal point of view.

I would like to thank Marco Sansottera for his guidance and help: he was never further than an e-mail when technical problems arose, and that happened more frequently than I would like to admit. So thanks for that, and for all the useful discussions along these years. I would also like to thank Christos Efthymiopoulos and Anne Lemaitre for their remarks and comments on the first version of the manuscript: this thesis was clearly enriched and improved by them.

I would like to express my gratitude to the Department of Mathematics for the warm welcome I received: one has indeed the impression of entering a small family, and it has been really nice to be part of that, if only for a limited period of time. Thanks also for having kindly supported my steady but slow learning of French. The infinite patience you always showed in waiting for me to finish a sentence was duly noted and very much appreciated.

In particular, thanks to Delphine and Pauline, who shared so many pleasant

moments inside and outside the University: I am going to cherish them fondly. I really hope you have been more entertained than disturbed by the sometimes sudden and vigorous laughs coming from the bureau 135.

All the merit (or fault?) for said laughs goes to Eve-Aline. I could write an entire page to properly thank her, but I will set for a shorter version. We might have been sorted together almost by chance, but surely it was a perfect match. I was lucky enough to find a wonderful colleague, guide and friend in the same person, and just a desk away. Thanks for having answered the weird French questions; for having listened me muttering in three languages, and for knowing to get worried when I got to Italian; for having understood and accepted that it is normal if I laugh without control for ten minutes for very stupid things; for having shared many movies (even the weird Japanese ones!); for our blackboard full of non-academic but nevertheless very important stuff. I have sometimes missed Home terribly, but having her next to me has soothed the feeling and helped me building a little *maison* in Namur has well.

A major contribution to the feeling of being home came from Céline (with Charley and the little Oscar), who has never stopped providing company and encouragements along the years.

Despite the distance, I had plenty of support from people scattered all around. I know it is not a given and I really appreciated and cherished it. In particular, there are some people that I have to thank explicitly.

Four years ago, during the redaction of *his* thesis, I spent months making sure Luca knew everything was going to be alright and he was "just" experiencing a normal Ph.D.-thesis blue. Little did I know that few years later our roles would be reversed and I would listen to variations of my own phrases. Thanks for all the "SCRIVI!".

I would like to thank my extended family for having endured the enormous sacrifice of having me far away: I am aware it was an incredible loss, for such is the joy I bring in all your lives! Know that I am grateful for the support I kept receiving in practical and abstract ways from all the three generations.

Le galline Alessandra, Alice, and Valeria (in rigorous alphabetical order, as always) are some of my firmest points. They bought tickets to come visiting in Namur even before I myself left Rome. This kind of friendship and support and will to not let go have been invaluable along these years.

Finally, I looked for something to write to properly thank Giovanni, I really did. I only came up with grandiose and soppy words he would be embarrassed by and I would later regret having shared with others. Fortunately, I know that he knows everything I would like to say.

Mara Volpi
Namur, 02 August 2019

Contents

Introduction **1**

Contributions **3**

Fundings **3**

I Preliminary 7

1 Exoplanetary systems **9**
1.1 Exoplanet population 9
1.2 Detection methods 11
1.2.1 Radial velocity method 11
1.2.2 Transit method 14
1.2.3 Other methods 17
1.3 Three-dimensional systems 21

2 Perturbation theory **25**
2.1 Normal forms 25
2.1.1 Lie series method 26
2.1.2 Particular normal forms 28
2.2 The three-body problem 30
2.2.1 Hamiltonian formulation and symmetries 30
2.2.2 Hamiltonian expansion 32
2.2.3 Secular Hamiltonian 33
2.2.4 Stability of planetary systems 36

II 3D systems with low eccentricities 39

3 A *reverse* KAM method 41
3.1 Motivation . . . 41
3.2 Construction of invariant tori for the secular model . . . 44
3.2.1 Preliminary set up for the Kolmogorov algorithm . . . 45
3.2.2 Formal construction of the Kolmogorov invariant tori . 47
3.3 Parametric study on the D_2 parameter . . . 49
3.4 Results . . . 52
3.5 Conclusions and perspectives . . . 53

III 3D systems with moderate to high eccentricities 59

4 Lidov-Kozai resonance and stability 61
4.1 Motivation . . . 61
4.2 Parametric study . . . 64
4.2.1 Methodology . . . 65
4.2.2 Accuracy of the analytical approach . . . 67
4.3 Results . . . 70
4.3.1 Extent of the LK regions . . . 70
4.3.2 Sensitivity to observational uncertainties . . . 80
4.3.3 Stability of planetary systems . . . 81
4.4 Conclusions . . . 85

5 Close-in planetary systems 87
5.1 Motivation . . . 87
5.2 Secular Hamiltonian with relativistic corrections . . . 88
5.3 Methodology . . . 89
5.4 Results . . . 90
5.4.1 Influence on the extent of the LK region . . . 90
5.4.2 Importance of the GR effects . . . 100
5.5 Conclusions . . . 107

Conclusions and Perspectives 109

Bibliography 113

Introduction

Our knowledge of the Universe has greatly improved over the last centuries. At the beginning, humankind thought that Earth was at the centre of the Universe. Then we discovered that our planet revolved around the Sun, and Earth lost its importance as a central point. Afterwards, it came the consciousness that neither the Solar System held any particular position in the Milky Way, nor our galaxy was special among the others. One of the last strongholds remaining was the belief that the Solar System was the only system hosting planets. That all came to an end in 1995, when Michel Mayor and Didier Queloz announced the discovery of a Jupiter-mass planet revolving around the Sun-like star 51 Pegasi.

Since that pivotal announcement, different techniques of detection have been developed and applied to the search of extrasolar planets, also named exoplanets, and thousands of new ones have been discovered. Their orbital parameters span a wide range of values, showing planets with characteristics that are very different from the ones of the Solar System. For example, the very first detected exoplanet belonged to a new category of planets, the so-called hot-Jupiters; namely, giant planets so close to the star that their orbital period is of just few days. Another striking new feature observed concerns the orbits: where the Solar System has planets on quasi-circular orbits, many exoplanets have very eccentric orbits. Lastly, we currently have proofs of at least three extrasolar systems with planets on highly mutually inclined orbits: K2-266 (15°), Kepler-108 (24°) and the most famous υ Andromedae (30°). Such three-dimensional architectures are very different from the almost coplanar case of our Solar System.

Despite the considerable amount of data collected in the last decades, our knowledge of the exact structure of the exosystems is scattered at best. This is mainly due to the limitations of the detection methods. All the different techniques suffer from technical biases and do not provide a full set of orbital

parameters for the exoplanets detected. The few examples for which complete information is available are due to the application of multiple techniques. In the present work, we are going to focus on two-planet systems observed via the radial velocity method. The major drawback of this method is that it provides no information about the inclinations of the planets of a system, both between them and with respect to the line of sight. This leads to not knowing the exact value of the masses and the eventual three-dimensional structure of the system.

The aim of the present work is to provide constraints for the values of the inclinations for systems detected via the radial velocity method. Since a chaotic evolution of the system would survive for just a small fraction of the lifetime of the system itself, the chances to observe such a temporary situation are very low. It is therefore reasonable to assume the long-term stability of the detected system. Through two different approaches, we then proceed in determining which spatial configurations of the detected systems could be compatible with such a long-term stability.

The thesis is divided in three parts. In the first part, we recall the preliminary concepts at the basis of our work. In Chap. 1 we review the characteristics of the exoplanet population known up to now, as well as the detection methods. In Chap. 2 we introduce the perturbation theory and the theoretical techniques used to tackle our problem.

In the second part (Chap. 3), we describe a first method to study the stability of three-dimensional systems. We apply a *reverse* KAM approach to determine the values of the mutual inclination between the orbital planes that are compatible with the stability in the KAM sense.

The third part concerns the second approach. In Chap. 4 we study the dynamics of the systems in the parameter space of the orbital inclinations with respect to the line of sight and of the mutual inclination between the planets. We study the stability of the systems in the sense of the regularity of the orbits. We explore which values of the parameters are compatible with the Lidov-Kozai long-term protection mechanism for highly three-dimensional systems. We add a further analysis of the regularity by means of a chaos indicator. In Chap. 5 systems with very close-in planets are considered, therefore we also take into account the corrections to the motions due to the effects of the general relativity. Finally, we draw our conclusions and discuss future developments and perspectives.

Contributions

- M. Volpi, U. Locatelli, M. Sansottera, *A reverse KAM method to estimate unknown mutual inclinations in exoplanetary systems*, Celestial Mechanics and Dynamical Astronomy 130:36, 2018, Chapter 3 of the thesis;
- M. Volpi, A. Roisin, A.-S. Libert, *The 3D secular dynamics of radial-velocity-detected planetary systems*, Astronomy & Astrophysics, 626:A74, 2019, Chapter 4 of the thesis.

A paper based on Chapter 5 is currently in preparation.

Fundings

The PhD thesis was supported by a FRIA fellowship (F.R.S.-FNRS). Computational resources have been provided by the PTCI (Consortium des Équipements de Calcul Intensif CECI), funded by the FNRS-FRFC, the Walloon Region, and the University of Namur (Conventions No. 2.5020.11, GEQ U.G006.15, 1610468 et RW/GEQ2016).

Notation

	Symbol	Meaning
Parameters	a	Semi-major axis
	e	Eccentricity
	i	Inclination
	i_{mut}	Mutual inclination
	ω	Argument of the pericenter
	$\bar{\omega}$	Longitude of the pericenter
	Ω	Longitude of the node
	λ	Mean longitude
	P	Orbital period
	$R_\star$	Star radius
	R_p	Planet radius
	$m_\star$	Mass of the star
	m_p	Mass of the planet
	K	Radial velocity semi-amplitude
	L	Star luminosity
	F	Star flux
	α	Astrometric signature

Units of Measure	AU	Astronomical unit
	pac	Parsec
	as	Arcsecond
	yr	Year
	d	Day
	$M_\odot$	Solar mass
	M_J	Jupiter mass
	$\mathrm{M}_\oplus$	Earth mass
	$^\circ$	Degree
Operators	$\{\cdot,\cdot\}$	Poisson Bracket
	$\langle\cdot\rangle_{\boldsymbol{\phi}}$	Average over the generic angle $\boldsymbol{\phi}$
	$\lceil\cdot\rceil_{\boldsymbol{\lambda}:K_F}$	Truncation of the expansion of $\cdot$ up to a trigonometric degree K_F in the generic angle $\boldsymbol{\lambda}$
Abbreviations	RV	Radial Velocity
	LK	Lidov-Kozai
	GR	General Relativity

Part I

Preliminary

Chapter 1

Exoplanetary systems

This chapter provides an overview of the characteristics of the exoplanets detected so far and describes the most relevant detection methods. It also depicts the three-dimensional planetary systems discovered up to now.

1.1 Exoplanet population

Since the discovery of the first exoplanet around the star 51 Pegasi (Mayor and Queloz, 1995), ground-based observations and dedicated space missions have led to an astonishing increase of discoveries. Up to now, the catalogues count around 4000 confirmed exoplanets. Fig. 1.1 shows the number of known exoplanets per year, highlighting the breakdown per detection method.

In light of such an extensive exoplanet-population record, formation and evolution models had to develop new theories in order to explain the new observations. The Solar System was the reference instance around which the models have been tailored, but it now appears to be a particular case, rather than the norm. The extrasolar systems in fact present a large variety concerning the values of the orbital parameters. As an example, Fig. 1.2 presents the orbital eccentricity of the known exoplanets with respect to the semi-major axis; the colour code quantifies the mass of the detected objects.

There are a few main differences with respect to the Solar System. The first one concerns the eccentricities. The planetary orbits of the Solar System are in fact all nearly circular: the mean eccentricity is 0.0776, with single values ranging between 0.0068 and 0.2051. On the other hand, the eccentricities observed for exoplanets span a much wider range, with a mean value of ~ 0.17: if most of them tend to be on the lower end of the range, there are several

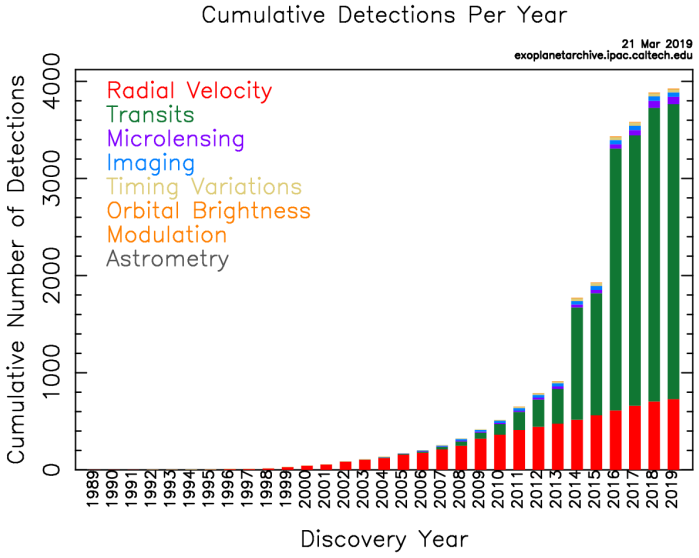

Figure 1.1 – Number of known exoplanets per year, coloured by detection method. Source: NASA Exoplanet Archive (`https://exoplanetarchive.pac.caltech.edu`).

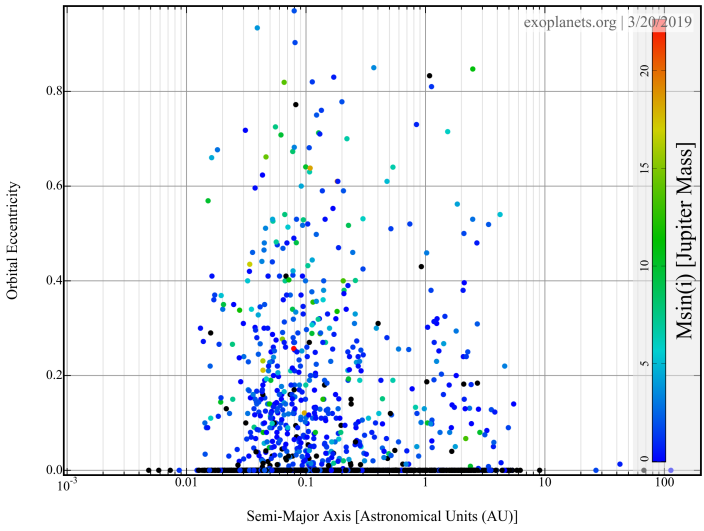

Figure 1.2 – Semi-major axis vs. eccentricity of the detected exoplanets. The colour scale indicates the mass of the planet expressed in Jupiter mass. Source: `exoplanets.org` (Han et al., 2014)

examples in which they assume exceptionally high values. The most extreme case reported is HD 20782b, whose eccentricity is accounted to be 0.97 (O'Toole et al., 2009).

The second major difference between the Solar System and the overall population of extrasolar systems lies in the mass distribution with respect to the semi-major axis. Our system has a neat configuration of small, rocky planets in the innermost part (but not closer than 0.3 AU), and gas/icy giants (being Jupiter the most massive) in the outer one. On the other hand, the first exoplanet observed, 51-Peg *b*, is a so-called *hot Jupiter*: a planet with a mass comparable to that of Jupiter and with a very short orbital period (typically a few days). In the following years, the majority of discovered exoplanets has proven to be close-in massive bodies. This category of planets was not expected from the classical formation theory made for the Solar System, and demanded a new approach to explain their existence. The significant proportion of hot Jupiters is surely to ascribe to observational biases. As we will discuss more in detail in the following section, detection methods tend to be more sensitive to planets that are very close to the host stars and have significant masses.

1.2 Detection methods

In order to discover exoplanets, several observational techniques have been developed during the last decades. Each of them has different characteristics and generally applies to targets of different nature. In this section we describe the five most widely adopted detection methods: radial velocity, transit, astrometry, imaging and microlensing. As shown by Fig. 1.1, the radial velocity and the transit methods are the most efficient and relevant methods in terms of number of discoveries. We then focus on these two in particular, describing briefly the other techniques.

All the data sets here mentioned are provided by The Extrasolar Planet Encyclopedia (`http://exoplanet.eu`, Schneider et al., 2011) and updated as of April 2019, unless otherwise stated.

1.2.1 Radial velocity method

The two-body problem prescribes the revolution of the bodies around their common centre of mass. In the case of a star-planet system, the movement of the star around the barycentre causes shifts of the light waves of its light spectrum: we observe shifts towards the red when the star is moving away from the observation point, and shifts towards the blue when approaching (see Fig. 1.3). The radial velocity (RV) method (or Doppler spectroscopy) measures these shifts in the light spectrum emitted by the star. The first RV surveys

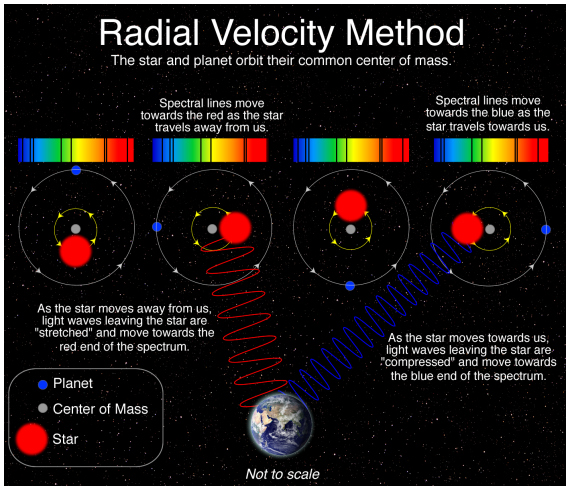

Figure 1.3 – Radial velocity method illustration. ©Las Cumbres Observatory Global Telescope Network.

were mainly designed to search for binary companions of main-sequence stars of modest mass ($\sim 1\,M_\odot$). Thus, the instruments did not initially have the sensitivity necessary to investigate the presence of exoplanets. However, as the accuracy improved, surveys started to observe many more stars for longer periods. This led to multiple observations of planets before the groundbreaking discovery of Mayor and Queloz (1995), but the announcements were careful and years had to pass before proper confirmation. For example, a planet of mass $1.7\,M_J$ was inferred around γ Cep by Campbell et al. (1988), but it was only confirmed in Hatzes et al. (2003). In the meantime, the first extrasolar planets were detected around the pulsar PSR 1257 12 (Wolszczan and Frail, 1992). The announcement of a hot Jupiter around 51 Peg solar-type star (Mayor and Queloz, 1995) opened substantial discussions. Such a short-period and giant planet was not in fact foreseen by the planetary models at the time. Since then, the Doppler spectroscopy has detected 817 planets divided in 612 systems, 142 of which are multiple.

The observations obtained by the RV method do not provide a complete set of orbital data for the planets. The shifts of the star light spectrum refer to the projection of the star motion along the line of sight. Therefore, it is not possible by RV alone to determine the orbital plane inclination i. A subset of the orbital parameters can be inferred: the eccentricity e, the argument of the pericenter ω, the orbital period P, and the position along the orbit at a particular reference time t_P. A quantity associated to exoplanets determined via this technique is the *radial velocity semi-amplitude* (see, e.g., Perryman

(2018))

$$K = \left(\frac{2\pi}{P}\right)^{1/3} \frac{m_p \sin i}{(m_\star + m_p)^{2/3}} \frac{1}{(1-e^2)^{\frac{1}{2}}} \tag{1.2.1}$$

where $m_\star$ and m_p are the mass of the star and of the planet, respectively. As a reference, the radial velocity semi-amplitude for Jupiter and Earth are $K_J = 12.5\,\mathrm{ms}^{-1}$ and $K_\oplus = 0.09\,\mathrm{ms}^{-1}$, respectively. The HARPS (High Accuracy Radial Velocity Planet Searcher) instrument was designed to achieve an accuracy $\sim 1\,\mathrm{ms}^{-1}$, and currently reaches a precision of $0.3 - 0.6\,\mathrm{ms}^{-1}$.

The quantities K, P and e are directly determined by the observations: whenever $m_\star$ can be estimated and supposing $m_p \ll m_\star$, it is possible to compute the value of $m_p \sin i$, but not of either of them separately. Therefore, the radial velocity method can only infer the minimal value $m_p \sin i$ for the mass of the planet. In light of this, it is actually not possible to distinguish, for example, between a low-mass planet whose orbital plane is aligned with the line of sight and a massive planet which is highly inclined with respect to the line of sight.

The RV-detected population

Let us now provide an overview of the characteristics of the exoplanet population discovered via the RV method. As we will show, the discoveries reflect the observational biases of the method, favouring massive planets on short-period orbits.

The early discoveries showed mostly hot Jupiters. As high-precision Doppler surveys have been carried in the last ~ 10 years only, the observation of bodies with $a \geqslant 3\,\mathrm{AU}$ is more difficult, and there is in fact a decrease in the number of planets found above such threshold. For this reason, planets with period $\mathrm{P} \geqslant 1000\,\mathrm{d}$ ($a \geqslant 2\,\mathrm{AU}$) are less certainly determined. Given the current data, projections have been made about the number of planets expected within 20 AU. Such a limit is given by formation theories: considering the physical properties of protoplanetary disks at such a distance, the time required for the formation of gas-giants would outdo the disk lifetime. Despite the uncertainties, even the most cautious models would consider that a significant population of exoplanets lies still undetected. Cumming et al. (2008) suggest that almost 20% of solar type stars might host a giant planet within 20 AU.

Extremely close-in planets ($\mathrm{P} \leqslant 6\,\mathrm{d}$) tend to display low eccentricities due to tidal effects, while further planets exhibit a huge variety of values, up to 0.97. An anti-correlation between eccentricities and multiplicity has been described in Limbach and Turner (2015): the higher the number of planets in the system, the lower the eccentricities. As a consequence, habitable planets might be more easily found in systems with a larger number of planets. In this perspective,

the lowly eccentric planets of the Solar System are, in fact, perfectly in line with the general exoplanet population, when the multiplicity of the system is taken into account. However, the determination of the eccentricities is not free from biases. For example, in Cumming et al. (2008), the authors evaluated the completeness of the KECK Planet Search and found that the highly-eccentric population (with $e \geqslant 0.6$) is not well constrained. Moreover, Rodigas and Hinz (2009) studied a possible bias related to undetected companions, highlighting that, for $0.1 < e < 0.3$, the probability to misinterpret, as a single planet in an eccentric orbit, a pair of a planet with a circular orbit and an unseen outer planet is estimated $\sim 13\%$.

As previously stated, the main restriction of the RV method lies in its incapability to determine the orbital inclination of a planet, and therefore its mass, since the proposed mass is only a minimal value. Although the RV method is more sensitive to massive planets, the majority of the detected planets have minimal masses smaller than 5 Jupiter masses. It is interesting to note that there are specific cases for which it is possible to combine different techniques in order to obtain additional constraints. The joined application of high-accuracy astrometry, for example, led to the determination of the masses of the υ Andromedae system planets c and d. Inclination constraints can be obtained also for systems discovered by means of the RV method but that later on have been found transiting as well.

1.2.2 Transit method

The transit method relies on the study of the light spectrum emitted by the host star. Whenever a planet crosses the line of sight of the observer, the light of the star is dimmed by its shadow. These alterations in the registered spectrum provide information about the body which is responsible for it (see Fig. 1.4 for an illustration of this effect).

In order to detect the variation, the star, the planet and the observer must be almost aligned. As such a particular configuration is required, the probability of detection is in general quite small. Moreover, the decrease in the stellar flux is considerably small. Indeed the star flux writes

$$F = \frac{L}{4\pi r^2} \tag{1.2.2}$$

and we define the transit depth as

$$\frac{\Delta F}{F} = \frac{R_p^2}{R_\star^2}\,, \tag{1.2.3}$$

where L is the luminosity of the star and r is the distance from the observer. As a reference, the transit depth for the Sun caused by Jupiter, Earth and Mars

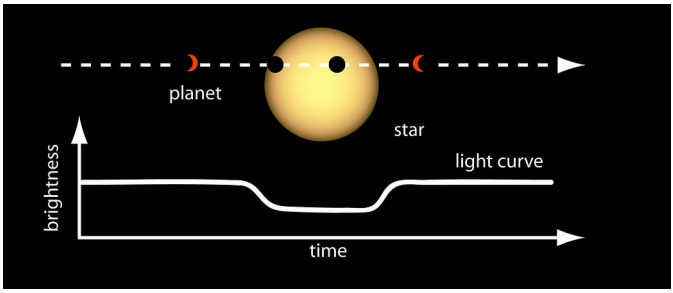

Figure 1.4 – Transit representation. ©NASA (`https://exoplanets.nasa.org`).

would be $\simeq 1.1 \times 10^{-2}$, $\simeq 8.4 \times 10^{-5}$ and $\simeq 3 \times 10^{-5}$, respectively. Ground-based telescopes have to deal with the interaction of the signal with the atmosphere, hence their accuracy is usually $\sim 10^{-3}$. Observations from space are highly more precise, reaching an accuracy of $\sim 10^{-4}$. For this reason, the launch of ESA's Corot[1](2006) and NASA's Kepler[2] (2009) missions has remarkably improved the detection rate.

The first detection by transit, HD 209458 *b*, was announced by Henry et al. (1999, 2000), as a second-step study of the planet that had already been discovered via radial velocity. The first transit observations were all following previous radial velocity measurements, but soon enough independent observations started. Especially after the launch of the space missions, the number of transiting planets has remarkably increased, reaching almost 3000 instances at the moment.

Let us note that a synergy with other techniques is required to gather further information on the transiting body, in particular to ensure its classification as a planet. Here we mention a few of the strategies applied. The simultaneous consideration of radial velocity data is a common process: supposing the orbital inclination to be $i \simeq 90^\circ$ (i.e., the orbital plane is close to the line of sight, otherwise there would be no transit), the two sets of data combined provide the parameters of the systems. Dynamical stability can act as a confirmation tool as well: Fabrycky et al. (2014) studied the multiple-planet systems listed in the results acquired by Kepler up until 2013, and confirmed around 95% of the observations with stability arguments. Direct imaging (see Sec. 1.2.3) is applied to discern eventual eclipsing binaries that could cause a signal similar to that of a transiting planet. Another example of confirmation strategy, more specific to Kepler, is the combination of its visible light signals with the infrared

[1]Convection, Rotation and planetary Transits, `http://sci.esa.int/corot/`
[2]`https://keplerscience.arc.nasa.gov/`

ones of Spitzer[3].

The schematic representation of the transit techniques given in Fig. 1.4 describes the general concept behind the observations. Additionally, there are several variations to the registered signal that provide further information about the planet detected.

The main phenomenon in the transit method is the *primary* eclipse: along its orbit, the planet crosses our line of sight and dims the light flux of the star. Moving away, thanks to the change of relative positions with the observer, the planet gradually begins to reflect the star light, reaching the peak of reflection right before passing behind the star. That is the so-called *secondary* eclipse. Useful data for the characterisation of the planet can be inferred by the difference between the signals of the primary and the secondary eclipse: they usually refer to the atmosphere of the planets, but they can also be used to better constrain their orbital properties.

For a single planet, the transits are regular over time, depending on the orbital period. Whenever the planet is interacting with other bodies (planets, exomoons, trojans), this regularity no longer applies[4]. The differences with the standard Keplerian behaviours are measured by the *transit timing variations* (TTVs). When the deviation is caused by interactions between planets, the TTVs have a strong dependency from the masses and the system architecture, and they allow, for example, to determine the masses that would be otherwise unknown.

Another particular feature can be observed when combining transit and radial velocity measurements: the Rossiter-McLaughlin effect, firstly noted in relation to binary systems (Rossiter (1924) and McLaughlin (1924)). It is based on the study of the variations of the star spectrum. As the star rotates, the half approaching the observer shows a blue shift in its spectrum, whereas the other half has red shifts. When transiting, a planet will shield different portions of the star, causing anomalies in the light spectrum emitted. Studying these alterations, it is possible to measure (if present) the spin-orbit misalignment between the star and the planet. For a review of the Rossiter-McLaughlin effect, see for example Gaudi and Winn (2007).

The transit-detected population

Although this detection method is again favouring massive planets on short period orbits, the transiting planet population shows a wide range in its characteristics. In terms of masses, for example, they vary between very low values

[3] `http://www.spitzer.caltech.edu/info/12-The-Mission`

[4] Other causes for such a disruption of the regularity are general relativity, oblateness of the host star, tidal interactions precessions and so on.

($0.02\,M_\oplus$ for Kepler-138$\,b$) to brown-dwarf values ($\sim 22\,M_J$ for CoRoT-3$\,b$), and beyond. This large variety applies to periods as well. Of the 2945 transiting planets actually detected, 2.5% have a period shorter than 1 d, 52% shorter than 10 d and 94% shorter than 100 d.

Many transiting systems do not have eccentricity constraints. This is often due to the fact that they are not suitable targets for observations via radial velocity. There are other means to determine their values. Mainly for close-in planets, in case of a registered secondary eclipse, the eccentricities can be inferred by comparison with the primary one. For multiple-planet systems showing TTVs, the eccentricity e and the planet mass m_p can be computed, although they are correlated. For the systems whose eccentricities have been determined, the same anti-correlation between eccentricity values and multiplicity of the planets discussed in Sec.1.2.1 have been found (Zinzi and Turrini, 2017).

As expected by the nature of the transit observations, orbital inclinations with respect to the plane of the sky are for the most part $\sim 90^\circ$. There are a few exceptions, with the most inclined case of Kepler-91$\,b$, showing an inclination of $\sim 68.5^\circ$.

When considering multiple-planet systems, a three-dimensional structure might be investigated. In the case of transit observations, there are some constraints that can be fixed for the mutual inclination between the planets. They may be obtained via different strategies: from the combination of transit and astrometry data, for example, or transit and radial velocity if the RV method has found a non-transiting planet. Transit signals alone can be sufficient to determine the mutual inclination whenever particular conditions have been observed in the same system, such as Rossiter-McLaughlin effect for multiple planets, changes in TTVs or in the transit duration and depth. In Sec. 1.3 we report a few examples of established 3D systems.

1.2.3 Other methods

As previously noted, the RV and the transit methods are the most efficient observational techniques currently available. Nevertheless, other methods are also used, and their contribution to complete data otherwise obtained has sometimes been decisive for crucial discoveries. In the following, we briefly describe several other methods.

Astrometry

Astrometry is the branch of astronomy that provides precise measurements of position and motion of celestial entities (from planetary system bodies to galaxies and clusters). In the framework of exoplanets, astrometry observations

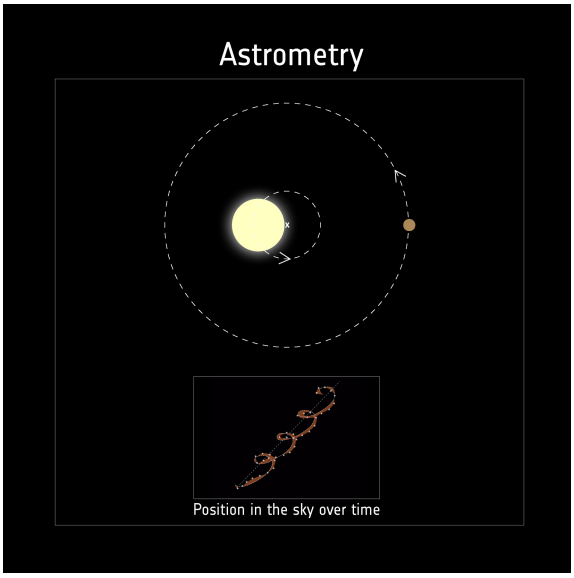

Figure 1.5 – Astrometry illustration. ©ESA (`https://www.esa.int`)

are based on the same phenomenon as the one considered by the RV method: the revolution of the star around the barycentre of the star-planet system (see Eq. 1.2.1). While the RV method measures the displacement of the star along the line of sight, astrometry data concern the projection of the movement on the plane of the sky (see Fig. 1.5).

The observable related to astrometry for planet detection is the astrometric signature α:

$$\alpha = \frac{m_p}{m_\star + m_p} a \simeq \frac{m_p}{m_\star} a = \left(\frac{m_p}{m_\star}\right)\left(\frac{a}{1\,\mathrm{AU}}\right)\left(\frac{d}{1\,\mathrm{pc}}\right)^{-1} \mathrm{as}, \tag{1.2.4}$$

where m_p and $m_\star$ are the planet and star masses, a is the semi-major axis of the planetary orbit (supposed circular), d is the distance of the star from Earth (expressed in parsecs). The Hipparcos (High Precision Parallax Collecting Satellite) mission[5] had an accuracy of $\sim 10^{-3}$ as. As a reference, the Sun-Jupiter system would have an astrometric signature $\alpha = 5 \cdot 10^{-4}$ as when observed from a distance $d = 10$ parsec, and $\alpha = 5 \cdot 10^{-5}$ as for $d = 100$ parsec. For this reason, up to now only 8 bodies discovered by astrometry are reported in The Extrasolar Planet Encyclopedia, and only HD 176051 b has a mass below the brown-dwarf limit of $13\,\mathrm{M}_J$ (see Muterspaugh et al. (2010)). The GAIA mission[6] launched in 2013 has an improved accuracy that goes from $\sim 10\,\mu$as

[5] `https://www.cosmos.esa.int/web/hipparcos`
[6] `https://www.cosmos.esa.int/web/gaia`

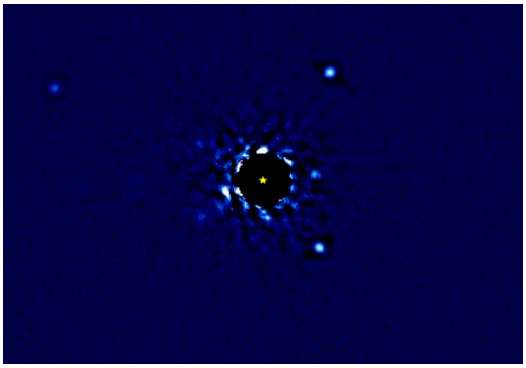

Figure 1.6 – Direct Imaging illustration of the four-planet system HR 8799. ©NASA (`https://exoplanets.nasa.org`), credits to Jason Wang and Christian Marois.

up to $\sim 300\,\mu$as depending on the stellar magnitude of the star taken into account. This should improve the astrometry detection record in the following years.

Despite the few occurrences of discoveries via astrometry itself, the method has been decisive to constrain observations obtained through other techniques. For example, the combination of the RV data and the astrometric ones of the Hipparcos mission led to the determination of constraints (when not precise values) of the planetary masses of numerous systems (see, e.g., Perryman (2018) for an overview).

Imaging

Contrary to the previous detection methods, imaging aims to acquire *direct* proof of the existence of an exoplanet by capturing proper images (see Fig. 1.6). There are different techniques applied to pursue the direct imaging of exoplanets: we will limit the present discussion to a general outline of the method. Its base concept is to consider the planet as a source of light, whether the host star's reflected light or the planet own emission. Direct imaging represents an impressive technical challenge, given the proximity of the planets (from the Earth perspective) to the evidently brighter star. At the same time, there are many benefits that come from this method. For example, it could allow the observation of planets much further the current limit of $a \gtrsim 20$ AU, or of the interaction between forming planets and protoplanetary disks in young systems.

Up to now, current imaging instruments are only able to capture images of giant planets that show sufficient own thermal emissions. Self-radiation-emitting giants are usually young and warm, therefore young stars ($10 - 100$ Myr) are

good candidates to host direct-imaging-detectable planets. The present instrumental development should ensure in the next years the detection of giants that reflect the host star light. Despite the foreseen improvements, Earth-like planets will still not be possible targets in the near future. Direct imaging can also be applied to known systems in case previous data infer the presence of an undetected body whose parameters cannot be further constrained otherwise.

Let us note that imaging has mainly led to the observations of planets revolving around brown dwarfs. The Exoplanet Encyclopedia registers 125 exoplanets discovered by direct imaging. Due to the current limitations of the method, a remarkable feature of the detections is that a relevant subset of the planets has been found on an orbit with extremely large semi-major axis, being $a \geqslant 100$ AU. As previously said, such extrasolar systems with this kind of structure could not be observed with any of the other methods. This ensures for direct imaging an important role in the future.

Gravitational microlensing

Gravitational lensing is a detection technique based on the distortion of the spacetime and the consequent deviation of the light prescribed by general relativity. It does require certain conditions to occur between three objects: an observer, a source of light in the background, and between the two a moving object in the foreground (the lens). The gravitational potential of the lens deviates the radiation emitted by the source: this disrupts the image perceived by the observer, in some cases even multiplying it. The relative motion between these three main objects determines time-dependent images, whose variations can last from hours to years, according to the type of source and lens.

There are different *regimes* of gravitational lensing, depending on the possibility to observe the effects in a proper or statistical sense and on the characteristics of the resulting images. The regime involved in the exoplanets' detection is the so-called gravitational *microlensing*, characterised by discrete and unresolved images. In this case, the primary lens is a Sun-like star: the two distorted images of the source that are generated are separated by ~ 1 mas, far below the threshold imposed by the resolution of ground-based instruments. When dealing with a star-planet system, both bodies work as lenses: in such circumstances, their disruptions of the source light can reveal the geometry of the system, as schematically shown in Fig. 1.7.

By its nature, gravitational microlensing requires the source, the lens and the observer to be aligned in a certain way. This particular configuration can not be predicted, therefore the observational surveys are required to monitor a large number of objects at the same time. For a successful observation, light sources generally have a distance of ~ 8 kpac from Earth: without lenses acting,

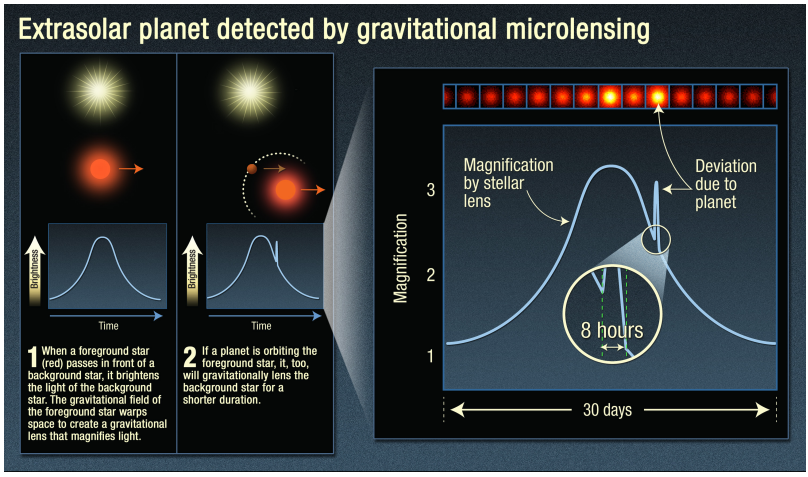

Figure 1.7 – Gravitational microlensing representation.
©NASA (`https://exoplanets.nasa.org`), credits to Kailash Sahu.

they are typically faint, if not invisible. When microlensing applies, the lenses most effectively detected are half-way (~ 4 kpac): this implies that they would be undetectable by other methods.

Although there had been numerous possible observations, the first confirmed discovery of an exoplanet by means of gravitational microlensing was announced in 2004 (OGLE-2003-BLG-235L b[7] (Bond et al., 2004)). Since then, more than 90 systems have been found thanks to this technique. The exoplanets discovered so far show a wide range of orbital parameters, for example, in mass and distance from the host star.

The principal limit of the gravitational microlensing method is that, given its nature, it is not possible to observe two times the same event. Therefore, as the observations are unique, they can not be confirmed.

1.3 Three-dimensional systems

As discussed in the previous sections, determining the possible three-dimensional architecture of a system is not a trivial task.

Despite the discovery of hundreds of planetary systems, information of their spatial configuration has only been derived for a dozen of them.

[7]OGLE is the Optical Gravitational Lens Experiment (Udalski, 2003). Together with MOA (Microlensing Observation in Astrophysics, Bond et al. (2001)), it is the most effective ground-based exoplanets' detector.

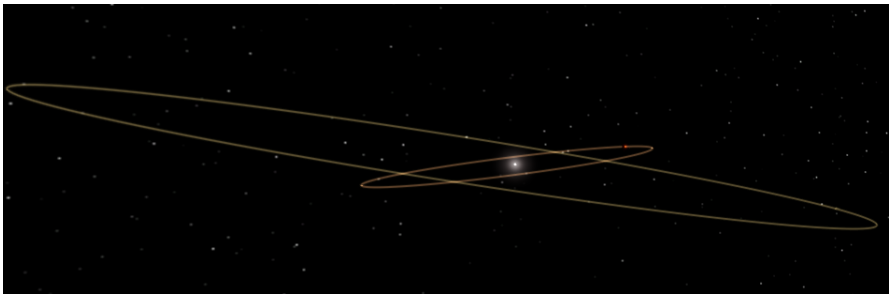

Figure 1.8 – υ Andromedae system (orbital parameters as in Table 16 of McArthur et al. (2010)). Created with "Universe Sandbox" (`http://universesandbox.com`).

More in-depth studies have been carried out in order to determine the mutual inclination between planets, and, in most of the cases, the conclusions delivered an upper bound for the mutual inclination of few degrees, with $i_{mut} \leqslant 10^\circ$.[8]

However, three systems have been characterised by a relevant mutual inclination between the planets. The most recent announcement is the system K2-266 (Rodriguez et al., 2018). The four confirmed planets and the two planet candidates revolve around the host star in an highly compact architecture ($a_{max} \sim 0.2546$ AU). The innermost, K2-266b, shows mutual inclinations between 12° and 15° with the other (possible) five planets of the system.

Another example of a three-dimensional (3D) system is Kepler-108 whose two giant planets have a mutual inclination of 24° (Mills and Fabrycky, 2017).

The most famous and well studied 3D system is surely υ Andromedae. It was announced by Butler et al. (1999) as the first multiple system to be discovered around a main-sequence star. In McArthur et al. (2010), the authors combined observational data obtained via RV method and astrometry to infer both the orbital inclinations of the planets c and d (and, therefore, their masses), and their mutual inclination of $29.9^\circ \pm 1^\circ$.

Coplanar configurations are straightforwardly coherent with the classical models of formation of planets within a dissipative disk. However, the existence of these prominently three-dimensional systems surely proves that mechanisms such as planet-disk interaction, planet-planet scattering and distant perturber interferences might play a relevant role in the establishment of inclined orbits.

The incomplete data that detection methods produce do not provide, in

[8] In particular: GJ 876 (Baluev, 2011), Kepler-9 (Holman et al., 2010), Kepler-10 (Batalha et al., 2011), Kepler-11 (Lissauer et al., 2011), Kepler-30 (Sanchis-Ojeda et al., 2012), Kepler-46 (Sanchis-Ojeda et al., 2012), Kepler-56 (Huber et al., 2013), Kepler-117 (Almenara et al., 2015), Kepler-419 (Dawson et al., 2014).

general, enough information to deduce the real structure of the exoplanetary systems discovered. Although several missions are planned to observe new stars searching for more new planets, others have been designed for a more focused study of already known systems (for example, ESA's CHEOPS[9]). A clear objective is to better characterise these systems, depicting the most complete picture possible.

Dynamical studies have already been used in the past to explore the stability of exoplanetary systems, either in coplanar or three-dimensional configurations. This allowed, if not to define precise values, to fix constraints for the unknown parameters. Our aim is to move consistently in this direction. Through different approaches, and in synergy with the observational information available, the objective is to determine boundaries in the parameter space that would ensure the stability of the system on the long term.

[9]Characterising Exoplanet Satellite, `http://sci.esa.int/cheops/`

Chapter 2

Perturbation theory

In this chapter we describe the general framework of normal forms and normalisation schemes. Moreover, we present the expansion of the Hamiltonian of the three-body problem and the two secular formulations (at order one and two in the masses) adopted in this work.

2.1 Normal forms

The existence of non-integrable systems has motivated the development of techniques aiming to obtain a close-enough approximation of the solution. In particular, nearly-integrable systems have been an optimal target to develop perturbation theory. Let us consider a set of canonical variables $(\boldsymbol{p},\boldsymbol{q}) \in \mathbb{R}^{2n}$. A system is said to be nearly-integrable if the associated Hamiltonian $H(\boldsymbol{p},\boldsymbol{q})$ can be written as

$$H(\boldsymbol{p},\boldsymbol{q}) = H_0(\boldsymbol{p},\boldsymbol{q}) + \varepsilon H_1(\boldsymbol{p},\boldsymbol{q})\,, \tag{2.1.1}$$

where H_0 is integrable and ε is a *small* parameter. Therefore the system can be interpreted as a small perturbation of an integrable problem. As the system is non-integrable, by definition it is not possible to derive an exact solution. Nevertheless, the Hamiltonian can be treated so to obtain an appropriate approximation. Applying transformations to transform the Hamiltonian into a normal form is a well-established technique. Normal forms are simplified formulations of the Hamiltonian useful to study the dynamics of the system. Normalisation algorithms are based on the application of canonical transformations. The goal is to identify a change of coordinates $(\boldsymbol{p},\boldsymbol{q}) = (\boldsymbol{p}(\boldsymbol{p}',\boldsymbol{q}'),\boldsymbol{q}(\boldsymbol{p}',\boldsymbol{q}'))$ such that the Hamiltonian can be re-formulated as

$$H'(\boldsymbol{p}',\boldsymbol{q}') = H(\boldsymbol{p}(\boldsymbol{p}',\boldsymbol{q}'),\boldsymbol{q}(\boldsymbol{p}',\boldsymbol{q}')) = Z(\boldsymbol{p}',\boldsymbol{q}') + R(\boldsymbol{p}',\boldsymbol{q}')\,, \tag{2.1.2}$$

where $Z(\boldsymbol{p}', \boldsymbol{q}')$ is an integrable normal form and $R(\boldsymbol{p}', \boldsymbol{q}')$ is the remainder. Given that the aim is to obtain an integrable approximation of $H(\boldsymbol{p}, \boldsymbol{q})$, the validity of the normalisation scheme is given by the size of the remainder $R(\boldsymbol{p}', \boldsymbol{q}')$. This is a crucial factor normalisation algorithms have to deal with while constructing the change of variables that leads to formulation (2.1.2).

2.1.1 Lie series method

One way to construct normal forms is given by the Lie series method (see for example Gröbner and Knapp, 1967; Giorgilli, 2015). Let us consider the set of canonical coordinates $(\boldsymbol{p}, \boldsymbol{q}) \in \mathbb{R}^{2n}$ and an holomorphic function $\chi(\boldsymbol{p}, \boldsymbol{q})$, that we can see as an autonomous Hamiltonian. We define the Lie derivative with respect to the function χ as

$$\mathcal{L}_\chi \cdot = \{\cdot, \chi\} \tag{2.1.3}$$

being $\{\cdot, \cdot\}$ the Poisson bracket defined as

$$\{f, g\} = \sum_{j=1}^{n} \frac{\partial f}{\partial q_j} \frac{\partial g}{\partial p_j} - \frac{\partial f}{\partial p_j} \frac{\partial g}{\partial q_j} \,. \tag{2.1.4}$$

We can then define the Lie series operator as

$$\exp(\varepsilon \mathcal{L}_\chi) \cdot = \sum_{j=0}^{\infty} \frac{\varepsilon^j}{j!} \mathcal{L}_\chi^j \cdot \,; \tag{2.1.5}$$

such an operator represents the time evolution of the canonical flow generated by the Hamiltonian χ. Given χ, applying the corresponding Lie series operator $\exp(\varepsilon \mathcal{L}_\chi)$ to the coordinates $\boldsymbol{p}$ and $\boldsymbol{q}$ amounts to perform a near-the-identity canonical transformation. We can in fact consider χ expressed in the new variables $\boldsymbol{p}'$ and $\boldsymbol{q}'$ and write:

$$\begin{aligned} \boldsymbol{p} = \exp(\varepsilon \mathcal{L}_\chi) \boldsymbol{p}' &= \boldsymbol{p}' - \varepsilon \frac{\partial \chi}{\partial \boldsymbol{q}'}\bigg|_{(\boldsymbol{p}', \boldsymbol{q}')} + \frac{\varepsilon^2}{2} \mathcal{L}_\chi \frac{\partial \chi}{\partial \boldsymbol{q}'}\bigg|_{(\boldsymbol{p}', \boldsymbol{q}')} + \dots \\ \boldsymbol{q} = \exp(\varepsilon \mathcal{L}_\chi) \boldsymbol{q}' &= \boldsymbol{q}' + \varepsilon \frac{\partial \chi}{\partial \boldsymbol{p}'}\bigg|_{(\boldsymbol{p}', \boldsymbol{q}')} + \frac{\varepsilon^2}{2} \mathcal{L}_\chi \frac{\partial \chi}{\partial \boldsymbol{p}'}\bigg|_{(\boldsymbol{p}', \boldsymbol{q}')} + \dots \,. \end{aligned} \tag{2.1.6}$$

The transformation of the coordinates $(\boldsymbol{p}, \boldsymbol{q})$ in $(\boldsymbol{p}', \boldsymbol{q}')$ easily translates in the transformation of a function $f(\boldsymbol{p}, \boldsymbol{q})$ in $f'(\boldsymbol{p}', \boldsymbol{q}')$ thanks to one of the properties of the Lie series, also known as the exchange theorem. It holds that

$$f(\boldsymbol{p}, \boldsymbol{q})\Big|_{\boldsymbol{p}=\exp(\varepsilon \mathcal{L}_\chi)\boldsymbol{p}', \boldsymbol{q}=\exp(\varepsilon \mathcal{L}_\chi)\boldsymbol{q}'} = \exp(\varepsilon \mathcal{L}_\chi) f(\boldsymbol{p}, \boldsymbol{q})\Big|_{(\boldsymbol{p}=\boldsymbol{p}', \boldsymbol{q}=\boldsymbol{q}')} \,. \tag{2.1.7}$$

Thus, instead of performing a change of variables, it is sufficient to apply the Lie series operator to the function itself in order to obtain the expansion in ε in the new set of coordinates.

Previously, we discussed the role of normalisation algorithms in the framework of nearly-integrable systems. The change of variables needed to rewrite the nearly-integrable Hamiltonian in normal form can be achieved by composition of near-the-identity canonical transformations constructed by means of the Lie series method. Let us consider the nearly-integrable function

$$h(\boldsymbol{p},\boldsymbol{q},\varepsilon) = h_0(\boldsymbol{p},\boldsymbol{q}) + \varepsilon h_1(\boldsymbol{p},\boldsymbol{q}) + \varepsilon^2 h_2(\boldsymbol{p},\boldsymbol{q}) + \dots \tag{2.1.8}$$

and its transformed expression $\bar{h}(\boldsymbol{p},\boldsymbol{q},\varepsilon) = \exp(\varepsilon\mathcal{L}_\chi)h$. From the linearity properties of the Lie series operator, it holds that

$$\exp(\varepsilon\mathcal{L}_\chi)h = \exp(\varepsilon\mathcal{L}_\chi)h_0 + \varepsilon\exp(\varepsilon\mathcal{L}_\chi)h_1 + \varepsilon^2\exp(\varepsilon\mathcal{L}_\chi)h_2 + \dots . \tag{2.1.9}$$

A visual representation of the transformation is given by the Lie triangle:

$$\begin{array}{ccccccc}
h_0 & & & & & & \\
\downarrow & & & & & & \\
\mathcal{L}_X h_0 & & h_1 & & & & \\
\downarrow & & \downarrow & & & & \\
\frac{1}{2}\mathcal{L}_X^2 h_0 & & \mathcal{L}_X h_1 & & h_2 & & \\
\downarrow & & \downarrow & & \downarrow & & \\
\frac{1}{3!}\mathcal{L}_X^3 h_0 & & \frac{1}{2}\mathcal{L}_X^2 h_1 & & \mathcal{L}_X h_2 & & h_3 \\
\vdots & & \vdots & & \vdots & & \vdots \qquad \ddots
\end{array} \tag{2.1.10}$$

On each row are displayed terms that are of the same order in ε, so that to obtain the term of order ε^j of the transformed function it is sufficient to sum up all the terms of the j-th row. Therefore, the expansion in ε of the function $\bar{h}$ writes

$$\bar{h}(\boldsymbol{p},\boldsymbol{q},\varepsilon) = \bar{h}_0(\boldsymbol{p},\boldsymbol{q}) + \varepsilon\bar{h}_1(\boldsymbol{p},\boldsymbol{q}) + \varepsilon^2\bar{h}_2(\boldsymbol{p},\boldsymbol{q}) + \dots , \tag{2.1.11}$$

being $\bar{h}_0 = h_0$ and, for $j \geqslant 1$,

$$\bar{h}_j = \sum_{k=0}^{j} \frac{1}{k!}\mathcal{L}_\chi^k h_{j-k} . \tag{2.1.12}$$

We explicitly describe in the following chapters how we applied the Lie series method. In Sect. 2.2.3 we describe how it is applied to obtain the secular formulation of the Hamiltonian at order two in the masses, while in Sect. 3.2.1 and in Sect. 3.2.2 the Lie series method is used to achieve the Birkhoff's and Kolmogorov's normal forms, respectively.

2.1.2 Particular normal forms

Since in the following we will heavily rely on normalisation schemes, we report here the theorems validating the normalisation schemes for the Kolmogorov's and Birkhoff's normal forms.

Birkhoff's normal form

Let us consider a smooth Hamiltonian H on the phase space $\mathbb{R}^{2n}$ having in the origin $(\mathbf{0},\mathbf{0})$ an elliptic equilibrium point. Therefore by definition there exists a set of canonical coordinates $(\boldsymbol{p},\boldsymbol{q})$ such that the Hamiltonian H writes

$$H(\boldsymbol{p},\boldsymbol{q}) = H_0(\boldsymbol{p},\boldsymbol{q}) + K(\boldsymbol{p},\boldsymbol{q})\,, \tag{2.1.13}$$

with

$$H_0(\boldsymbol{p},\boldsymbol{q}) = \sum_{j=1}^{n} \omega_j \frac{p_j^2+q_j^2}{2} \tag{2.1.14}$$

and K a real smooth function having a zero of order 3 in the origin.

The Birkhoff theorem states the following (see for example Moser (1968)).

Theorem 1 *For any positive $r \geqslant 0$, there exist a neighbourhood U_r of the origin and a canonical transformation $\tau_r : (\boldsymbol{p},\boldsymbol{q}) \in U_r \to (\boldsymbol{p}',\boldsymbol{q}') \in \mathbb{R}^{2n}$ such that the system* (2.1.13) *is transformed in Birkhoff normal form up to order r:*

$$H^{(r)} = H \circ \tau_r = H_0 + Z^{(r)} + R^{(r)}\,, \tag{2.1.15}$$

where $Z^{(r)}$ is a polynomial of degree $r+2$ such that $\{H_0, Z^{(r)}\} = 0$ and $R^{(r)}$ is small, i.e.*,*

$$|R^{(r)}| \leqslant k_r |(\boldsymbol{p},\boldsymbol{q})|^{r+3}, \quad \forall (\boldsymbol{p},\boldsymbol{q}) \in U_r\,. \tag{2.1.16}$$

Furthermore, the transformation τ_r is close to the identity:

$$|(\boldsymbol{p},\boldsymbol{q}) - \tau_r(\boldsymbol{p},\boldsymbol{q})| \leqslant k_r |(\boldsymbol{p},\boldsymbol{q})|^2, \quad \forall (\boldsymbol{p},\boldsymbol{q}) \in U_r\,, \tag{2.1.17}$$

and the same holds for τ_r^{-1}.

Moreover, if $\boldsymbol{\omega}$ is non resonant up to order r then $Z^{(r)}$ depends only on the new actions

$$I_j' = \frac{(p_j')^2 + (q_j')^2}{2}\,. \tag{2.1.18}$$

The Birkhoff's normal form constitutes one of the most direct and common examples of normalisation of an Hamiltonian, as its aim is to obtain a formulation depending only on the actions up to a certain order r. In Sect. 3.2.1 we implement the Birkhoff's normal form to eliminate the degeneracy of the secular Hamiltonian at order two in the masses as one of the preparatory steps to finally construct a Kolmogorov's normal form.

Kolmogorov's normal form

The main objective of the KAM theory is the study of the persistence of quasi-periodic motions of integrable Hamiltonian systems under small perturbations. The development of such a theory was due to the necessity to solve stability problems found in celestial mechanics.

The first instance of the theorem was proposed by Andrey Kolmogorov in 1954 (see Kolmogorov (1954) for the original work and Chierchia (2008) for a review). Its formulation is recalled here.

Theorem 2 *Let H be a real-analytic Hamiltonian*

$$(\boldsymbol{p},\boldsymbol{q},\varepsilon)\in\mathcal{M}^{2n}\times(-\varepsilon_0,\varepsilon_0):=B\times\mathbb{T}^n\times(-\varepsilon_0,\varepsilon_0)\to H(\boldsymbol{p},\boldsymbol{q};\varepsilon), \tag{2.1.19}$$

being B a n-ball around the origin in $\mathbb{R}^n$, $\mathbb{T}^n$ the n-dimensional torus, ε_0 a real positive and ε a real small parameter. The phase space $\mathcal{M}^{2n}$ is considered with the standard symplectic form $dp\wedge dq=\sum_{j=1}^n dp_j\wedge dq_j$ so that for each ε, the Hamiltonian flow $\phi_H^t:\mathcal{M}^{2n}\to\mathcal{M}^{2n}$ is the solution at the time t of the following Cauchy problem:

$$\begin{cases}\dot{\boldsymbol{p}}=-\nabla_{\mathbf{q}}H(\boldsymbol{p},\boldsymbol{q};\varepsilon)\\ \dot{\boldsymbol{q}}=\nabla_{\mathbf{p}}H(\boldsymbol{p},\boldsymbol{q};\varepsilon)\end{cases},\quad \textit{with}\quad \begin{cases}\boldsymbol{p}(0)=\boldsymbol{p_0}\\ \boldsymbol{q}(0)=\boldsymbol{q_0}\end{cases}. \tag{2.1.20}$$

Let $H_0(\boldsymbol{p},\boldsymbol{q}):=H(\boldsymbol{p},\boldsymbol{q};0)$ be of the form

$$H_0(\boldsymbol{p},\boldsymbol{q})=E+\boldsymbol{\omega}\cdot\boldsymbol{p}+Q(\boldsymbol{p},\boldsymbol{q}) \tag{2.1.21}$$

such that $Q=\mathcal{O}(|\boldsymbol{p}|^2)$, $E\in\mathbb{R}$ and $\boldsymbol{\omega}\in\mathbb{R}^n$ satisfies a Diophantine condition, namely there exist constants γ and τ for which

$$|\boldsymbol{\omega}\cdot\boldsymbol{n}|\geqslant\frac{\gamma}{|\boldsymbol{n}|^\tau},\quad\forall\,\boldsymbol{n}\in\mathbb{Z}^n\backslash\{0\}. \tag{2.1.22}$$

Let assume H_0 to be non-degenerate in the sense that

$$\det\langle\partial_{\mathrm{p}}^2\mathrm{Q}(0,\cdot)\rangle\neq 0, \tag{2.1.23}$$

being $\langle\cdot\rangle$ the average over $\mathbb{T}^n$. Then, there exist $0<\bar\varepsilon\leqslant\varepsilon_0$, a ball $\bar B\subset B$ centred in the origin of $\mathbb{R}^n$ and a real-analytic symplectic transformation

$$\bar\phi:\bar B\times\mathbb{T}^n\to\mathcal{M}^{2n}$$

depending analytically also on $\varepsilon\in(-\varepsilon_0,\varepsilon_0)$, such that $\bar\phi|_{\varepsilon=0}$ is the identity map and, for any $|\varepsilon|<\bar\varepsilon$,

$$H\circ\bar\phi(\boldsymbol{p}',\boldsymbol{q}')=\bar K(\boldsymbol{p},\boldsymbol{q};\varepsilon)=\bar E(\varepsilon)+\boldsymbol{\omega}\cdot\boldsymbol{p}'+\bar Q(\boldsymbol{p},\boldsymbol{q};\varepsilon)$$

with $\bar Q=\mathcal{O}(|\boldsymbol{p}'|^2)$.

Following this first formulation, many developments and extensions have been proposed, notably by Moser (1962) and Arnol'd (1963), who provided a precise demonstration of the Kolmogorov's theorem. For this reason, the theory is known by the acronym KAM.

The KAM theorem finds its natural application in the $(n+1)$-body planetary problem: disregarding the gravitational attraction between the planets, the Hamiltonian describing the system is the sum of n Keplerian problems that are integrable. The interaction between the planets then plays the role of a perturbation of an integrable problem. The "smallness" of such a perturbation is guaranteed by the ratio of the planetary and stellar masses.

Benettin et al. (1984) proved the KAM theorem following the original scheme by Kolmogorov, but using the Lie method to define the canonical transformations. This provides two benefits. The first one is that it avoids any inversion and therefore any use of the implicit-function theorem, as it is required in the original scheme. Secondly, as it involves only simple algebraic operations, it is easily implemented on a computer.

2.2 The three-body problem

The focus of the present work will be on exoplanetary systems consisting in a host star and two planets. In the following, the central star will be indicated by the index 0, while the two planets will be marked by the indexes 1 (inner) and 2 (outer). Therefore, we study a three-body problem. When considering a two-body gravitational system, we face an integrable problem whose solution has been known since the works of Kepler in the seventeenth century. Unfortunately, the integrability of the two-body problem does not extend to systems of three bodies. The nature of the three-body planetary case is particular: as the masses of the planets are much smaller than the one of the star ($m_1, m_2 \ll m_0$), their mutual gravitational attraction is small compared to the ones acting between the star and each planet. Thus it is a nearly-integrable problem, and therefore particularly suitable to undergo a normalisation algorithm.

2.2.1 Hamiltonian formulation and symmetries

The three-body problem possesses two intrinsic symmetries. Exploiting their properties, it is possible to reduce the initial 9 degrees of freedom (d.o.f.) of the system, therefore simplifying its dynamical analysis.

First of all, it is invariant for translations in the $\mathbb{R}^3$ space: this corresponds to the invariance of the centre of mass. Once this feature is taken into account, we obtain a 6-d.o.f problem. Such a reduction can be operated by adopting

heliocentric canonical variables. The Hamiltonian in heliocentric canonical coordinates $(\boldsymbol{r}, \tilde{\boldsymbol{r}})$ (see, for example, Laskar (1989b)) writes

$$H(\boldsymbol{r}, \tilde{\boldsymbol{r}}) = T^{(0)}(\tilde{\boldsymbol{r}}) + U^{(0)}(\boldsymbol{r}) + T^{(1)}(\tilde{\boldsymbol{r}}) + U^{(1)}(\boldsymbol{r}), \tag{2.2.1}$$

where

$$\begin{aligned} T^{(0)}(\tilde{\boldsymbol{r}}) &= \frac{1}{2} \sum_{j=1}^{2} \|\tilde{\boldsymbol{r}}_j\|^2 \left(\frac{1}{m_0} + \frac{1}{m_j} \right), \\ U^{(0)}(\boldsymbol{r}) &= -\mathcal{G} \sum_{j=1}^{2} \frac{m_0 m_j}{\|\boldsymbol{r}_j\|}, \\ T^{(1)}(\tilde{\boldsymbol{r}}) &= \frac{\tilde{\boldsymbol{r}}_1 \cdot \tilde{\boldsymbol{r}}_2}{m_0}, \\ U^{(1)}(\boldsymbol{r}) &= -\mathcal{G} \left(\frac{m_1 m_2}{\|\boldsymbol{r}_1 - \boldsymbol{r}_2\|} \right). \end{aligned} \tag{2.2.2}$$

The terms $T^{(0)}$ and $U^{(0)}$, $T^{(1)}$ and $U^{(1)}$ represent the kinetic and potential energies of the integrable part (two uncoupled Keplerian problems) and the ones of the perturbing function, respectively. We will adopt the set of canonical variables defined by Poincaré:

$$\begin{aligned} \Lambda_j &= \frac{m_0 m_j}{m_0 + m_j} \sqrt{\mathcal{G}(m_0 + m_j) a_j}, \\ \lambda_j &= M_j + \bar{\omega}_j, \\ \xi_j &= \sqrt{2\Lambda_j} \sqrt{1 - \sqrt{1 - e_j^2}} \cos \bar{\omega}_j, \\ \eta_j &= -\sqrt{2\Lambda_j} \sqrt{1 - \sqrt{1 - e_j^2}} \sin \bar{\omega}_j, \\ p_j &= \sqrt{2\Lambda_j} \sqrt{\sqrt{1 - e_j^2}(1 - \cos i_j)} \cos \Omega_j, \\ q_j &= -\sqrt{2\Lambda_j} \sqrt{\sqrt{1 - e_j^2}(1 - \cos i_j)} \sin \Omega_j, \end{aligned} \tag{2.2.3}$$

where a_j, e_j, i_j, M_j, $\bar{\omega}_j$, Ω_j are the semi-major axis, the eccentricity, the inclination, the mean anomaly, the longitude of the pericenter and the longitude of the node of the j-th planet, respectively.

The second symmetry is with respect to rotations. This is linked to the conservation of both the norm and the direction of the total angular momentum $\boldsymbol{C}$ of the system. When including this feature in the formulation of the problem (Poincaré (1893), Laskar (1989b)), the d.o.f. decrease to 4. The reduction to 4 d.o.f. can be performed by adopting the Laplace plane as reference plane. The Laplace plane is defined as the plane perpendicular to the total angular

momentum of the system. As we are considering only conservative forces, the total angular momentum is an invariant of the system. Consequently, the Laplace plane is invariant as well. The choice of this particular plane as reference implies that the following holds:

$$\Omega_1 - \Omega_2 = \pi \tag{2.2.4}$$

$$\Lambda_1\sqrt{1-e_1^2}\cos i_1 + \Lambda_2\sqrt{1-e_2^2}\cos i_2 = C\,, \tag{2.2.5}$$

$$\Lambda_1\sqrt{1-e_1^2}\sin i_1 - \Lambda_2\sqrt{1-e_2^2}\sin i_2 = 0\,. \tag{2.2.6}$$

We then find relations between the eccentricities and the inclinations. Therefore, the system can be described using the adapted heliocentric Poincaré variables:

$$\begin{aligned}
\Lambda_j &= \frac{m_0 m_j}{m_0+m_j}\sqrt{\mathcal{G}(m_0+m_j)a_j}\,,\\
\lambda_j &= M_j + \omega_j\,,\\
\xi_j &= \sqrt{2\Lambda_j}\sqrt{1-\sqrt{1-e_j^2}}\cos\omega_j\,,\\
\eta_j &= -\sqrt{2\Lambda_j}\sqrt{1-\sqrt{1-e_j^2}}\sin\omega_j\,,
\end{aligned} \tag{2.2.7}$$

being ω_j the argument of the pericenter of the j-th planet.

2.2.2 Hamiltonian expansion

In this work we expand the Hamiltonian both in the Poincaré variables (2.2.7) and, following Robutel (1995), in the parameter D_2 defined as

$$D_2 = \frac{(\Lambda_1+\Lambda_2)^2 - C^2}{\Lambda_1\Lambda_2}\,, \tag{2.2.8}$$

where C is the norm of the total angular momentum. The parameter D_2 can be seen as a normalised angular momentum deficit (hereafter AMD), similar to the one introduced in Laskar (1997)[1]. By definition, D_2 is quadratic in eccentricities or inclinations. This parameter is therefore a measure of the difference between the actual total angular momentum and the one of a similar system having circular and co-planar orbits (for which $D_2 = 0$).

Let us note that, combining (2.2.5), (2.2.6) and (2.2.8), we obtain the relation between the mutual inclination of the two orbital planes referred to the

[1]Precisely, being C the total angular momentum, i.e., $C = \sum_{k=1}^{2}\Lambda_k\sqrt{1-e_k^2}\cos i_k$, the angular momentum deficit is defined as $AMD = \sum_{k=1}^{2}\Lambda_k\Big(1-\sqrt{1-e_k^2}\cos i_k\Big)$.

Laplace plane and the parameter D_2:

$$i_1 + i_2 = \operatorname{acos}\left(\frac{\Lambda_1^2 e_1^2 + \Lambda_2^2 e_2^2 + (2 - D_2)\Lambda_1\Lambda_2}{2\Lambda_1\Lambda_2\sqrt{1-e_1^2}\sqrt{1-e_2^2}}\right). \tag{2.2.9}$$

Such an Hamiltonian expansion in Poincaré variables and D_2 parameter has already been implemented in Locatelli and Giorgilli (2000): the main difference with respect to that approach is that in that work the parameter D_2 was replaced by its particular value (computed for the Sun-Jupiter-Saturn system). On the contrary, in our case D_2 is kept as as a free parameter in the expansions.

Before performing the expansion, we introduce the translation $L_j = \Lambda_j - \Lambda_j^*$, where Λ_j^* is the value of Λ_j for the *observed* semi-major axis a_j. The Hamiltonian expansion in power series of the variables $\mathbf{L}$, $\boldsymbol{\xi}$, $\boldsymbol{\eta}$ and the parameter D_2, and in Fourier series of $\boldsymbol{\lambda}$ writes

$$H^{(\mathcal{T}_F)} = \sum_{j_1=1}^{\infty} h_{j_1,0}^{(\mathrm{Kep})}(\mathbf{L}) + \mu \sum_{s=0}^{\infty}\sum_{j_1=0}^{\infty}\sum_{j_2=0}^{\infty} D_2^s\, h_{s;j_1,j_2}^{(\mathcal{T}_F)}(\mathbf{L},\boldsymbol{\lambda},\boldsymbol{\xi},\boldsymbol{\eta}), \tag{2.2.10}$$

where $\mu = \max\{m_1/m_0, m_2/m_0\}$ and

- $h_{j_1,0}^{(\mathrm{Kep})}$ is a homogeneous polynomial function of degree j_1 in $\mathbf{L}$; in particular, $h_{1,0}^{(\mathrm{Kep})} = \boldsymbol{n}^* \cdot \mathbf{L}$, where the components of the angular velocity vector $\boldsymbol{n}^*$ are defined by the third Kepler law;
- $h_{s;j_1,j_2}^{(\mathcal{T}_F)}$ is a homogeneous polynomial function of degree j_1 in $\mathbf{L}$, degree j_2 in $\boldsymbol{\xi}$ and $\boldsymbol{\eta}$, and with coefficients that are trigonometric polynomials in $\boldsymbol{\lambda}$, related to the term D_2^s.

The superscript $\mathcal{T}_F$ stresses the fact that $H^{(\mathcal{T}_F)}$ is the Hamiltonian obtained after having applied a translation of the fast actions.

2.2.3 Secular Hamiltonian

In this work we will select systems whose planets are far from mean-motion resonances. As we are interested in ensuring the long-term stability of the systems, we will study their *secular* evolution, discarding short-period effects. We mentioned in the Introduction that the work here presented tackles the same problem through two different approaches. The first difference between them is the formulation of the secular Hamiltonian. Two different secular formulations will be adopted, depending on the goal pursued.

The two different secular approximations of the Hamiltonian at order one and two in the masses are described hereafter.

The secular Hamiltonian at order one in the masses

The secular Hamiltonian at order one in the masses is obtained by averaging the Hamiltonian described by Eq. (2.2.10) with respect to the fast angles $\boldsymbol{\lambda}$. This approximation implies that the value of $\boldsymbol{\Lambda}$, and consequently the ones of the semi-major axis are constant. Such an averaging is obtained by solving the integral

$$\overline{H^{(\mathcal{T}_F)}} = \frac{1}{4\pi^2} \iint\limits_{[0,2\pi]^2} H^{(\mathcal{T}_F)} \mathrm{d}\lambda_1 \mathrm{d}\lambda_2 \,. \tag{2.2.11}$$

Computing $\overline{H^{(\mathcal{T}_F)}}$ is equivalent to discard any term of $H^{(\mathcal{T}_F)}$ that depends on any combination of the fast angles λ_i. For this reason, the approximation at order one in the masses is also known as the averaging by scissors. The resulting Hamiltonian, setting $H^{(sec1)} = \overline{H^{(\mathcal{T}_F)}}$, writes

$$H^{(sec1)}(D_2, \boldsymbol{\xi}, \boldsymbol{\eta}) = \sum_{j=0}^{ORDECC/2} \mathcal{C}_{j,\boldsymbol{m},\boldsymbol{n}} D_2^j \sum_{\boldsymbol{m}+\boldsymbol{n}=0}^{ORDECC-j} \boldsymbol{\xi}^{\boldsymbol{m}} \boldsymbol{\eta}^{\boldsymbol{n}} \,, \tag{2.2.12}$$

where $ORDECC$ indicates the maximal order in eccentricities considered, here fixed to 12. In non-resonant cases, the secular Hamiltonian at the first order in the masses describes efficiently the dynamics of the problem (see for example Libert and Sansottera (2013)), and will be used in Chap 4.

The secular Hamiltonian at order two in the masses

The Kolmogorov normalisation scheme described in Sect. 2.1.2 can be used to produce the secular approximation at order two in the masses (see, e.g., Locatelli and Giorgilli (2000); Libert and Sansottera (2013)). This means that in our model the torus corresponding to $\mathbf{L} = 0$ in the new coordinates will be invariant up to order two in the masses. For this aim, we proceed by averaging over the fast angles the terms of the Hamiltonian (2.2.10) that do not depend or are linear in the actions $\mathbf{L}$. This elimination is obtained via a composition of two Kolmogorov-like steps.

First, the transformed Hamiltonian writes, in the Lie series formalism,

$$\exp \mathcal{L}_{\chi_1^{(\mathcal{O}2)}} H^{(\mathcal{T}_F)} = \sum_{j=0}^{\infty} \frac{1}{j!} \mathcal{L}^j_{\chi_1^{(\mathcal{O}2)}} H^{(\mathcal{T}_F)} \,, \tag{2.2.13}$$

where the generating function $\chi_1^{(\mathcal{O}2)}$ is determined as the solution of the following homological equation

$$\sum_{i=1}^{2} n_i^* \cdot \frac{\partial \chi_1^{(\mathcal{O}2)}}{\partial \lambda_i} + \mu \sum_{\substack{s=0\,,\, j_2=0 \\ 2s+j_2 \leqslant N_S}} \left[D_2^s h_{s;0,j_2}^{(\mathcal{T}_F)} \right]_{\boldsymbol{\lambda}:K_F} = \mu \sum_{\substack{s=0\,,\, j_2=0 \\ 2s+j_2 \leqslant N_S}} D_2^s \left\langle h_{s;0,j_2}^{(\mathcal{T}_F)} \right\rangle_{\boldsymbol{\lambda}} \,, \tag{2.2.14}$$

being $\langle\cdot\rangle_{\boldsymbol{\phi}}$ the average over the generic angles $\boldsymbol{\phi}$. In the previous formula, we have denoted with $\lceil g\rfloor_{\boldsymbol{\lambda}:K_F}$ the truncation of the expansion of the generic function g up to a trigonometric degree K_F. The parameter K_F is fixed so as to include the main quasi-resonance of the system on hand: for instance, let us suppose the system is near to a $k_1^*:k_2^*$ resonance, then we set $K_F \geqslant |k_1^*|+|k_2^*|$. Moreover, in (2.2.14) the integer parameter N_S rules the considered order of magnitude in eccentricity and inclination: the choice of the particular value of N_S is again related to the main quasi-resonance of the system. In fact, from the d'Alembert rule we know that the terms containing the harmonics $(k_1^*\lambda_1 - k_2^*\lambda_2)$ have an order in eccentricity and inclination greater or equal to $|k_1^* - k_2^*|$ and with the same parity. Therefore, in order to include the effects of the $k_1^*:k_2^*$ resonance in the generating function $\chi_1^{(\mathcal{O}2)}$, we have to truncate the expansion up to $N_S \geqslant |k_1^* - k_2^*|$. This constraint takes into account that both $\boldsymbol{\xi}$ and $\boldsymbol{\eta}$ are linear in the eccentricities and D_2 is quadratic in eccentricities or inclinations.

The second Kolmogorov-like step is performed in an analogous way so as to introduce the secular Hamiltonian at order two in the masses $H^{(\mathcal{O}2)} = \exp\mathcal{L}_{\chi_2^{(\mathcal{O}2)}} \circ \exp\mathcal{L}_{\chi_1^{(\mathcal{O}2)}} H^{(\mathcal{T}_F)}$, where the new generating function $\chi_2^{(\mathcal{O}2)}$ is the solution of the homological equation

$$\begin{aligned}\sum_{i=1}^{2} n_i^* \cdot \frac{\partial \chi_2^{(\mathcal{O}2)}}{\partial \lambda_i} + \mu \sum_{\substack{s=0,\, j_2=0 \\ 2s+j_2\leqslant N_S}} \left\lceil D_2^s h_{s;1,j_2}^{(\mathcal{T}_F)} \right\rfloor_{\boldsymbol{\lambda}:K_F} + \mathcal{L}_{\chi_1^{(\mathcal{O}2)}} h_{2,0}^{(\mathrm{Kep})} \\ = \mu \sum_{\substack{s=0,\, j_2=0 \\ 2s+j_2\leqslant N_S}} D_2^s \left\langle h_{s;1,j_2}^{(\mathcal{T}_F)} \right\rangle_{\boldsymbol{\lambda}} .\end{aligned} \tag{2.2.15}$$

As already mentioned, we will focus on the secular part of the Hamiltonian $\langle H^{(\mathcal{O}2)}\rangle_{\boldsymbol{\lambda}}$: for such an Hamiltonian, the actions $\mathbf{L}$ are first integrals. We consider the basic approximation of the fast dynamics corresponding to quasi-periodic motions with an angular velocity vector equal to $\boldsymbol{n}^*$, by setting $\mathbf{L} = 0$.

Let us define

$$\begin{aligned}\widetilde{H} =& H^{(\mathcal{T}_F)} + \frac{1}{2}\left\{\chi_1^{(\mathcal{O}2)}, \mathcal{L}_{\chi_1^{(\mathcal{O}2)}} h_{2,0}^{(\mathrm{Kep})}\right\}_{\boldsymbol{L},\boldsymbol{\lambda}} \\ &+ \left\{\chi_1^{(\mathcal{O}2)}, \mu \sum_{\substack{s=0,\, j_2=0 \\ 2s+j_2\leqslant N_S}} D_2^s \tilde{h}_{s;1,j_2}^{(\mathcal{T}_F)}\right\}_{\boldsymbol{L},\boldsymbol{\lambda}} + \frac{1}{2}\left\{\chi_1^{(\mathcal{O}2)}, \mu \sum_{\substack{s=0,\, j_2=0 \\ 2s+j_2\leqslant N_S}} D_2^s \tilde{h}_{s;0,j_2}^{(\mathcal{T}_F)}\right\}_{\boldsymbol{\xi},\boldsymbol{\eta}},\end{aligned} \tag{2.2.16}$$

where $\{\cdot,\cdot\}_{\boldsymbol{L},\boldsymbol{\lambda}}$ and $\{\cdot,\cdot\}_{\boldsymbol{\xi},\boldsymbol{\eta}}$ are the terms of the Poisson bracket involving only the derivatives with respect to the variables $(\boldsymbol{L},\boldsymbol{\lambda})$ and $(\boldsymbol{\xi},\boldsymbol{\eta})$, respectively.

Then, according to Locatelli and Giorgilli (2000), we have that

$$\langle H^{(\mathcal{O}2)} \rangle_{\boldsymbol{\lambda}} \Big|_{\mathbf{L}=\mathbf{0}} = \langle \widetilde{H} \rangle_{\boldsymbol{\lambda}} \Big|_{\mathbf{L}=\mathbf{0}} + \mathcal{O}(\mu^3) \,.$$

We can finally introduce our secular model up to order two in the masses, by setting

$$H^{(\mathrm{sec2})}(D_2, \boldsymbol{\xi}, \boldsymbol{\eta}) = \left[\langle \widetilde{H} \rangle_{\boldsymbol{\lambda}} \Big|_{\mathbf{L}=\mathbf{0}} \right]_{(D_2, \boldsymbol{\xi}, \boldsymbol{\eta}) : 2N_S} , \tag{2.2.17}$$

where $\left[\langle \widetilde{H} \rangle_{\boldsymbol{\lambda}} \Big|_{\mathbf{L}=\mathbf{0}} \right]_{(D_2, \boldsymbol{\xi}, \boldsymbol{\eta}) : 2N_S}$ indicates the averaged expansion (over the fast angles $\boldsymbol{\lambda}$) of the part of $\widetilde{H}$ that is both independent from the actions $\mathbf{L}$ and truncated up to a total order of magnitude N_S in eccentricity and inclination. This means that a monomial $D_2^s \boldsymbol{\xi}^{\boldsymbol{m}_1} \boldsymbol{\eta}^{\boldsymbol{m}_2}$ is included in the truncation if and only if $2s + |\boldsymbol{m}_1| + |\boldsymbol{m}_2| \leqslant 2N_S$. By comparing (2.2.16) and (2.2.17), one can notice that our secular Hamiltonian model represented by $H^{(\mathrm{sec2})}$ does not depend on the second generating function $\chi_2^{(\mathcal{O}2)}$ whose explicit calculation is therefore unnecessary.

The explicit form of (2.2.17) writes

$$H^{(\mathrm{sec2})} = h_{1,1}^{(\mathrm{sec})} + \sum_{s=2}^{N_S} \sum_{l=1}^{s} D_2^{s-l} h_{s,l}^{(\mathrm{sec})} , \tag{2.2.18}$$

where $h_{s,l}$ is a homogeneous polynomial function of degree $2l$ in $\boldsymbol{\xi}$ and $\boldsymbol{\eta}$, for all $1 \leqslant l \leqslant s \leqslant N_S$. The even parity of the exponents is determined by the D'Alembert rules: having removed all the harmonics, the order in eccentricity that the terms must held is of the same parity of zero. The expansion of the final Hamiltonian $H^{(\mathrm{sec2})}$ presents terms in D_2, $\boldsymbol{\xi}$ and $\boldsymbol{\eta}$ up to a degree that is twice the one of the truncated expansions of $\chi_1^{(\mathcal{O}2)}$ as it is determined by (2.2.14): this is set to ensure that all the terms generated by the Poisson brackets in (2.2.16) are going to be taken into account. The secular Hamiltonian at order two in the masses is at the basis of the analytical approach developed in the next chapter to asses the stability of planetary systems by a reverse KAM method.

2.2.4 Stability of planetary systems

The first studies on the stability of planetary systems concerned obviously the Solar System. While they have been carried on since antiquity, the first main results are due to Lagrange and Laplace, who proved how the long-term variations of the planetary semi-major axis due to the mutual gravitational interactions vanish when considering only the first order in the masses. In later works, they showed that the eccentricities and inclinations of the planets of the Solar System experience only small variations of their values (see for example

Laskar (2012)). After that, Poincaré proved that the three-body problem is not integrable, thus stopping the search for exact solutions. Moving forward, the development of computers and algebraic manipulators allowed more precise and long-term numerical integrations, which revealed that the Solar System is chaotic, in the sense that a small modification in the initial conditions may lead to a drastic change in the evolution of the system. In Laskar (1989a) the Lyapunov time of the Solar System was estimated to be 5 million years. This result has been then confirmed by Sussman and Wisdom (1992).

Other definitions of the stability of a planetary system are present in the literature, especially for studies concerning extrasolar systems. The Hill stability for example prescribes that the orbits of the planets do not cross each other. This implies that the bodies of the system do not undergo close encounters or disruption. Some authors define the stability *in the astronomical sense*, considering the system stable whenever no merging or ejection of planets occur for the period of interest (possibly long, but finite), or when the evolution is robust against sufficiently small perturbations (see for example Lissauer (1999)). Recently, Laskar and Petit (2017) proposed a simplified criterion on the stability of quasi-planar systems, denoted AMD-stability and based on the computation of the angular momentum deficit. It appears clear that different definitions of the stability of a planetary systems can be used, depending on the context and the question to be solved.

In the present work we follow two different approaches to assess the stability of extrasolar systems. In Chap. 3 we study the stability in the KAM sense and define the system stable if it is possible to construct the Kolmogorov's normal form described in Sect. 2.1.2. This requires the convergence of the constructing algorithm and generally imposes strict requirements on the initial conditions. In Chap. 4 and in Chap. 5, we study the stability of planetary systems, by referring to the secular equilibria of the three-body problem, in particular the ones associated to the Lidov-Kozai resonance. Moreover, in Chap. 4 we complete our analysis on the whole parameter space by means of a chaos indicator, differentiating between stable periodic orbits, quasi-periodic (or close to stable periodic) orbits and chaotic orbits.

Part II

3D systems with low eccentricities

Chapter 3

A *reverse* KAM method

As previously discussed in Chap. 1, the orbital characteristics of the extrasolar systems detected so far are quite different from those of the Solar System. In this first approach, we intend to analyse the long-term evolution of detected exoplanets in a spirit similar to the classical studies of stability of the Solar System.

This chapter describes the methodology and the results presented in Volpi et al. (2018). This work has been developed in collaboration with Prof. Ugo Locatelli (Università degli studi di Roma "Tor Vergata") and Dr. Marco Sansottera (Università degli studi di Milano).

3.1 Motivation

Multiplanetary extrasolar systems raise new interesting challenges concerning the mathematical treatment of the orbital dynamics. For instance, in the Solar System the eccentricities of the celestial bodies play the role of small parameters in the power series expansions considered in classical perturbation theory. On the other hand, the eccentricities of the detected planets in extrasolar systems are often so large (see, e.g., Butler et al. (2006)) that they prevent the convergence of the Laplacian expansion of the disturbing function (see, e.g., Ferraz-Mello (1994)). Nevertheless, accurate analytical results based on classical expansions have been obtained even for systems having moderate to high eccentricities via high-order expansions (see, e.g., Libert and Henrard (2005) and Libert and Sansottera (2013)).

In Sect. 1.2.1 we mentioned the strengths and the observational biases of the RV method. Given its sensitivity to massive bodies, RV based observations

are expected to capture information about the *skeleton* of an extrasolar system, i.e., its major planets. As a main drawback, the RV method cannot detect the inclinations of the orbital planes with respect to the plane of the sky; moreover, its measure of the mass of each planet is affected by the uncertainty factor $\sin i$, being i the inclination of the orbital plane with respect to the tangent plane to the celestial sphere (see, e.g., Beaugé et al. (2012)). However, assuming that the detected systems are long-term stable (otherwise their observation would be an extremely rare event), ranges of the most probable values of the inclinations can be deduced by prescribing the long-time stability of the system. This is done for instance in Laskar and Correia (2009), where the properties of the numerically computed orbital motions are investigated by using the frequency analysis method (see Laskar (2003) and references therein for an introduction to this kind of numerical explorations).

We propose a novel procedure: a *reverse KAM approach* by using normal forms depending on a free parameter related to the unknown mutual inclinations between their orbital planes. Our approach is based on a careful adaptation of the algorithm constructing the Kolmogorov's normal form (see Sect. 2.1.2) for the secular part of the Sun–Jupiter–Saturn (SJS) system, as done for example in Locatelli and Giorgilli (2000). The differences between the two contexts are remarkable. In Locatelli and Giorgilli (2000) the parameters and the orbital elements of the SJS system were very well known; all these data were used to prove the existence of KAM tori confining the motion and, therefore, the stability of the secular model. Here, we deal with systems for which some of the orbital elements are unknown: we aim to infer information about their values by prescribing the stability and therefore requiring that the algorithm constructing KAM tori is convergent. Actually, from a practical point of view, its implementation is rather delicate. For instance, we use the interval arithmetic to represent the coefficients of the secular expansions; this allows us to consider sets of values of the free parameter in a comprehensive way instead of studying many different numerical integrations, each corresponding to a single value of that same parameter ranging in a suitably chosen discrete grid. Thus, our implementation is an interesting example of alternative use of validated numerics outside the context of a rigorous proof where it is often used (see, e.g., Celletti et al. (2000)). We emphasise that this is done by handling the difficulty due to the fact that the free parameter, related to the unknown mutual inclination, directly contributes to the so-called Laplace-Lagrange approximation (see, e.g., Libert and Sansottera (2013)). Therefore, it affects the secular frequencies possibly introducing dangerous resonance relations.

We think that our approach can interestingly complement some recent results: in particular, the concept of "AMD-stability" introduced in Laskar and Petit (2017) to analyse the dynamics of the multiplanetary extrasolar systems

(see also Petit et al. (2017) for an extension to the resonant case). Roughly, that criterion requires that the AMD (see definition in Sect. 2.2.2) is smaller than a critical threshold, in order to ensure that the planetary orbits cannot collide; therefore, the system is considered to be AMD-stable. In Laskar and Petit (2017) five planetary systems are recognised to belong to the so-called subcategory of "*hierarchical AMD-stable systems that are AMD-unstable but become AMD-stable when they are split into two parts*". Among them, the Solar System is a typical example when considering the two subsystems formed by the giant planets on one side and the inner ones on the other. We emphasise that AMD-stability of the giant planets is not sufficient to prove the global stability of the system as it does not provide a detailed enough information about the regularity of their motions. Indeed, it is well known that the chaoticity of the secular motions of the inner planets is induced by the gravitational perturbations due to Jupiter (see Laskar (1990)). Because of this chaoticity, it has been possible to select some scenarios (depicted by suitably chosen numerical integrations) leading to the ejection of Mercury or to destructive collisions between the terrestrial planets in a few billions of years (see Laskar (1989a) in the context of the secular dynamics and Laskar and Gastineau (2009), respectively). It is very natural to expect that these destabilising effects would act dramatically faster, if also the secular dynamics of the outer system was chaotic, instead of being extremely regular as it has shown to be (see, e.g., Laskar (1996)). A deeper knowledge of the dynamics of the outer planets is therefore crucial in order to prove the effective (or long-time) stability of the complete system. When a specific extrasolar system cannot be classified as AMD-stable but only hierarchical AMD-stable, the problem of ensuring its stability properties can be attacked by following a strategy that is based on our reverse KAM approach, as outlined below.

In the case of hierarchical AMD-stable systems, when successful, our approach can ensure that there are values of the inclinations for which the subsystem formed by the major planets is stable in a much stronger sense with respect to the AMD-criterion: the eventual diffusion would be so weak that the orbit could not significantly go away from a KAM torus before an extremely[1] long interval of time (see Giorgilli et al. (2017)). In such a situation, the motion of the biggest planets is indistinguishable from a quasi-periodic one. Such a preliminary result would be essential in order to prove (at least) the metastability of the less massive planets over times that are comparable with the expected lifetime of the system. This highlights the usefulness of our reverse KAM ap-

[1] Actually, when the mild hypotheses assumed in Morbidelli and Giorgilli (1995) are satisfied, the diffusion time is estimated to be super-exponentially big. This means that its order of magnitude is given by the exponential of the exponential of the inverse of a fractional power of the distance from a reference KAM torus.

proach.

We apply here the KAM-stability approach to three multiplanetary extrasolar systems, i.e. HD 1413199, HD 143761 and HD 40307 systems, that have low eccentricities and are far from mean-motion resonances. It should be noted that the two systems HD 141399 and HD 40307 have more than two planets. These systems were previously studied by Laskar and Petit (2017) and classified as hierarchical AMD-stable and AMD-unstable respectively. In order to achieve this classification, the authors defined an AMD-stability coefficient for every adjacent pair of planets, and from the different coefficients, derived the AMD-stability of the whole system. In the same spirit, we only focus here on a pair of adjacent planets and compare the results between the works. For the hierarchical AMD-stable HD 141399, we choose the two more massive planets c and d. For the AMD-unstable HD 40307, whose pairs of planets are all AMD-unstable, we select the two planets that have the smallest eccentricities (c and d). We stress that, for these two systems, no deduction on the stability of the whole system can be deduced from the present work.

This represents the first step in the direction of a complete proof of the so-called *effective stability* of such exoplanetary systems, when they are studied in the framework of models including all their already discovered planets (see Sansottera et al. (2013) for a recent application of these concepts to the secular dynamics of the Sun–Jupiter–Saturn–Uranus system). Of course, the whole implementation of our strategy is not priceless: the required amount of computations (mainly by the algebraic manipulations of the expansions) is extremely demanding.

3.2 Construction of invariant tori for the secular model

As already mentioned, our approach is based on a careful adaptation of that described in Locatelli and Giorgilli (2000). The expansion of the Hamiltonian in heliocentric Poincaré coordinates and in the parameter D_2 has been described in Sect. 2.2.2, while in Sect. 2.2.3 we have thoroughly detailed the construction of the secular Hamiltonian at order two in the masses. For completeness, we recall the final expression obtained:

$$H^{(\mathrm{sec2})} = h^{(\mathrm{sec})}_{1,1} + \sum_{s=2}^{N_S} \sum_{l=1}^{s} D_2^{s-l} h^{(\mathrm{sec})}_{s,l}, \tag{3.2.1}$$

where $h^{(\mathrm{sec})}_{s,l}$ is a homogeneous polynomial function of degree $2l$ in $\boldsymbol{\xi}$ and $\boldsymbol{\eta}$, for all $1 \leqslant l \leqslant s \leqslant N_S$.

3.2.1 Preliminary set up for the Kolmogorov algorithm

We will perform a series of preliminary transformations in order to obtain the most convenient formulation of our Hamiltonian for the construction of the invariant tori. Firstly, we will diagonalise the quadratic part of the Hamiltonian; secondly, we will transform the variables into an action-angle set; we will then proceed with a partial Birkhoff's normalisation, so as to remove the degeneration of the unperturbed Hamiltonian; finally, we will shift the origin of the actions so that they are centred around a value consistent with the observations. We will indicate with Roman numbers the intermediate Hamiltonians and generating functions necessary to determine the Hamiltonian $H^{(0)}$, that is suitable to start the Kolmogorov normalisation procedure.

It is well known that under mild assumptions on the quadratic part of the Hamiltonian which are satisfied in our case (see Sect. 3 of Biasco et al. (2006) where such hypotheses are shown to be generically fulfilled for a planar model of the Solar System), one can find a canonical transformation $(\boldsymbol{\xi},\boldsymbol{\eta}) = \mathcal{D}(\boldsymbol{x},\boldsymbol{y})$ with the following properties: (i) the map $(\boldsymbol{\xi},\boldsymbol{\eta}) = \big(\boldsymbol{\xi}(\boldsymbol{x}),\boldsymbol{\eta}(\boldsymbol{y})\big)$ is linear, (ii) $\mathcal{D}$ diagonalises the quadratic part of the Hamiltonian, so that we can write $h^{(\mathrm{sec})}_{1,1}$ in the new coordinates as $\sum_{j=1}^{2}\nu_j(x_j^2+y_j^2)/2$, where both the entries of the vector $\boldsymbol{\nu}$ have the same sign.

Action–angle variables are introduced via the canonical transformation

$$x_j = \sqrt{2I_j}\cos\phi_j\ , \qquad y_j = \sqrt{2I_j}\sin\phi_j\ , \qquad j=1,2\ . \tag{3.2.2}$$

With these two last changes of coordinates the Hamiltonian (3.2.1) takes the form

$$H^{(\mathrm{I})}(\boldsymbol{I},\boldsymbol{\phi}) = \boldsymbol{\nu}\cdot\boldsymbol{I} + \sum_{s=2}^{\infty}\sum_{l=1}^{s} D_2^{s-l} h^{(\mathrm{I})}_{s;l}(\boldsymbol{I},\boldsymbol{\phi})\ , \tag{3.2.3}$$

where $h^{(\mathrm{I})}_{s;l}$ is an homogeneous polynomial function of degree $2l$ in the square roots of actions $\boldsymbol{I}$ and a trigonometric polynomial of degree $2s$ in the angles $\boldsymbol{\phi}$, i.e., it writes

$$h^{(\mathrm{I})}_{s,l}(\boldsymbol{I},\boldsymbol{\phi}) = \sum_{i_1+i_2=2l}\ \sum_{j_1=0}^{i_1}\sum_{j_2=0}^{i_2} c^{(\mathrm{I})}_{s;i_1,i_2;j_1,j_2}\sqrt{I_1^{i_1}I_2^{i_2}}\cos\big[(i_1-2j_1)\phi_1+(i_2-2j_2)\phi_2\big]. \tag{3.2.4}$$

In the previous formula only cosines occur because of the parity relation due to the d'Alembert rules.

Let us stress that our aim is to provide ranges of inclinations which are compatible with the stability of the system. These intervals of values are obtained as a function of the parameter D_2. Thus it is crucial to keep D_2 as a parameter in the Hamiltonian expansion as long as possible. We now proceed

with a partial Birkhoff's normalisation in order to remove the degeneration of the unperturbed Hamiltonian (as we previously mentioned in Sect. 2.1.2). We can visualise the Hamiltonian (3.2.3) as

$$H^{(\mathrm{I})}(\boldsymbol{I},\boldsymbol{\phi}) = \sum_{\boldsymbol{\nu}\cdot\boldsymbol{I}} \begin{matrix} \\ \\ \\ \\ D_2\, h^{(\mathrm{I})}_{2;1} \end{matrix} \begin{matrix} \\ \\ \\ h^{(\mathrm{I})}_{2;2} \\ D_2\, h^{(\mathrm{I})}_{3;1} \end{matrix} \begin{matrix} \\ \\ h^{(\mathrm{I})}_{3;3} \\ D_2\, h^{(\mathrm{I})}_{3;2} \\ D_2^2\, h^{(\mathrm{I})}_{4;1} \end{matrix} \begin{matrix} \\ h^{(\mathrm{I})}_{4;4} \\ D_2\, h^{(\mathrm{I})}_{4;3} \\ D_2^2\, h^{(\mathrm{I})}_{4;2} \\ D_2^3\, h^{(\mathrm{I})}_{4;1} \end{matrix} \begin{matrix} \ddots \\ \dots \\ \dots \\ \dots \\ \dots \end{matrix} . \tag{3.2.5}$$

This writing highlights two features of each term: the size of the perturbation in eccentricity and inclination is determined by the columns; the degree in actions depends on the rows. Our aim is then to remove the dependency on the angle variables up to the third column. We determine the first two generating functions by solving the two homological equations

$$\{\mathcal{B}^{(\mathrm{II})}_1, \boldsymbol{\nu}\cdot\boldsymbol{I}\} - D_2\, h^{(\mathrm{I})}_{2;1} = D_2 Z_{2;1} \tag{3.2.6}$$

and

$$\{\mathcal{B}^{(\mathrm{II})}_2, \boldsymbol{\nu}\cdot\boldsymbol{I}\} - h^{(\mathrm{I})}_{2;2} = Z_{2;2}\,, \tag{3.2.7}$$

where $Z_{s;l}$ is the average of $h^{(\mathrm{I})}_{s;l}$ over the angles $\boldsymbol{\phi}$.

The transformed Hamiltonian is computed as

$$H^{(\mathrm{II})} = \exp\mathcal{L}_{\mathcal{B}^{(\mathrm{II})}_2} \circ \exp\mathcal{L}_{\mathcal{B}^{(\mathrm{II})}_1} H^{(\mathrm{I})}\,. \tag{3.2.8}$$

Let us stress that $\exp\mathcal{L}_{\mathcal{B}^{(\mathrm{II})}_1} H^{(\mathrm{I})}$ does not produce any contribution to the term $h^{(\mathrm{I})}_{2;2}$: this justifies the term appearing in (3.2.7) for the generating function. At this point, all the terms up to order 4 in eccentricity and inclination do not depend on the fast angles and the Hamiltonian reads

$$H^{(\mathrm{II})}(\boldsymbol{I},\boldsymbol{\phi}) = \boldsymbol{\nu}\cdot\boldsymbol{I} + D_2\, Z_{2;1}(\boldsymbol{I}) + Z_{2;2}(\boldsymbol{I}) + \sum_{s=3}^{\infty}\sum_{l=1}^{s} D_2^{s-l} h^{(\mathrm{II})}_{s;l}(\boldsymbol{I},\boldsymbol{\phi})\,. \tag{3.2.9}$$

Analogously, we compute the generating functions $\mathcal{B}^{(\mathrm{III})}_1$, $\mathcal{B}^{(\mathrm{III})}_2$, $\mathcal{B}^{(\mathrm{III})}_3$ in order to eliminate the dependency on the angle variables of the terms of order 6 in eccentricity and inclinations. Finally, our Hamiltonian is computed as

$$H^{(\mathrm{III})} = \exp\mathcal{L}_{\mathcal{B}^{(\mathrm{III})}_3} \circ \exp\mathcal{L}_{\mathcal{B}^{(\mathrm{III})}_2} \circ \exp\mathcal{L}_{\mathcal{B}^{(\mathrm{III})}_1} H^{(\mathrm{II})}\,. \tag{3.2.10}$$

The last preliminary transformation of the Hamiltonian consists in a translation of the actions. Being the action vector $\boldsymbol{I}$ nearly constant, i.e., $\boldsymbol{I}(t) \simeq \boldsymbol{I}(0)$, we shift the origin of the action about $\boldsymbol{I}(0) = \boldsymbol{I}^*$. This is done using a canonical transformation $\mathcal{T}(\boldsymbol{I}, \boldsymbol{\phi}) = (\boldsymbol{p} + \boldsymbol{I}^*, \boldsymbol{q})$. The transformed Hamiltonian is given by

$$H^{(0)}(\boldsymbol{p}, \boldsymbol{q}) = H^{(\mathrm{III})} \circ \mathcal{T}(\boldsymbol{I}, \boldsymbol{\phi}) \,.$$

3.2.2 Formal construction of the Kolmogorov invariant tori

We will now proceed with the construction of the Kolmogorov invariant tori. Firstly, we compute the expansion of Hamiltonian $H^{(0)}$, that can be visually arranged as

$$H^{(0)}(\boldsymbol{p}, \boldsymbol{q}) = \sum \begin{array}{ccccccc} \vdots & & \vdots & \vdots & \vdots & \vdots & \vdots \\ f_2^{(0,0)(\boldsymbol{p})} & & f_2^{(0,1)}(\boldsymbol{p}, \boldsymbol{q}) & \dots & f_2^{(0,s)}(\boldsymbol{p}, \boldsymbol{q}) & \dots & \\ \boldsymbol{\omega}^{(0)} \cdot \boldsymbol{p} & & f_1^{(0,1)}(\boldsymbol{p}, \boldsymbol{q}) & \dots & f_1^{(0,s)}(\boldsymbol{p}, \boldsymbol{q}) & \dots & , \\ 0 & & f_0^{(0,1)}(\boldsymbol{q}) & \dots & f_0^{(0,s)}(\boldsymbol{q}) & \dots & \end{array} \tag{3.2.11}$$

being the generic term $f_j^{(0,s)} \in \mathcal{P}_{j,2s}$: this means that it is a homogeneous polynomial of degree j in the actions $\boldsymbol{p}$ and a trigonometric polynomial of degree $2s$ in $\boldsymbol{q}$. In order to adopt the classical notation of the Kolmogorov theorem, we renamed the frequencies $\boldsymbol{\nu}$ appearing in Sect. 3.2.1 as $\boldsymbol{\omega}$.

There is a striking difference between the visual schemes (3.2.5) and (3.2.11): in the latter, we do not keep track of the expansions in powers of D_2. This is due to the fact that, in the explicit applications, we replace the parameter D_2 with convenient intervals of values. In Sect. 3.3 we will discuss in more detail this technical point, that is not essential for the comprehension of the normalisation scheme.

Let us emphasise that the parameter $\boldsymbol{I}^*$ plays a key role in the convergence of the expansion. As it is discussed in Locatelli and Giorgilli (2000) and Giorgilli et al. (2017), the size of the term $f_j^{(0,s)}$ has an upper bound that is i) of order $\|\boldsymbol{I}^*\|^s$ and ii) inversely proportional to the l-th power of the minimum component of the vector $\boldsymbol{I}^*$. Therefore the parameter $\boldsymbol{I}^*$ rules the convergence of the series with respect to the index s; according to the definitions in the previous sections, it is a small quantity because $\boldsymbol{I}^*$ is quadratic in eccentricities or inclinations.

The Kolmogorov's normalisation algorithm requires to remove the dependency on the angle variables of all the terms of the Hamiltonian (3.2.11) of degree 0 or 1 in the actions $\boldsymbol{p}$. In order to do that, we start by determining the

generating function $\chi_1^{(1)}$ such that

$$\{\chi_1^{(1)}, \boldsymbol{\omega}^{(0)} \cdot \boldsymbol{p}\} + f_0^{(0,1)} = 0\,, \tag{3.2.12}$$

where $\chi_1^{(1)}$ is a trigonometric polynomial of degree 2.

We will then obtain a new Hamiltonian

$$\hat{H}^{(1)} = \exp \mathcal{L}_{\chi_1^{(1)}} H^{(0)}\,, \tag{3.2.13}$$

whose generic term of the expansion is $\hat{f}_j^{(1,s)} \in \mathcal{P}_{j,2s}$. As a consequence of equation (3.2.12), we have that $\hat{f}_0^{(1,1)} = 0$.

We proceed in an analogous way to complete this first Kolmogorov's normalisation step: we compute the generating function $\chi_2^{(1)}(\boldsymbol{p}, \boldsymbol{q})$ such that

$$\{\chi_2^{(1)}, \boldsymbol{\omega}^{(0)} \cdot \boldsymbol{p}\} + \hat{f}_1^{(1,1)} = \langle \hat{f}_1^{(1,1)} \rangle_{\boldsymbol{q}}\,; \tag{3.2.14}$$

then, $\chi_2^{(1)}$ will be linear in $\boldsymbol{p}$ and of order 2 in $\boldsymbol{q}$. Let us stress that it is possible to solve the previous homological equations (3.2.12) and (3.2.14), provided that $|\boldsymbol{k} \cdot \boldsymbol{\omega}^{(0)}| > 0$ for $\boldsymbol{k} \in \mathbb{Z}_2$ with $|\boldsymbol{k}| = 1, 2$, being $|\boldsymbol{k}| = |k_1| + |k_2|$.

Therefore, we will obtain the new Hamiltonian $H^{(1)} = \exp \mathcal{L}_{\chi_2^{(1)}} \hat{H}^{(1)}$, whose generic term is now $f_j^{(1,s)} \in \mathcal{P}_{j,2s}$. In the following it lies a profound difference with respect to previous works (see for example Locatelli and Giorgilli (2000)): due to the way $\chi_2^{(1)}$ was determined, we have that

$$f_1^{(1,1)} = \hat{f}_1^{(1,1)} + \mathcal{L}_{\chi_2^{(1)}} \boldsymbol{\omega}^{(0)} \cdot \boldsymbol{p} = \langle \hat{f}_1^{(1,1)} \rangle_{\boldsymbol{q}}\,. \tag{3.2.15}$$

Therefore, $f_1^{(1,1)}$ is an homogeneous polynomial of degree 1 in $\boldsymbol{p}$ and independent from $\boldsymbol{q}$: hence, it shares the same functional properties of the term $\boldsymbol{\omega}^{(0)} \cdot \boldsymbol{p}$. We then set for appropriate values of $\boldsymbol{\omega}^{(1)}$

$$\boldsymbol{\omega}^{(1)} \cdot \boldsymbol{p} = \boldsymbol{\omega}^{(0)} \cdot \boldsymbol{p} + \langle \hat{f}_1^{(1,1)} \rangle_{\boldsymbol{q}}\,, \tag{3.2.16}$$

hence changing the frequency vector associated to the searched invariant tori. Let us note that a slightly different scheme could be implemented. The standard approach would fix the value of the frequencies $\boldsymbol{\omega} = \boldsymbol{\omega}^{(0)}$, thus requiring a different definition of the generating functions. We plan to follow this strategy and compare the results provided by the two different approaches in the future.

The generic r-th normalisation step is performed in the same way provided that the following non-resonance condition holds true:

$$|\boldsymbol{k} \cdot \boldsymbol{\omega}^{(r-1)}| > 0\ , \qquad \forall\ \boldsymbol{k} \in \mathbb{Z}_2 \backslash \{\boldsymbol{0}\} \text{ with } |\boldsymbol{k}| \leqslant 2r\ . \tag{3.2.17}$$

One can start from an expansion of the Hamiltonian $H^{(r-1)}$ of the same form as in (3.2.11), where the upper index 0 is replaced by $r-1$. Hence, the generating functions $\chi_1^{(r)}$, $\chi_2^{(r)}$ are introduced by solving the homological equations obtained by replacing the upper index 1 with r in formulas (3.2.12) and (3.2.14).

The new Hamiltonian is therefore given by

$$H^{(r)} = \exp \mathcal{L}_{\chi_2^{(r)}} \hat{H}^{(r)} \quad \text{with} \quad \hat{H}^{(r)} = \exp \mathcal{L}_{\chi_1^{(r)}} H^{(r-1)} . \tag{3.2.18}$$

In order to better understand the ultimate goal of this algorithm constructing invariant tori, let us suppose to be able to iterate it *ad infinitum*. We would end up with a Hamiltonian of the form

$$H^{(\infty)}(\boldsymbol{p}, \boldsymbol{q}) = \boldsymbol{\omega}^{(\infty)} \cdot \boldsymbol{p} + \mathcal{O}(\|\boldsymbol{p}\|^2) . \tag{3.2.19}$$

Writing the equations of motion derived from the previous Hamiltonian, it appears evident that the torus $\{\boldsymbol{p} = \boldsymbol{0}\,,\ \boldsymbol{q} \in \mathbb{T}^2\}$ is invariant.

3.3 Parametric study on the D_2 parameter

By borrowing the techniques used in Giorgilli et al. (2014) to ensure the existence of elliptic tori for planetary systems, one could prove the convergence of the algorithm described in the previous section under very general conditions. In practice, this means that: (i) the perturbation (ruled by $\boldsymbol{I}^*$) is small enough; (ii) the Hessian of the main quadratic term $f_2^{(0,0)}(\boldsymbol{p})$ is non-degenerate; (iii) the initial frequencies $\boldsymbol{\omega}^{(0)}$ belong to a suitable set having non-zero Lebesgue measure.

Here we do not investigate theoretically the convergence of the algorithm that is instead numerically analysed. In the spirit of a *reverse KAM approach*, we claim that some initial conditions originate motions that are inside a stable region when the convergence is evident from a numerical point of view.

We want to investigate the stability of extrasolar planetary systems for the widest possible ranges of D_2 (i.e., mutual inclinations) and we want to take into account the uncertainties on other orbital elements due to the observational limitations. Therefore, we have found convenient to represent the coefficients of the expansions of the Hamiltonian with intervals. Let us emphasise that such an approach based on interval arithmetic allows us to cover completely a set of values of the orbital elements. This provides a key advantage to the normal form approach with respect to the explorations purely based on numerical integrations. In fact, when dealing with numeric parametrical analysis the latter methods require to consider grids of values of the initial conditions; moreover, the synthetic coverage provided by the normal form approach (implemented with interval arithmetic) is not possible.

When dealing with the proof of any KAM-type statement, it is essential to establish an iterative scheme of estimates producing suitable majorants. The ultimate goal of such a scheme is proving that the norms of the two sequences of generating functions (i.e., $\chi_1^{(r)}$ and $\chi_2^{(r)}$ in our settings) decrease exponentially. Therefore, when such a behaviour is met in the plot of the norms of the generating functions, this is the clear signature of the existence of invariant KAM tori. In the case of a forced pendulum Hamiltonian model (see Celletti et al. (2000)), the study of the behaviour of $\chi_2^{(r)}$ succeeded in extrapolating a good approximation of the breakdown of the golden ratio invariant torus. As previously discussed, the existence of KAM tori implies the long-time stability of the dynamics in a region surrounding them. Therefore, this argument ensures that the stability in KAM sense is firmly related to the convergence of the generating functions.

To fix the ideas, let us consider the specific case of the extrasolar multiplanetary system HD 40307, whose orbital parameters are reported in Tab. 3.1. The plots of the norms of the generating functions $\chi_2^{(r)}$ are shown in Fig. 3.1 for two different ranges of values of the parameter D_2. The norm $\|\chi_2^{(r)}\|$ is nothing but the sum of the absolute values of the coefficients of the terms appearing in its expansion. We decide to focus on the behaviour of $\chi_2^{(r)}$ instead of the one of $\chi_1^{(r)}$ because we observed that the former ones are bigger than the latters. On the top panel of Fig. 3.1, for D_2 values in the range $[0.0164, 0.0564]$ we can appreciate that the decrease of $\|\chi_2^{(r)}\|$ is sharp and quite regular; we associate this behaviour to the convergence of the algorithm. Often the algorithm crashes because the coefficients in the expansions of the Hamiltonians inflate to the point where the non-resonant condition (3.2.17) is not satisfied anymore. By comparison, the decrease of the norms in the plot on the bottom of Fig. 3.1, for D_2 values in the range $[0.0814, 0.0864]$, is notably slower than the one on the top; for instance, the norm of the last computed generating function on the bottom is 6 orders of magnitude bigger than the corresponding on the top.

Obviously we aim to automatise the identification of the converging procedures to avoid a visual inspection for each specific instance. Having fixed the maximal normalisation order at $\bar{r} = 33$, in our codes the non-convergence is established if at least one of the following tests is true:

1. the ratio $\|\chi_2^{(r)}\| / \|\chi_2^{(1)}\|$ is greater than 0.9^{r-1} for some r;
2. the norm $\|\chi_2^{(\bar{r})}\|$ is greater than $10^{-9} \|\chi_2^{(1)}\|$.

Otherwise, we consider that the algorithm might be iterated *ad infinitum*, so to ensure the existence of the KAM tori.

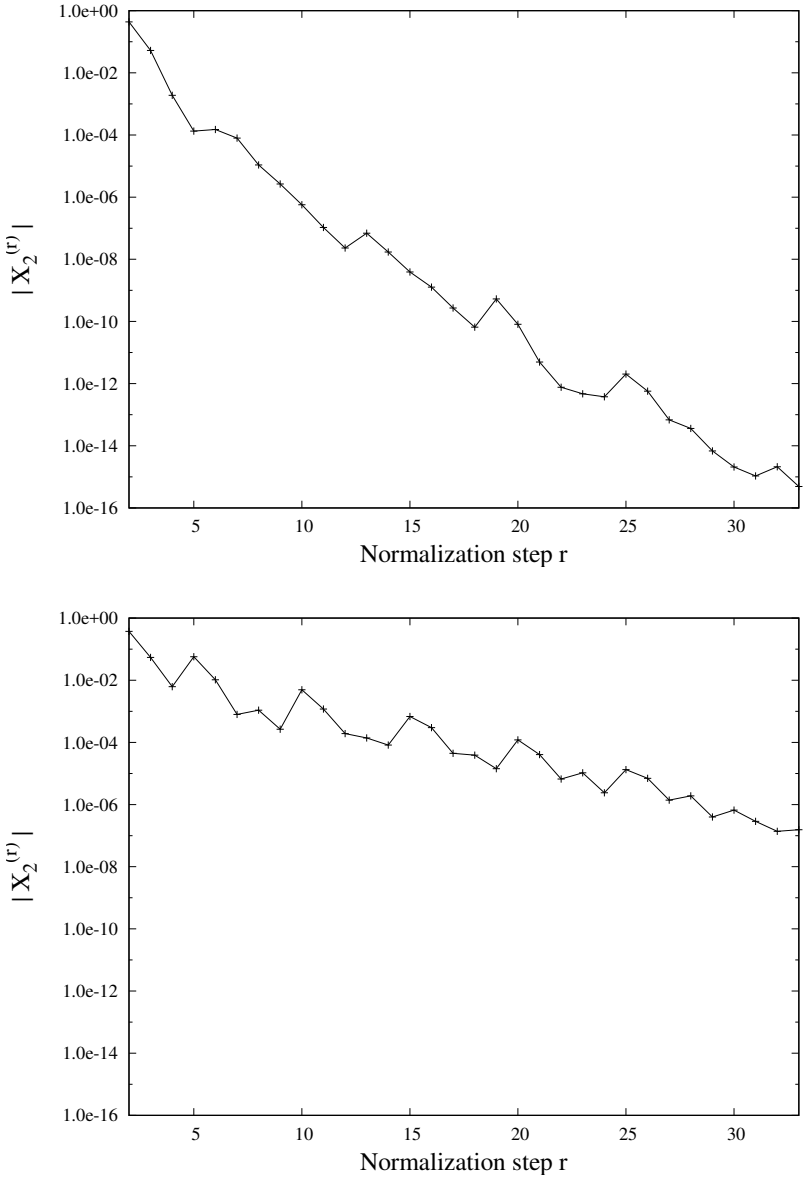

Figure 3.1 – Results relative to HD 40307. Behaviour of the norms of the generating functions $\chi_2^{(r)}$ as a function of the normalisation step r. On the top, for values of $D_2 \in [0.0164, 0.0564]$. On the bottom for values of $D_2 \in [0.0814, 0.0864]$. The orbital parameters of the system are listed in Tab. 3.1.

3.4 Results

In this section, we explicitly apply our approach to the three selected extrasolar systems described in Sect. 3.1. In Tab. 3.1 we report the orbital parameters of the systems considered: for simplicity in the following we use as planetary masses the minimal ones listed there.

System	Planet	$m \sin i$ $[M_J]$	M_{Star} $[M_\odot]$	a [AU]	e	ω [°]
HD 141399	c	1.33	1.14	0.704	0.048 ± 0.009	220 ± 40
	d	1.18		2.14	0.074 ± 0.025	220 ± 30
HD 143761	b	1.045	0.99	0.228	0.037 ± 0.004	270.6 ± 6
	c	0.079		0.427	0.050 ± 0.004	175 ± 125
HD 40307	c	0.0202	0.77	0.081	0.060 ± 0.005	234 ± 1
	d	0.0275		0.134	0.070 ± 0.005	170 ± 10

Table 3.1 – Orbital parameters of the systems considered to apply the computational algorithm for the parametric study on D_2. For each column the unit of measure is reported in square brackets. The angle i refers to the inclination of the orbital plane with respect to the line of sight.

For the sake of completeness, we detail some of the parameters ruling the *finite size* of the expansions of the Hamiltonians introduced in our formal algorithm (Sect. 3.2). In Tab. 3.2 we list the values of the integer parameters K_F and N_S and the mean-motion resonance that is considered to play the major role in the perturbation of the non-resonant fast dynamics. Let us recall that K_F gives the limitation on the generating function $\chi_1^{(\mathcal{O}2)}$ that is needed to construct the approximation at order 2 in the masses; moreover, N_S fixes the maximal order in $e^2 + i^2$ for the secular Hamiltonian $H^{(\mathrm{sec2})}$ (see Sect. 2.2.3). The series appearing in Eq. (3.2.3) and defining $H^{(\mathrm{I})}$ is truncated at the final value $s = 15$; the same limitation is imposed on the expansions of $H^{(\mathrm{II})}$ and $H^{(\mathrm{III})}$. Finally, the maximal degree in the actions $\boldsymbol{p}$ is fixed at 4 for the expansions of all the Hamiltonians $H^{(r)}$ involved in the normalisation up to order $\bar{r} = 33$.

In Fig. 3.2 we present two plots relative to HD 141399. On the top, we show the True/False output which results from the tests on the convergence described in Sect. 3.3: to each value of the parameter D_2 we assign 1 if the system is convergent, 0 otherwise. On the bottom, we show the plot of the mutual inclination as the function of the parameter D_2 described by relation (2.2.9).

System	Nearest resonance	K_F	N_S
HD 141399	5 : 1	12	8
HD 143761	5 : 2	8	6
HD 40307	2 : 1	6	8

Table 3.2 – Nearest resonance and values of the integer parameters K_F and N_S (as described in Section 2.2.3) for each system.

By means of the interval arithmetic, we can take into account the observational errors on the orbital parameters of the system, e.g., the eccentricities (as shown in Tab. 3.1). Therefore, for each value of the parameter D_2 we obtain a range of values for the mutual inclination. For this reason, in all the plots concerning the mutual inclination (right of Fig. 3.2 and Fig. 3.3) a central value with error-bars is drawn on the y coordinate. In Fig. 3.3, we show the results for the systems HD 143761 (top panel) and HD 40307 (bottom panel). The behaviour of the mean value of the mutual inclinations is mainly due to relation (2.2.9). The jump observed in the thick lines of the plots can be related to numerical reasons. As negative values of the mutual inclination are not acceptable, the error bars are smoothed so to never include values below the zero. The jump occurs at the first value of D_2 such that the error bars do not need to be corrected anymore.

We can summarise the results provided by our implementation of the Kolmogorov's normalisation scheme as follows: the systems HD 141399, HD 143761 and HD 40307 are stable in the KAM sense, for mutual inclinations up to 18°, 10° and 15°, respectively. In this context, if we would have taken into account the magnifying factor $1/\sin i_j$ for the mass of the j-th planet, we expect that the previous maximal mutual inclinations would be slightly lower, except in the extreme case in which i_j are close to zero. Indeed, the main impact of considering larger masses would be increasing the size of the correcting terms of order two in the masses with respect to those of order one in the secular Hamiltonian $H^{(\mathrm{sec})}$.

3.5 Conclusions and perspectives

Up to our knowledge, this is the first application to extrasolar planetary systems of an explicit algorithm constructing KAM tori. As it is discussed in the previous sections, actually we have not applied a statement of the KAM theorem. Instead, we have exploited a keystone of the proof, i.e., the study of the convergence of the generating functions. In this respect we can say that our

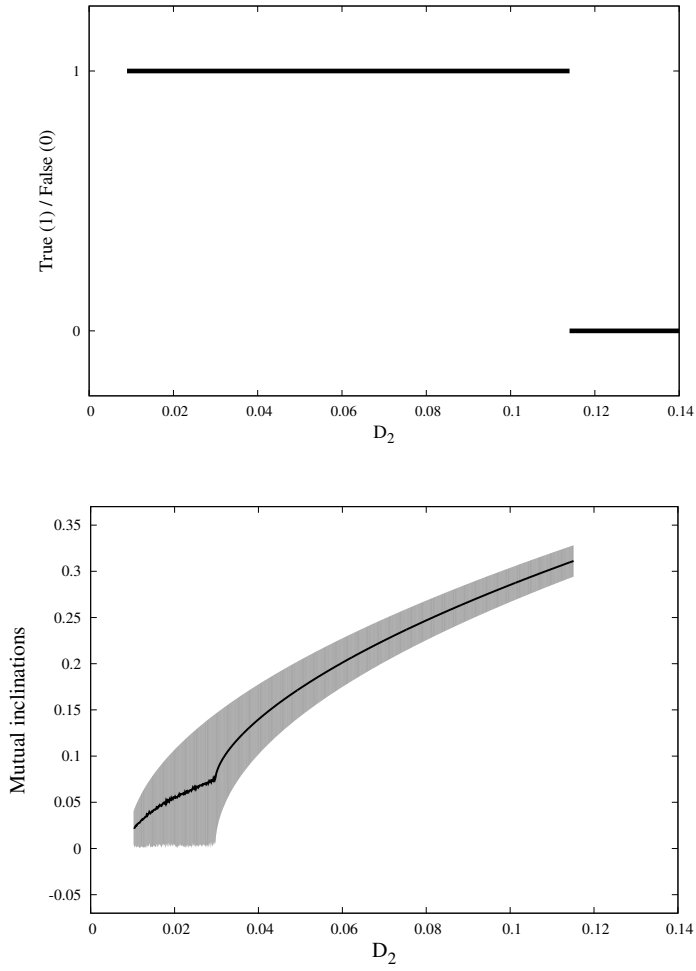

Figure 3.2 – Results relative to HD 141399. On the top, the True/False output regarding the convergence of the algorithm. On the bottom, the range of values of the mutual inclination (in radians), where the thick line represents the mean value of the inclination interval. Both the plots are drawn as functions of the parameter D_2.

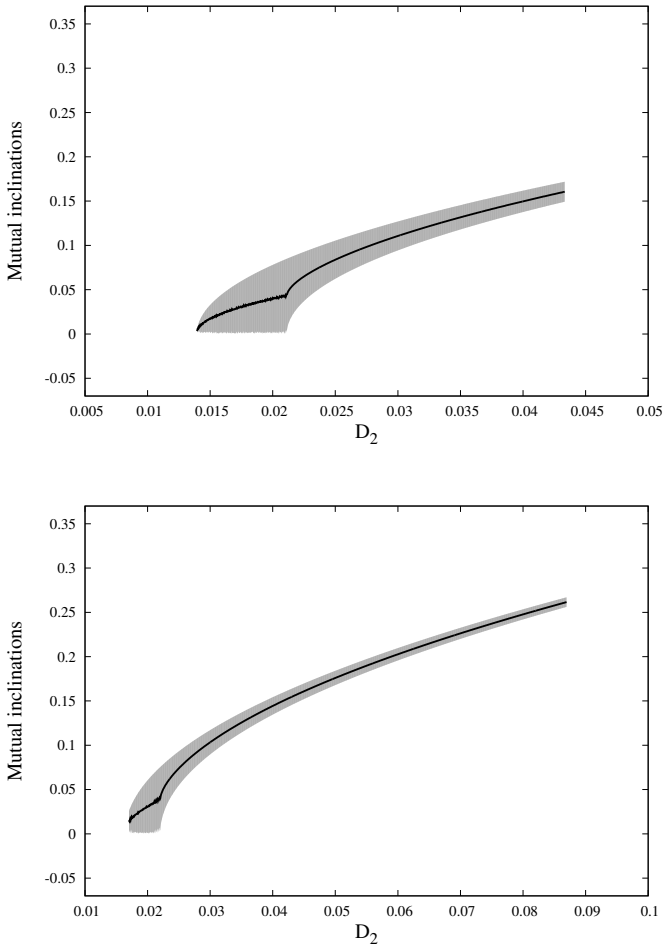

Figure 3.3 – Plots of the mutual inclination as a function of the parameter D_2. On the top, the results relative to HD 143761. On the bottom, those for HD 40307.

approach is computer aided: the norms of some of the initial generating functions are evaluated after having explicitly calculated their expansions, instead of being analytically estimated. The eventual convergent character of the constructing algorithm in its entirety is inferred by the behaviour of said norms. Our results should legitimately be included in the list of the applications of KAM theory to realistic physical models (see, e.g., Celletti (1994); Celletti and Chierchia (2007); Gabern et al. (2005)). In fact, for what concerns the tori that are invariant with respect to the secular Hamiltonian and characterised by the complete circulation of the arguments of the pericenters, the values of the mutual inclinations for which the Lidov-Kozai resonant region takes place can be considered as a natural upper limit[2]. In extrasolar systems such a critical value of the mutual inclinations is usually located at about 40° (see, e.g., Libert and Tsiganis (2009)). Therefore, for the three systems here considered, our results about the stability in the KAM sense cover a set of values whose extension ranges between 25% and 50% of the Lidov-Kozai limit. The inclusion of the Lidov-Kozai resonance region will be the subject of the next chapter.

We shall now point out the weaknesses of our approach. Our constructing algorithm does not work when the eccentricities of the planets are not small. In fact, the procedure has generated divergent series when it has been applied to the systems HD 109271, HD 155358 and HD 4732; in all of them there is at least one of the planets whose eccentricity is between 0.1 and 0.25. Thus, it seems that our approach is limited to systems with planetary eccentricities smaller than 0.1. Since we are able to produce results for small inclinations of the major planets of the systems, the ideal situation is very similar to that of the Solar System. This is not surprising, since the whole approach has been adapted from the one described in Locatelli and Giorgilli (2000), which in turn has been tailored to the Jovian planets. In particular, the series expansion of the three-body planetary Hamiltonian is in power series of some coordinates and parameters that are of the same order of the eccentricities and the inclinations.

A natural goal for the future would be to remove the limitations affecting the approach described in this work. We think that some of them are intrinsic in the definition of stability that we assumed. Actually, since the beginning we postulated that the motions of the major planets are quasi-periodic and their orbits lie on KAM tori constructed with expansions in small eccentricities and inclinations. Such a prescription is extremely strict. In our opinion, any

[2]In the Laplace plane frame, the region of the Lidov-Kozai resonance is characterised by the libration of the argument of the pericenter of the inner planet. The implicit adoption of such a frame has been essential in order to perform the reduction of the angular momentum sketched in Sect. 2.2.2. Therefore, the comparison between our results and those for that resonant region is valid because also our Hamiltonian model is written in the secular canonical coordinates with respect to the Laplace plane.

substantial improvement of the method will be based on a clever weakening of this assumption. This should be done by identifying a suitable integrable approximation of the secular dynamics that can be shown to be convergent even for large eccentricities. In the very different context of the orbits of the Trojan bodies, this change of attitude has been shown to produce substantial enhancements (see Páez and Locatelli (2015); Páez et al. (2016)). In future works, we plan to extend this kind of ideas to the problem of determining values of the inclinations consistent with (a suitable type of) stability.

Part III

3D systems with moderate to high eccentricities

Chapter 4

Lidov-Kozai resonance and stability

In this chapter, we propose a second approach to study the long-term stability of extrasolar systems. The differences with the previous approach based on the KAM theory are noticeable.

This chapter describes the methodology and the results presented in Volpi et al. (2019).

4.1 Motivation

Firstly, with the reverse KAM approach (see Chap. 3) we focused our parametric study on the mutual inclination between the planets. For what concerns the masses of the planets, we took the minimal values provided by the observations (see Sect. 1.2.1). In the second approach we consider a more realistic view of extrasolar systems, since we also take into account different values of the inclination i of the orbital planes with respect to the line of sight. This implies considering different values of the masses of the planets. It also means that we will have to handle a higher number of parameters in the study.

Secondly, as discussed in Chap. 2 we should carefully differentiate the meaning of the term "stability". In the framework of extrasolar planetary problems, we say that a system is stable *in a KAM sense* whenever the algorithm for the construction of the invariant tori converges (as per Sect. 3.1). We should consider that the implementation of the algorithm intrinsically restrains the subset of the parametric space for which the convergence is guaranteed. In other words, the normalisation scheme is highly demanding in terms of require-

Table 4.1 – Orbital parameters of the selected systems.

System		$m \sin i\,(M_J)$	$M_{\rm Star}\,(M_\odot)$	a	e	ω	References
HD 11506	b	3.44	1.19	2.43	0.22	257.8	Tuomi and Kotiranta (2009)
	c	0.82		0.639	0.42	234.9	
HD 12661	b	2.3 ($\pm$0.19)	1.07	0.831 ($\pm$0.048)	0.378 ($\pm$0.0077)	296 ($\pm$1.5)	Wright et al. (2009)
	c	1.57 ($\pm$0.07)		2.56 ($\pm$0.17)	0.031 ($\pm$0.022)	165 ($\pm$0.0)	
HD 134987	b	1.59	1.07	0.81	0.233	252.7	Jones et al. (2010)
	c	0.82		5.8	0.12	195	
HD 142	b	1.25 ($\pm$0.15)	1.1	1.02 ($\pm$0.03)	0.17 ($\pm$0.06)	327 ($\pm$26)	Wittenmyer et al. (2012)
	c	5.3 ($\pm$0.7)		6.8 ($\pm$0.5)	0.21 ($\pm$0.07)	250 ($\pm$20)	
HD 154857	b	2.24	1.718	1.291	0.46	57	Wittenmyer et al. (2014)
	c	2.58		5.36	0.06	32	
HD 164922	b	0.3385	0.874	2.115	0.126	129	Fulton et al. (2016)
	c	0.0406		0.3351	0.22	81	
HD 169830	b	2.88	1.4	0.81	0.31	148	Mayor et al. (2004)
	c	4.04		3.6	0.33	252	
HD 207832	b	0.56	0.94	0.57	0.13	130.8	Haghighipour et al. (2012)
	c	0.73		2.112	0.27	121.6	
HD 4732	b	2.37	1.74	1.19	0.13	35	Sato et al. (2013)
	c	2.37		4.6	0.23	118	
HD 74156	b	1.778	1.24	0.2916	0.638	175.35	Feng et al. (2015)
	c	7.997		3.82	0.3829	268.9	

ments that the initial conditions have to satisfy (as it is discussed in Sect. 3.5). The stability concept as intended from now on, however, is different. Without undergoing the process to construct the KAM tori (and thus requiring the convergence of the constructing algorithm), we mean to determine the 3D configurations whose associated orbit is regular, and we will provide an analytical comprehension of the results in terms of the stable equilibria of the secular Hamiltonian formulation.

A few studies on the dynamics of extrasolar systems have been devoted to the 3D problem. Analytical works of Michtchenko et al. (2006), Libert and Henrard (2007), and Libert and Henrard (2008) investigated the secular evolution of 3D exosystems which are not in a mean-motion resonance. They showed that mutually inclined planetary systems can be long-term stable. In particular, these works focused on the analysis of the equilibria of the 3D planetary three-body problem, showing the generation of stable Lidov-Kozai (LK) equilibria (Lidov (1962), Kozai (1962)) through bifurcation from a central equilibrium, which itself becomes unstable at high mutual inclination. Thus, around the stability islands of the LK resonance, which offers a secular phase-protection mechanism and ensures the stability of the system, chaotic motion of the planets occurs, limiting the possible 3D configurations of planetary systems.

Using n-body simulations, Libert and Tsiganis (2009) investigated the possibility that five extrasolar two-planet systems, namely υ Andromedae, HD 12661, HD 169830, HD 74156 and HD 155358, are actually in a LK-resonant state for mutual inclinations in the range $[40^\circ, 60^\circ]$. They showed that the physical and orbital parameters of four of the systems are consistent with a LK-type orbital motion, at some specific values of the mutual inclination, while around $30\% - 50\%$ of the simulations generally lead to chaotic motion. The work also suggests that the extent of the LK-resonant region deeply varies for each planetary system considered.

Extensive long-term n-body integrations of five hierarchical multi-planetary systems (HD 11964, HD 38529, HD 108874, HD 168443 and HD 190360) were performed by Veras and Ford (2010). They showed a wide variety of dynamical behaviours when assuming different line-of-sight and relative inclinations. They often reported LK-oscillations for stable highly inclined systems.

In the spirit of Libert and Tsiganis (2009), we aim to determine the possible 3D architectures of RV-detected systems by identifying ranges of values for the mutual inclinations which ensure the long-term stability of the systems. Particular attention will be given to the possibility of the detected extrasolar systems to be in a LK-resonant state, since it offers a secular phase-protection mechanism for mutually inclined systems, even though the two orbits may suffer large variations both in eccentricity and inclination. Indeed, the variations occur in a coherent way, such that close approaches do not occur and the

system remains stable.

Our analytical approach is based on the adoption of the secular Hamiltonian at order one in the masses, described in Sect. 2.2.3. For completeness, we re-write its formulation:

$$H(D_2,\boldsymbol{\xi},\boldsymbol{\eta}) = \sum_{j=0}^{ORDECC/2} \mathcal{C}_{j,\boldsymbol{m},\boldsymbol{n}} D_2^j \sum_{\boldsymbol{m}+\boldsymbol{n}=0}^{ORDECC-j} \boldsymbol{\xi}^{\boldsymbol{m}}\boldsymbol{\eta}^{\boldsymbol{n}}\,, \tag{4.1.1}$$

recalling that

$$\begin{aligned} \xi_j &= \sqrt{2\Lambda_j}\sqrt{1-\sqrt{1-e_j^2}}\cos\omega_j\,,\\ \eta_j &= -\sqrt{2\Lambda_j}\sqrt{1-\sqrt{1-e_j^2}}\sin\omega_j\,, \end{aligned} \tag{4.1.2}$$

and where $ORDECC$ indicates the maximal order in eccentricities considered, here fixed to 12. We recall that this Hamiltonian has only two degrees of freedom, with the semi-major axis being constant in the secular approach. It has been shown in previous works (see, for example, Libert and Henrard (2007), Libert and Sansottera (2013)) that, if the planetary system is far from a mean-motion resonance, the secular approximation at the first order in the masses is accurate enough to describe the evolution of the system. Such analytical approach is of interest for the present purpose, since, being faster than pure n-body simulations which also consider small-period effects, it allows to perform an extensive parametric exploration at a reasonable computational cost. Moreover, we will show that the analytical expansion is highly reliable, fulfilling its task up to high values of the mutual inclination.

The goal of the present work is twofold. On the one hand, we study the 3D secular dynamics of ten RV-detected extrasolar systems, identifying for each one the values of the inclination i of the orbital plane with respect to the line of sight and of the mutual inclination i_{mut} inducing a LK-resonant behaviour of the system. On the other hand, through numerical explorations performed with a chaos detector, we identify the ranges of values for which a long-term stability of the orbits is observed, unveiling for each system the extent of the chaotic region around the LK stability islands.

4.2 Parametric study

In the following, we describe the parametric study realised in the present work. The selection of the systems considered here is described in Sect. 4.2.1, and the accuracy of the analytical expansion for the secular evolution of the selected systems is discussed in Sect. 4.2.2.

4.2.1 Methodology

The present work aims to identify the possible 3D architectures of RV-detected extrasolar systems. From the online database `exoplanets.eu` (Schneider et al., 2011) we selected all the two-planet systems which fulfil the following criteria: (a) the semi-major axis of the outer planet is smaller than 10 AU (systems with significant planet-planet interactions); (b) the system is not close to a mean-motion resonance[1]; (c) the initial planetary eccentricities are lower than 0.65; (d) the masses of the planets are smaller than $10\,M_J$; (e) the orbital period of the inner planet is larger than 45 days (no significant relativistic or tidal effects induced by the star, see Chap. 5). The orbital parameters of the 10 selected systems are listed in Table 4.1, as well as the reference from which they have been derived.

In this work, the secular evolutions of the systems are considered when varying the mutual inclination i_{mut} and the orbital plane inclination i with respect to the plane of the sky. It is important to note that, although the inclinations i_1 and i_2 of the two orbital planes may differ, we decide here to set the same value $i_1 = i_2 = i$ for both planes. Thus both masses are varied using the same scaling factor $\sin i$.

In the general reference frame, the following relation holds:

$$\cos i_{mut} = \cos i_1 \cos i_2 + \sin i_1 \sin i_2 \cos \Delta\Omega\,, \tag{4.2.1}$$

being $\Delta\Omega = \Omega_1 - \Omega_2$. It should be noted that Eq. (4.2.1) can be solved if $i_{mut} \leqslant 2i$, thus for a given value of i it determines boundaries for the compatible values of i_{mut}. Since $i_1 = i_2 = i$, having fixed the values of i_{mut}, we can determine the value of the longitudes of the nodes by setting $\Omega_1 = \Delta\Omega$ and $\Omega_2 = 0$, thus obtaining the complete set of initial conditions. A consequent change of coordinates to the Laplace plane is finally performed by using the relations (2.2.5) and (2.2.6) valid in the Laplace plane.

For our parametric study, we vary the value of the mutual inclination i_{mut} from 0° to 80° with an increasing step of 0.5°, while the common orbital plane inclination i runs from 5° to 90° with an increasing step of 5°. As the coefficients $\mathcal{C}_{j,\boldsymbol{m},\boldsymbol{n}}$ in Eq. (4.1.1) depend on $\boldsymbol{L}$, and therefore on the masses of the planets, we recompute them for each value of i. Regarding the integration of the secular approach, we implement a Runge-Kutta of order 4 scheme, fixing the integration time to 10^6 yr with an integration step of 1 yr, and the energy preservation is monitored along the integration.

Table 4.2 – Convergence *au sens des astronomes* for the 10 systems. The value H_j corresponds to the sum of the absolute values of the terms of the Hamiltonian (4.1.1) of order j in eccentricities and inclinations (see definition in Eq. (4.2.3)). The last column gives the relative error between the secular Hamiltonian computed by numerical quadrature and the expansion (4.1.1). The values are computed for the initial condition $(i_{mut}, i) = (50°, 50°)$.

System	H_2	H_4	H_6	H_8	H_{10}	H_{12}	H_{12}/H_2	Relative error
HD 11506	4.78e-05	7.98e-05	1.44e-04	1.44e-04	6.56e-05	1.21e-05	$\mathcal{O}(10^{-1})$	1.62e-04
HD 12661	4.88e-05	7.24e-05	7.33e-05	3.96e-05	9.69e-06	9.25e-07	$\mathcal{O}(10^{-2})$	1.42e-04
HD 134987	5.48e-07	3.27e-08	1.70e-09	1.93e-10	1.14e-11	1.62e-12	$\mathcal{O}(10^{-6})$	1.10e-05
HD 142	4.70e-06	1.80e-06	1.85e-07	8.29e-08	1.75e-08	4.73e-09	$\mathcal{O}(10^{-3})$	1.34e-04
HD 154857	2.85e-05	1.41e-06	1.51e-07	8.06e-08	1.38e-08	2.14e-09	$\mathcal{O}(10^{-5})$	9.33e-05
HD 164922	1.77e-07	1.44e-08	7.87e-10	1.07e-10	7.51e-12	1.05e-12	$\mathcal{O}(10^{-6})$	1.03e-05
HD 169830	5.65e-05	6.70e-05	1.39e-04	1.77e-04	9.35e-05	1.92e-05	$\mathcal{O}(10^{-1})$	1.46e-04
HD 207832	1.69e-06	8.50e-07	4.65e-07	3.626e-07	1.08e-07	1.40e-08	$\mathcal{O}(10^{-3})$	5.28e-05
HD 4732	7.83e-06	1.79e-06	2.59e-06	2.29e-07	5.11e-08	5.80e-09	$\mathcal{O}(10^{-4})$	7.58e-05
HD 74156	4.37e-05	7.89e-05	7.23e-05	1.48e-04	1.25e-04	5.52e-05	$\mathcal{O}(1)$	1.01e-04

4.2.2 Accuracy of the analytical approach

Before discussing the results of our parametric study, we need to ensure that the Hamiltonian formulation (4.1.1) provides an accurate description of the planetary dynamics for all sets of parameters considered in the study, in particular for high values of the mutual inclination i_{mut}. As already shown in previous papers (e.g. Libert and Henrard (2005) for the coplanar problem, Libert and Henrard (2007) for the 3D problem), the series of the secular terms converge better than the full perturbation. However, the higher the value of D_2, the weaker the convergence, as expected. In the following, we discuss the numerical convergence of the expansion for the selected extrasolar systems, also called *convergence au sens des astronomes*, as opposed to the mathematical convergence (Poincaré (1893)).

In Table 4.2, are listed, for the 10 systems, the contributions to the Hamiltonian value of the terms from order 2 to order 12 in eccentricities and inclinations (i.e., $j+m+n$ in Eq. (4.1.1)). The entries are the sums of the absolute value of the terms appearing at a given order, computed at the orbital parameters given in Table 4.1 and at $i = 50^\circ$ and $i_{mut} = 50^\circ$, in order to evaluate the *convergence au sens des astronomes* at high mutual inclination. Whenever we fix the value of i_{mut}, we can evaluate the parameter D_2 and rearrange the expression (4.1.1) into

$$H(\boldsymbol{\xi},\boldsymbol{\eta}) = \sum_{\boldsymbol{m}+\boldsymbol{n}=0}^{ORDECC/2} \bar{\mathcal{C}}_{\boldsymbol{m},\boldsymbol{n}} \boldsymbol{\xi}^{\boldsymbol{m}} \boldsymbol{\eta}^{\boldsymbol{n}} . \tag{4.2.2}$$

Therefore, we have that

$$H_{2i} = \sum_{\boldsymbol{m}+\boldsymbol{n}=i} \left| \bar{\mathcal{C}}_{\boldsymbol{m},\boldsymbol{n}} \boldsymbol{\xi}^{\boldsymbol{m}} \boldsymbol{\eta}^{\boldsymbol{n}} \right|. \tag{4.2.3}$$

The numerical convergence of the expansion at high mutual inclination is obvious for most of the systems. However, when the decrease of the terms is less marked, we should keep in mind that results at higher mutual inclinations should be analysed with caution. This is the case, in particular, for the systems HD 11506, HD 12661, HD 169830 and HD 74156. Moreover, the last column of Table 4.1 gives an estimation of the remainder of the truncated expansion. It shows the relative error between the secular Hamiltonian computed by numerical quadrature and our polynomial formulation (4.1.1), confirming the previous observations.

To further illustrate the accuracy of our analytical approach, we show in Fig. 4.1 and Fig. 4.2 the evolutions of HD 12661 given by the analytical expansion (4.1.1) (red curves) for the mutual inclinations $i_{mut} = 20^\circ, 40^\circ, 50^\circ$

[1] A system is close to the $k_2 : k_1$ mean-motion resonance if there exist $k_1, k_2 \in \mathbb{N}$ such that $n_1 k_1 - n_2 k_2 \simeq 0$, where n_1, n_2 are the mean motions.

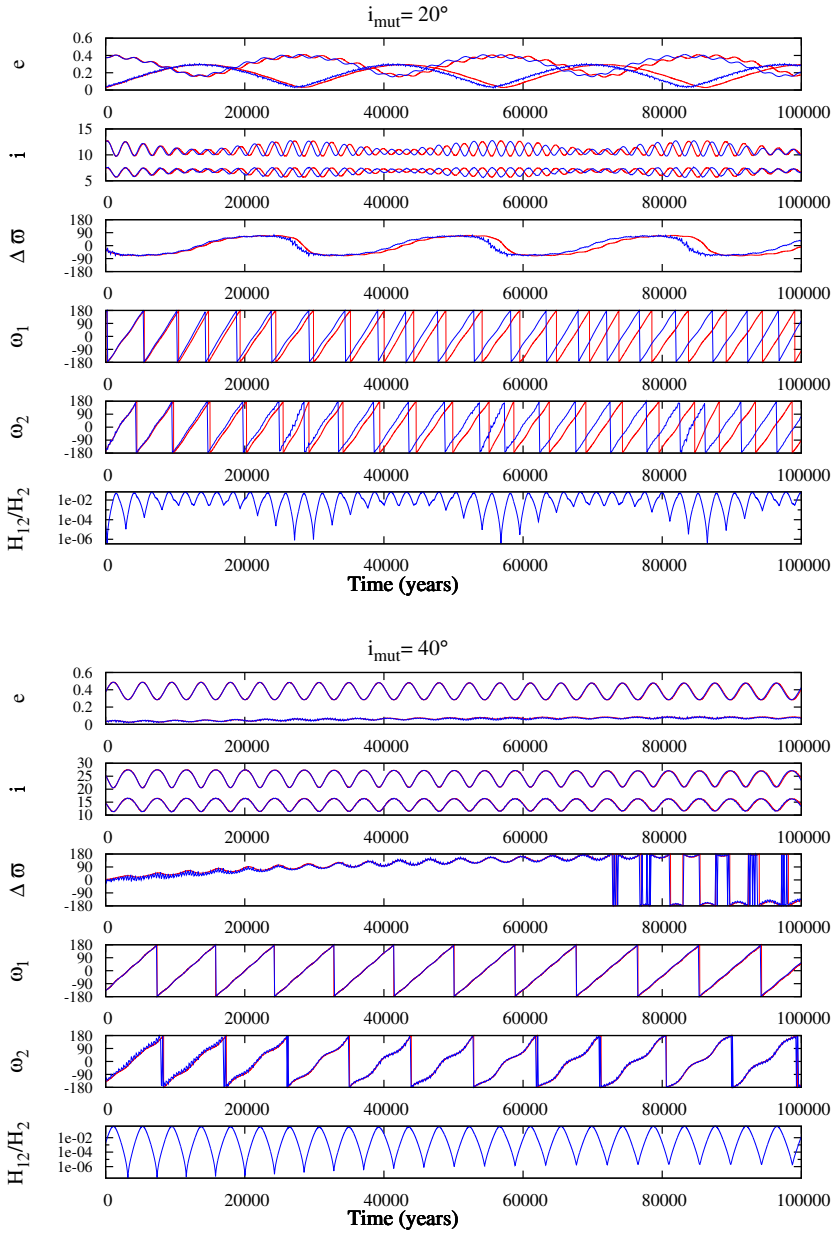

Figure 4.1 – Dynamical evolutions of the HD 12661 system given by the analytical expansion (in red) and by n-body simulations (in blue), for $i_{mut} = 20°$ (top), 40° (bottom). The inclination of the orbital plane is fixed to $i = 50°$.

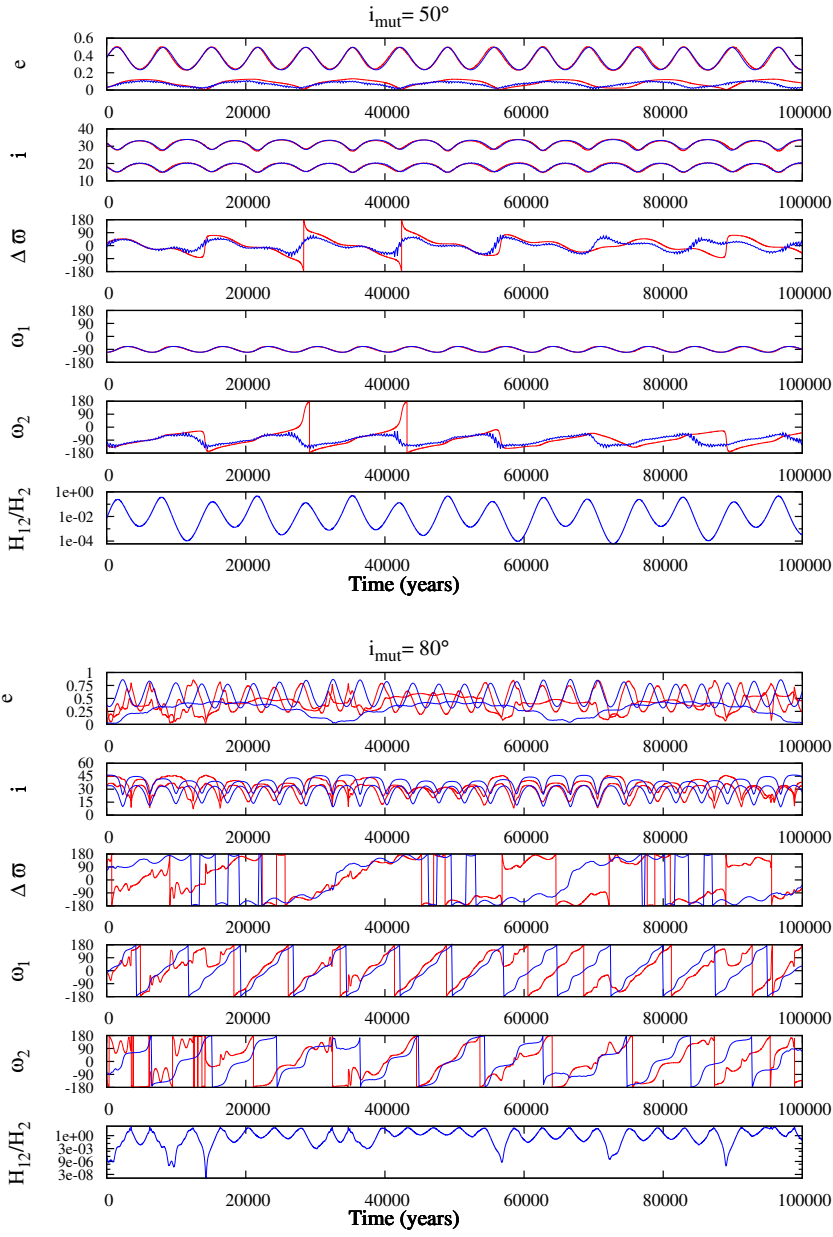

Figure 4.2 – Dynamical evolutions of the HD 12661 system given by the analytical expansion (in red) and by n-body simulations (in blue), for $i_{mut} = 50°$ (top) and 80° (bottom). The inclination of the orbital plane is fixed to $i = 50°$.

and 80° (i is fixed to 50°), and compare them to the evolutions obtained by the numerical integration of the three-body problem with the SWIFT package (Levison and Duncan (1994), blue curves). Although the numerical convergence observed in Table 4.2 is not excellent for HD 12661, the agreement of the analytical approach with the numerical integration of the full problem is very good. The dynamical evolutions are well reproduced up to high values of the mutual inclination ($i_{mut} = 20°, 40°, 50°$). Only small differences in the periods are observed and can be attributed to the short-period terms not considered in our secular formulation. For very high values ($i_{mut} = 80°$), the dynamical evolutions given by the two methods no longer coincide, but follow the same trend. The accuracy of the analytical approach is also monitored along the evolutions in the last panels of the plots of Fig. 4.1 and Fig. 4.2 by computing the quantity H_{12}/H_2, introduced in Table 4.2. This quantity reaches higher maximal values when increasing the mutual inclination i_{mut}. As it will be shown in Sect. 4.3.3, the orbits are generally chaotic for high values of the mutual inclination.

4.3 Results

The question of the 3D secular dynamics of RV-detected planetary systems is addressed here in two directions. Firstly, we focus on identifying the inclination values for which a LK-resonant regime is observed in our parametric study. Secondly, the long-term stability of the mutually inclined systems is unveiled by means of a chaos detector.

4.3.1 Extent of the LK regions

Regarding the possible 3D configurations of extrasolar systems, we are particularly interested in the LK resonance. This protective mechanism ensures that the system remains stable, despite large eccentricities and inclinations variations. It is characterised, in the Laplace-plane reference frame, by the coupled variation of the eccentricity and the inclination of the inner planet, and the libration of the argument of the pericenter of the same planet around ±90° (Lidov (1962), Kozai (1962)).

As a first example, we investigate the dynamics of the HD 12661 extrasolar system. In the top panel of Fig. 4.3, we show, for varying (i_{mut}, i) values, the maximal eccentricity of the inner planet reached during the dynamical evolution of the system, i.e.

$$e_{1_{max}} = \max_t e_1(t)\,, \tag{4.3.1}$$

being $e_1(t)$ the eccentricity of the inner planet at time t. Let us note that this quantity is often used to determine the regularity of planetary orbits, since for

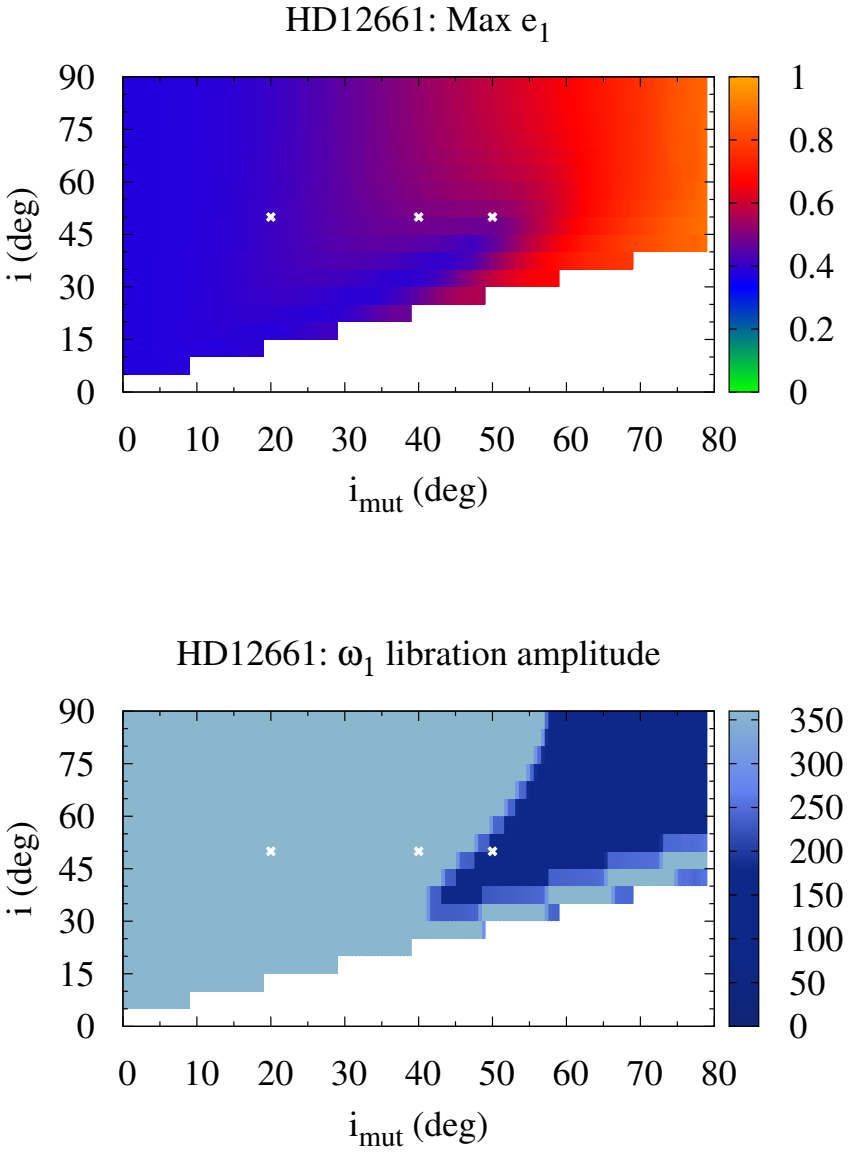

Figure 4.3 – Long-term evolution of the HD 12661 system when varying the mutual inclination i_{mut} (x-axis) and the inclination of the orbital plane i (y-axis), both expressed in degrees. Top panel: the maximal eccentricity of the inner planet, as defined by Eq. (4.3.1). Bottom panel: the libration amplitude of the argument of the pericenter ω_1 (in degrees), as defined by Eq. (4.3.2). The three highlighted points are related to the representative planes shown in Fig. 4.4.

low ($e \lesssim 0.2$) and high ($e \gtrsim 0.8$) eccentricity values it is generally found in good agreement with chaos indicators (see for instance (Funk et al., 2011)). On the bottom panel, we report, for all the considered (i_{mut}, i) values, the libration amplitude of the angle ω_1, defined as

$$\text{libr\_ampl}\,(\omega_1) = \max_t \omega_1(t) - \min_t \omega_1(t)\,. \tag{4.3.2}$$

This value will serve as a guide for the detection of the LK-resonant behaviours characterised by the libration of ω_1, and thus by a small value of libr_ampl (ω_1).

When following an horizontal line in Fig. 4.3, the mutual inclination i_{mut} varies while the orbital inclination i, and thus the planetary masses, are kept fixed. On the other hand, the inclination of the common orbital plane decreases when moving down along a vertical line, while the planetary masses increase accordingly. As previously stated, this implies the re-computation of the coefficients $\mathcal{C}_{j,\boldsymbol{m},\boldsymbol{n}}$ of Eq. (4.1.1). Let us recall that all (i_{mut}, i) pairs can not be considered here since, for fixed $i_1 = i_2 = i$ values, Eq. (4.2.1) can not be solved for all the mutual inclinations.

We see that the eccentricity variations of 3D configurations of HD 12661 are small[2] for low mutual inclinations (blue colour in the top panel of Fig. 4.3) and become large for high mutual inclinations (red colour). Additionally, the argument of the pericenter ω_1 circulates for low i_{mut} values (light blue colour in the bottom panel of Fig. 4.3) and librates for high i_{mut} values (dark blue colour). Thus, for high mutual inclinations, the system is in a LK-resonant state.

To visualise the different dynamics, we draw, for a given D_2 value, the level curves of Hamiltonian (4.1.1) in the representative plane $(e_1 \sin\omega_1, e_2 \sin\omega_2)$ where both pericenter arguments are fixed to $\pm 90^\circ$ (see Libert and Henrard (2007) for more details on the representative plane). This plane is neither a phase portrait, nor a surface of section, since the problem is four-dimensional. However, nearly all the orbits will cross the representative plane in several points of intersection on a same energy curve. Fig. 4.4 shows the representative planes of HD 12661 for $i_{mut} = 20^\circ$ (i.e., $D_2 = 0.35$, top left panel), 40° (i.e., $D_2 = 0.67$, top right panel) and 50° (i.e., $D_2 = 0.90$, bottom panel), the inclination of the orbital plane being fixed to 50°. These three system configurations are also indicated with white crosses in Fig 4.3 and their dynamical evolutions are those presented in Fig. 4.1 and Fig. 4.2.

For low values of i_{mut}, circular orbits ($e_1 = e_2 = 0$) constitute a point of stable equilibrium (top left panel of Fig. 4.4). As we increase the mutual inclination (top right and bottom panels of Fig. 4.4), the central equilibrium becomes unstable and bifurcates into the two stable LK equilibria. The red

[2]It is recalled that the initial inner eccentricity is 0.377.

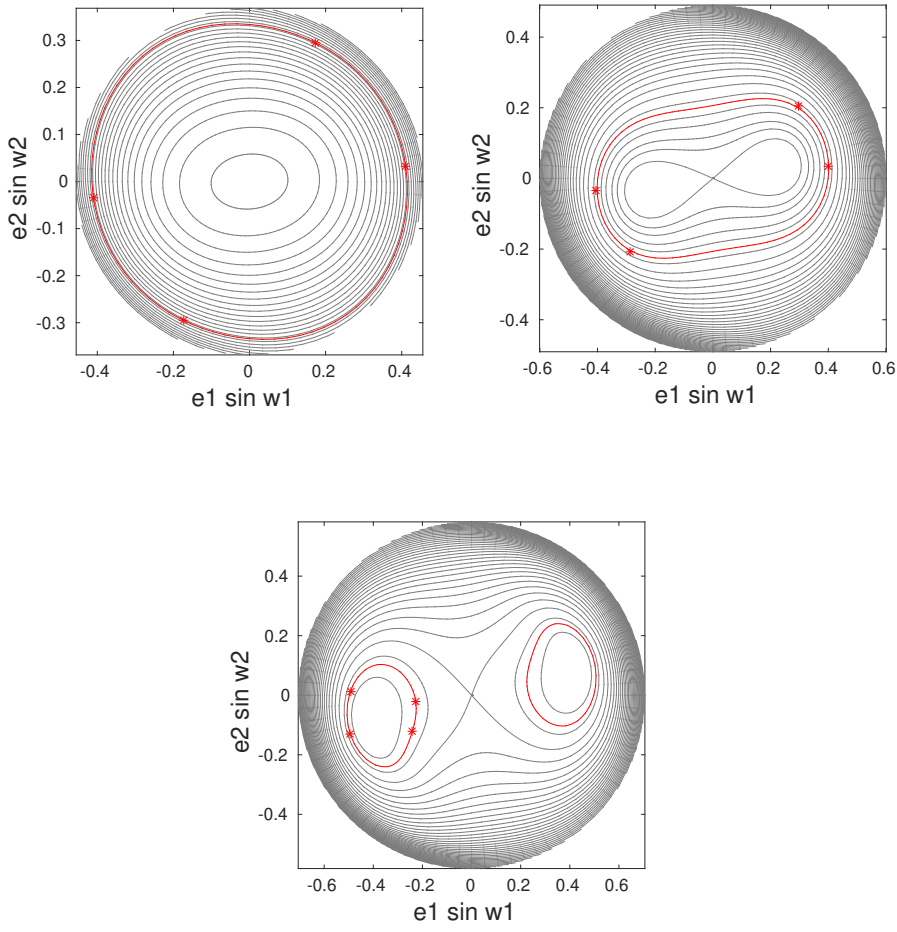

Figure 4.4 – Representative plane for the HD 12661 system, having fixed the inclination of the orbital plane to $i = 50°$, for $i_{mut} = 20°$ (top left panel), $i_{mut} = 40°$ (top right panel) and $i_{mut} = 50°$ (bottom panel). The level curve of Hamiltonian relative to the orbital parameters of HD 12661 is highlighted in red. The crosses indicate the intersections of the orbit with the representative plane.

crosses represent the intersections of the evolution of the mutually inclined HD 12661 system with the representative plane. For low mutual inclinations, the crosses are located on both sides of the representative plane, so the argument of the inner pericenter circulates. For $i_{mut} = 50^\circ$ (bottom panel of Fig. 4.4), the crosses are inside the LK island in the left side of the representative plane, associated with the libration of ω_1 around 270° (as it can also be observed in the top dynamical evolution shown in Fig. 4.2). We see that the corresponding white cross on the bottom of Fig. 4.3 is likewise located inside the dark blue region of the LK resonance.

The critical value of the mutual inclination, which corresponds to the change of stability of the central equilibrium, depends on the mass and semi-major axis ratios (see, e.g., Libert and Henrard (2007)) and is typically around $40^\circ - 45^\circ$ for mass ratios between 0.5 and 2. The linear stability of the central equilibrium can be studied by following the same approach adopted, for example, in Henrard and Lemaître (2005) and Libert and Henrard (2007). Around an equilibrium point $(\boldsymbol{\xi}^*, \boldsymbol{\eta}^*)$, the quadratic approximation of the Hamiltonian (4.1.1) can be written as

$$2\mathcal{Q} = a_{11}s_1^2 + 2a_{12}s_1^2 s_2^2 + a_{22}s_2^2 + b_{11}S_1^2 + 2b_{12}S_1S_2 + b_{22}S_2^2\,, \tag{4.3.3}$$

where

$$a_{i,j} = \left.\frac{\partial^2 \mathcal{Q}}{\partial\xi_i \partial\xi_j}\right|_{(\boldsymbol{\xi}^*,\boldsymbol{\eta}^*)}, \quad b_{i,j} = \left.\frac{\partial^2 \mathcal{Q}}{\partial\eta_i \partial\eta_j}\right|_{(\boldsymbol{\xi}^*,\boldsymbol{\eta}^*)} \qquad (i,j=1,2) \tag{4.3.4}$$

and (s_i, S_i) are the increments relative to the variables (ξ_i, η_i). Applying the untangling transformation described in detail in Henrard and Lemaître (2005), we obtain a new formulation of the Hamiltonian, that now writes as a linear combination of squares:

$$2\mathcal{Q} = (c_{11}\tilde{s}_1^2 + d_{11}\tilde{S}_1^2) + (c_{22}\tilde{s}_2^2 + d_{22}\tilde{S}_2^2)\,, \tag{4.3.5}$$

being $(\tilde{s}_i, \tilde{S}_i)$ (for $i,j = 1,2$) the new variables. Studying the sign of the products $c_{ii}d_{ii}$ we can determine the linear stability: when it is positive the corresponding degree of freedom is linearly stable, otherwise it is linearly unstable. The linear frequencies can be easily computed when $c_{ii}d_{ii} > 0$, by introducing a new set of action-angle variables

$$\tilde{s}_i = \sqrt{2R_iR_i^*}\sin r_i\,, \quad \tilde{S}_i = \sqrt{2R_i/R_i^*}\cos r_i\,, \tag{4.3.6}$$

where $R_i^* = \sqrt{d_{ii}/c_{ii}}$. We finally obtain the following simplified form of the Hamiltonian:

$$\mathcal{Q} = \sqrt{c_{11}d_{11}}R_1 + \sqrt{c_{22}d_{22}}R_2\,. \tag{4.3.7}$$

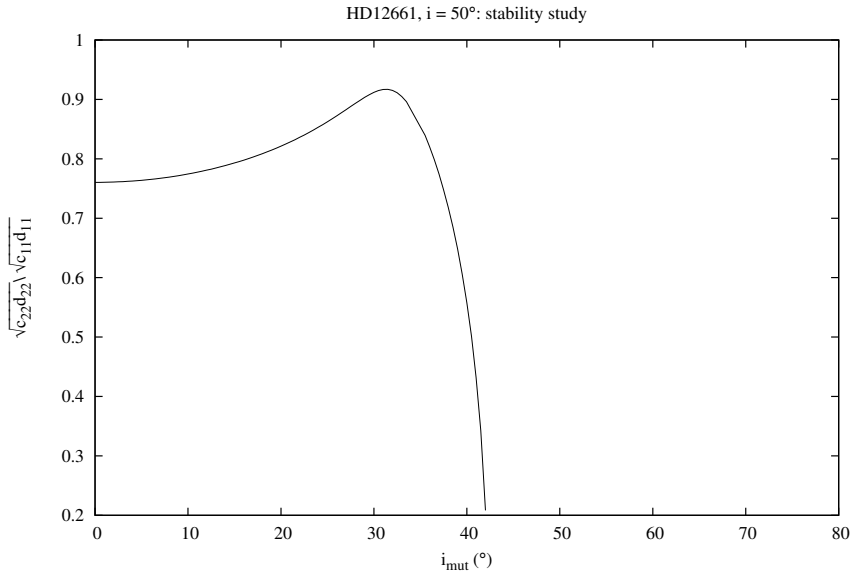

Figure 4.5 – Evolution of the ratio of the linear frequencies $\sqrt{c_{11}d_{11}}$ and $\sqrt{c_{22}d_{22}}$ as defined by Eq. (4.3.7), relative to the central equilibrium point of the system HD 12661, having fixed $i = 50°$.

In Fig. 4.5 we show, for the system HD 12661 with $i = 50^\circ$, the evolution of the ratio between the two linear frequencies $\sqrt{c_{11}d_{11}}$ and $\sqrt{c_{22}d_{22}}$, associated to the stable central equilibrium, when increasing the value of the mutual inclination. The ratio is positive up to $\sim 42^\circ$ of mutual inclination, when we observe a change of stability of the central equilibrium.

For increasing mutual inclinations, the stable LK equilibria created by the bifurcation of the central equilibrium reach higher inner eccentricity values and the orbit of the considered system possibly crosses the representative plane inside a LK island, as observed in Fig. 4.4. Therefore, the dark blue LK region in Fig. 4.3 starts around $40^\circ - 55^\circ$, the exact value for the change of dynamics depending on the inclination of the orbital plane since the expansion (4.1.1) depends on the inclination i via the planetary mass.

Let us note that, even if the numerical convergence of the analytical expansion of HD 12661 system is not excellent (see Table 4.2), the LK-resonant region perfectly matches the one obtained with n-body simulations additionally performed for validation, except at very high mutual inclinations ($i_{mut} \geqslant 70^\circ$). Indeed, for HD 12661 and HD 74156 systems, a destabilisation of the orbits is observed at very high mutual inclinations and slightly reduces the stable LK region.

A second example is shown in Fig. 4.6 for the HD 11506 system. The LK region is now located at smaller mutual inclinations, making visible the right border of the LK region. For each i value, the interval of mutual inclinations associated with the libration of the angle ω_1 begins at $\sim 40^\circ$, whereas its amplitude depends on i. No spatial configuration of HD 11506 can be found in a LK-resonant state for a mutual inclination higher than 65°.

Let us note that some additional dark-blue points can be observed for low values of the inclinations of the orbital plane i. These systems are close to the separatrix of the LK resonance and will be destabilised on a longer time scale, as it will be shown in the next section.

In Fig. 4.7 we display the libration amplitude of the argument of the pericenter of the inner planet for the 10 systems considered here. All the graphs do show a LK region. In other words, all the selected RV-detected systems, when considered with a significant mutual inclination, have physical and orbital parameters compatible with a LK-resonant state. Table 4.3 summarises information on the extent of the LK region for each system. The second and third columns display the minimum values of the mutual inclination i_{mut} (with an accuracy of 1°) and the orbital inclination i, respectively, for which a libration of the argument of the pericenter ω_1 is observed. The percentage of initial conditions inside the (dark blue) LK region is given in the fourth column. The last column reports the percentage of chaos in the whole set of initial conditions and will be discussed in Section 4.3.3.

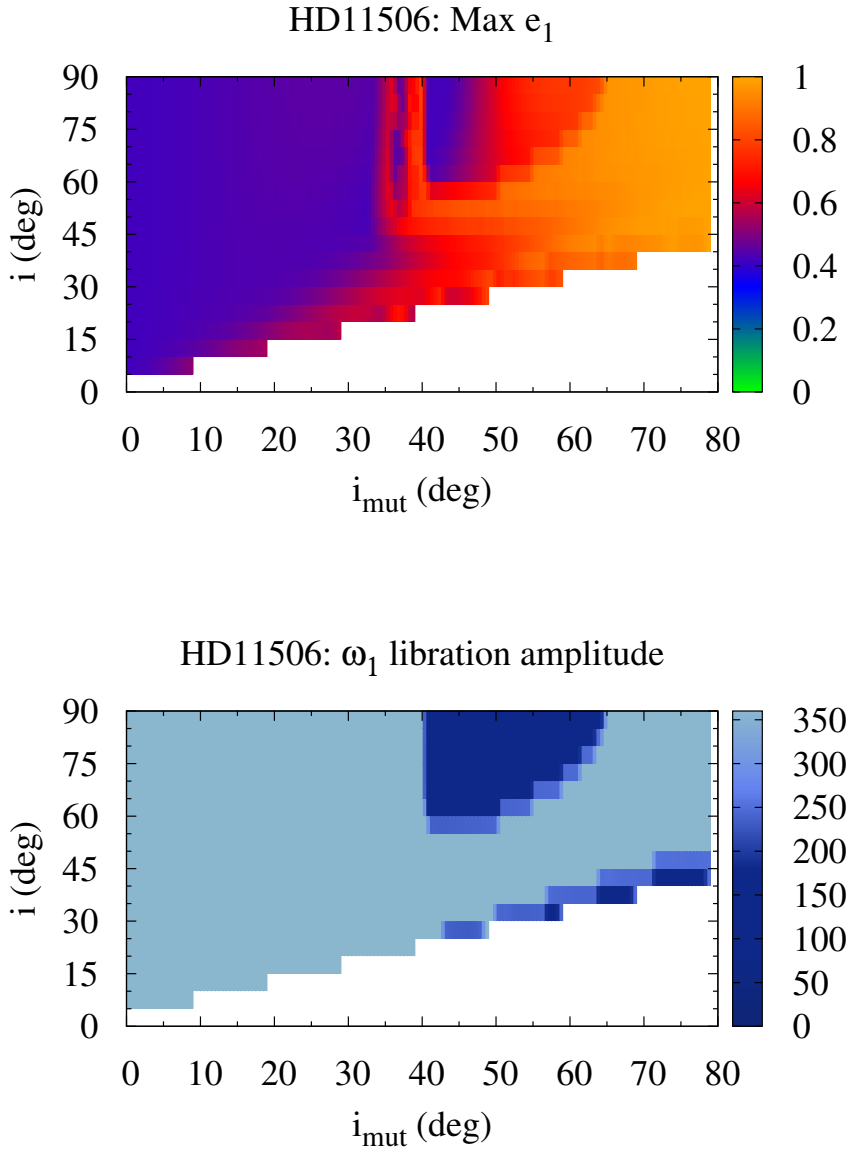

Figure 4.6 – Same as Fig. 4.3 for HD 11506 system.

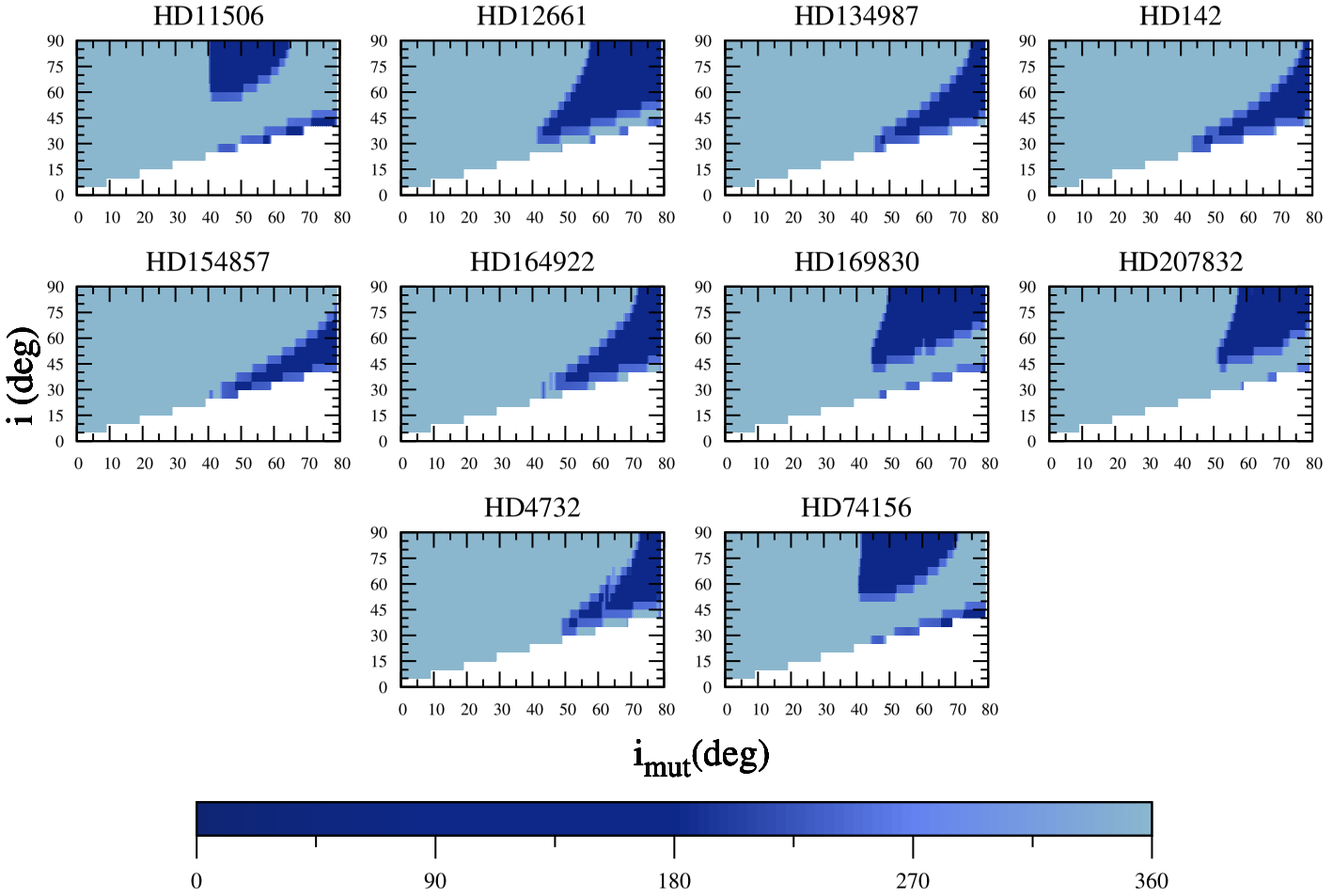

Figure 4.7 – Libration amplitude of ω_1 for the 10 systems considered here, when varying the mutual inclination i_{mut} (x-axis) and the inclination of the orbital plane i (y-axis).

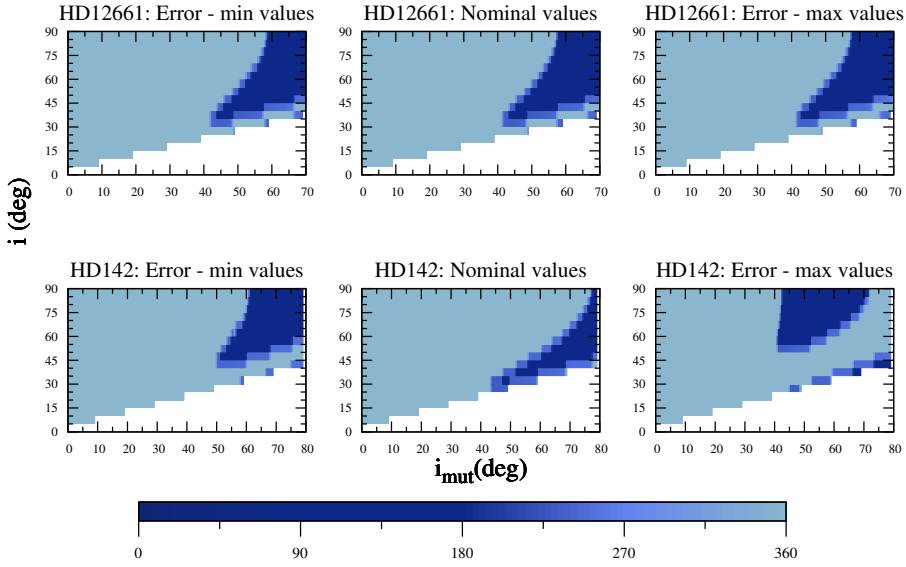

Figure 4.8 – Libration amplitude of ω_1, as in Fig. 4.7, for HD 12661 (top) and HD 142 (bottom) systems, when considering the minimal values (left), the nominal values (middle) and the maximal values (right) of the orbital parameters.

Table 4.3 – Extent of the LK region for the 10 systems. For each system, we indicate the minimum i_{mut} (second column) and i (third column) values of the LK region where libration of ω_1 is observed in Fig. 4.7, the percentage of initial conditions for which a LK-resonant state is observed (fourth column) and the percentage of initial conditions classified as chaotic by the chaos indicator (fifth column).

System	$\min i_{mut}$ (°)	$\min i$ (°)	LK (%)	chaos (%)
HD 11506	41	30	15	39
HD 12661	43	30	24	49
HD 134987	46	30	13	–
HD 142	44	30	11	2
HD 154857	41	30	10	2
HD 164922	43	30	23	–
HD 169830	45	25	23	19
HD 207832	50	35	17	20
HD 4732	49	35	12	15
HD 74156	41	30	20	2

4.3.2 Sensitivity to observational uncertainties

So far, we have considered the nominal values of the orbital parameters given by the observations. However, due to the limitations of the detection techniques, observational data come with relevant uncertainties, and to explore the influence of such uncertainties on the previous results is relevant. As typical examples, we show in Fig. 4.8 the extent of the LK region for HD 12661 and HD 142 systems, when considering extremal orbital parameters within the confidence regions given by the observations, instead of the best-fit parameter values. The errors on each orbital parameter are listed in Table 4.1 for both planetary systems. Two extremal cases are examined in the following, where the minimal/maximal values are adopted for all the parameters simultaneously.

In the case of the HD 12661 system, the location and extent of the LK region are very similar when adopting the minimal values (top left panel of Fig. 4.8), the nominal values (top middle) and the maximal values (top right) of the orbital parameters. Concerning HD 142, the situation is quite different. We observe, in the bottom panels of Fig. 4.8, a significant variation of the LK region in its extent and shape, probably due to the greater size of the observational errors on the different orbital elements.

As a result, the location and extent of the LK resonance regions are sensitive to observational uncertainties in the orbital elements, especially when they are

significant, and this should be taken into account in detailed studies of the selected systems. Nevertheless, we stress that, when considering extremal values within the confidence regions, the dynamics remains qualitatively the same with the existence of stable LK islands at high mutual inclinations for both systems.

4.3.3 Stability of planetary systems

In this section, we aim to determine if the LK-resonant state of a 3D planetary system is essential to ensure its long-term stability. To do so, we have used the Mean Exponential Growth factor of Nearby Orbits (MEGNO) chaos indicator, briefly described in the following (for an extensive discussion on the properties of the MEGNO, see Cincotta and Simo (2000) and Maffione et al. (2011)).

Let $H(\mathbf{p},\mathbf{q})$ with $\mathbf{p},\mathbf{q} \in \mathbb{R}^n$ be an autonomous Hamiltonian of n degrees of freedom. The Hamiltonian vector field can be expressed as

$$\dot{\mathbf{x}} = J\nabla_{\mathbf{x}}\mathcal{H}\mathbf{x} \tag{4.3.8}$$

where $\mathbf{x} = \begin{pmatrix} \mathbf{p} \\ \mathbf{q} \end{pmatrix} \in \mathbb{R}^{2n}$ and $\mathrm{J} = \begin{bmatrix} 0_n & -1_n \\ 1_n & 0_n \end{bmatrix}$, being 1_n and 0_n the unitary and null $n \times n$ matrices, respectively. In order to apply the MEGNO chaos indicator, we need to compute the evolution of deviation vectors $\boldsymbol{\delta}(t)$. These vectors satisfy the variational equations

$$\dot{\boldsymbol{\delta}}(t) = J\nabla^2_{\mathbf{x}}\mathcal{H}\boldsymbol{\delta}(t), \tag{4.3.9}$$

being $\nabla^2_{\mathbf{x}}\mathcal{H}$ the Hessian matrix of the Hamiltonian. As in Cincotta and Simo (2000), the Mean Exponential Growth Factor is defined as

$$Y(t) = \frac{2}{t}\int_0^t \frac{\dot{\delta}(s)}{\delta(s)}\,ds \tag{4.3.10}$$

where $\delta(s)$ is the Euclidean norm of $\boldsymbol{\delta}(s)$. We consider here the *mean* MEGNO, i.e., the time-averaged MEGNO:

$$\bar{Y}(t) = \frac{1}{t}\int_0^t Y(s)\,ds. \tag{4.3.11}$$

The limit for $t \to \infty$ provides a good characterisation of the orbits. The MEGNO chaos indicator is particularly convenient since we have:

- $lim_{t\to\infty}\bar{Y}(t) = 0$ for stable periodic orbits,
- $lim_{t\to\infty}\bar{Y}(t) = 2$ for quasi-periodic orbits and for orbits close to stable periodic ones,
- for irregular orbits, $\bar{Y}(t)$ diverges with time.

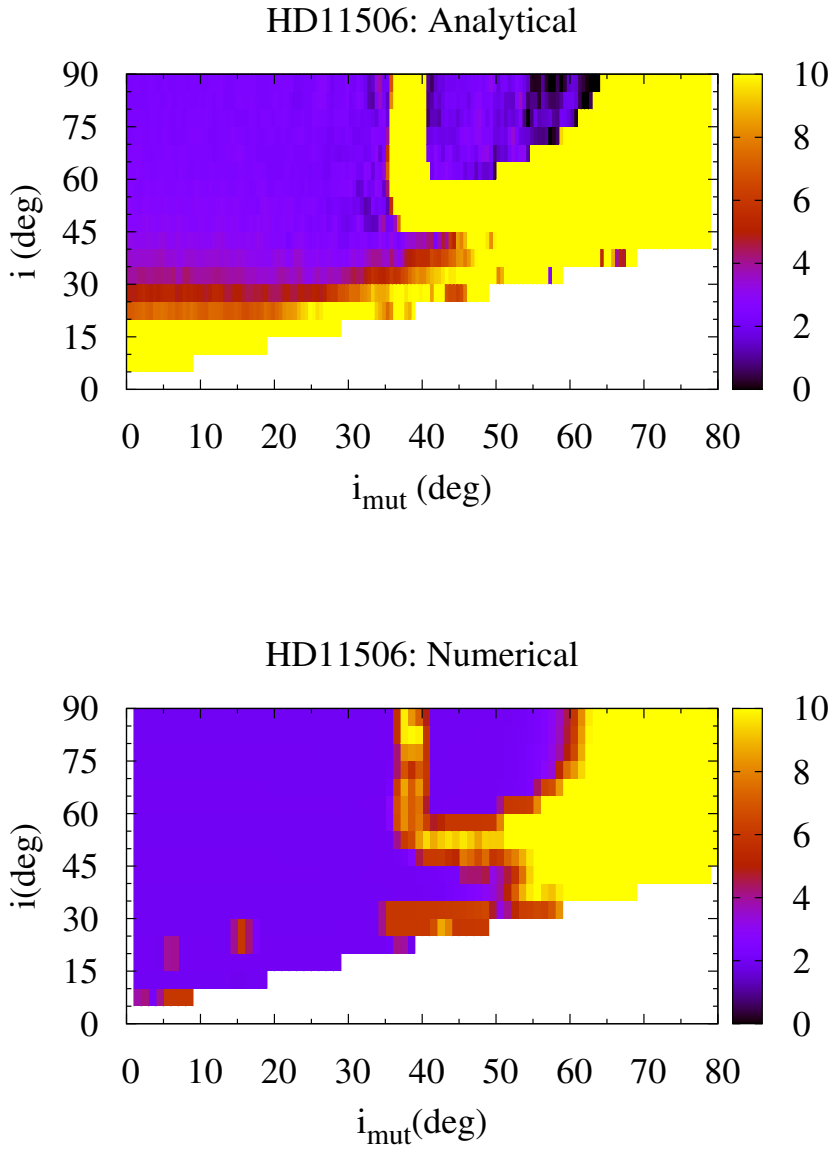

Figure 4.9 – Mean MEGNO values for HD 11506 system given by our analytical approach (top panel) and n-body simulations (bottom panel).

For each set of initial conditions we choose the initial deviation vector $\boldsymbol{\delta}(0)$ as a random unitary vector. We then study its evolution along the orbit and compute the corresponding evolution of the mean MEGNO. Two main factors have motivated the choice of this chaos indicator. First, it requires the study of the evolution of only one deviation vector, saving valuable computational time. Second, it returns an absolute value, as it classifies each orbit independently.

As previously noted, the LK-resonant state is surrounded by a chaotic zone associated with the bifurcation of the central equilibrium at null eccentricities. Therefore, a chaos indicator can be useful to highlight the extent of the chaotic zone and identify with precision the (i_{mut}, i) values ensuring the regularity of the orbits for a long time.

On the top panel of Fig. 4.9, we show the values of the mean MEGNO for HD 11506 computed with our analytical approach. We can appreciate how the region at high inclinations characterised as regular by the mean MEGNO (purple colour) clearly superimposes with the LK-resonant region identified in Fig 4.6. The surrounding chaotic region displayed in yellow extends up to high mutual inclinations, showing that highly mutually inclined configurations of HD 11506 system can only be expected in a LK-resonant state. Regarding low mutual inclinations, nearly all spatial configurations present regular motion up to a mutual inclination of $\sim 35^\circ$, where the LK resonance comes into play.

A comparison with n-body simulations (short-period effects included) is given on the bottom panel of Fig. 4.9, where numerical integrations have been carried out with SWIFT (for every 1° instead of 0.5° to reduce the computational cost). The two panels look very similar, showing that our secular approach is reliable for systems which are far from a mean-motion resonance.

Similar observations can be made for the 10 extrasolar systems considered here. In Fig. 4.10, the chaotic region associated to a mean MEGNO value greater than 8 with our analytical approach, is indicated in white on the plot showing the libration amplitude of ω_1 (Fig. 4.7). Also, more information on the extent of the chaotic zone for each system can be found in the last column of Table 4.3. The chaotic region around the stable LK islands is broad for half of the systems (HD 11506, HD 12661, HD 169830, HD 207832 and HD 4732), moderate for HD 142, HD 15487 and HD 74156 systems, and not significant for HD 134987 and HD 164922 systems, given the integration timescale and the grid of initial conditions considered. For the first category of systems, long-term regular evolutions of the orbits are only possible for low mutual inclinations and, for higher mutual inclinations, in the LK region, while in the two other cases regular evolutions are also observed at high mutual inclinations outside the LK regions.

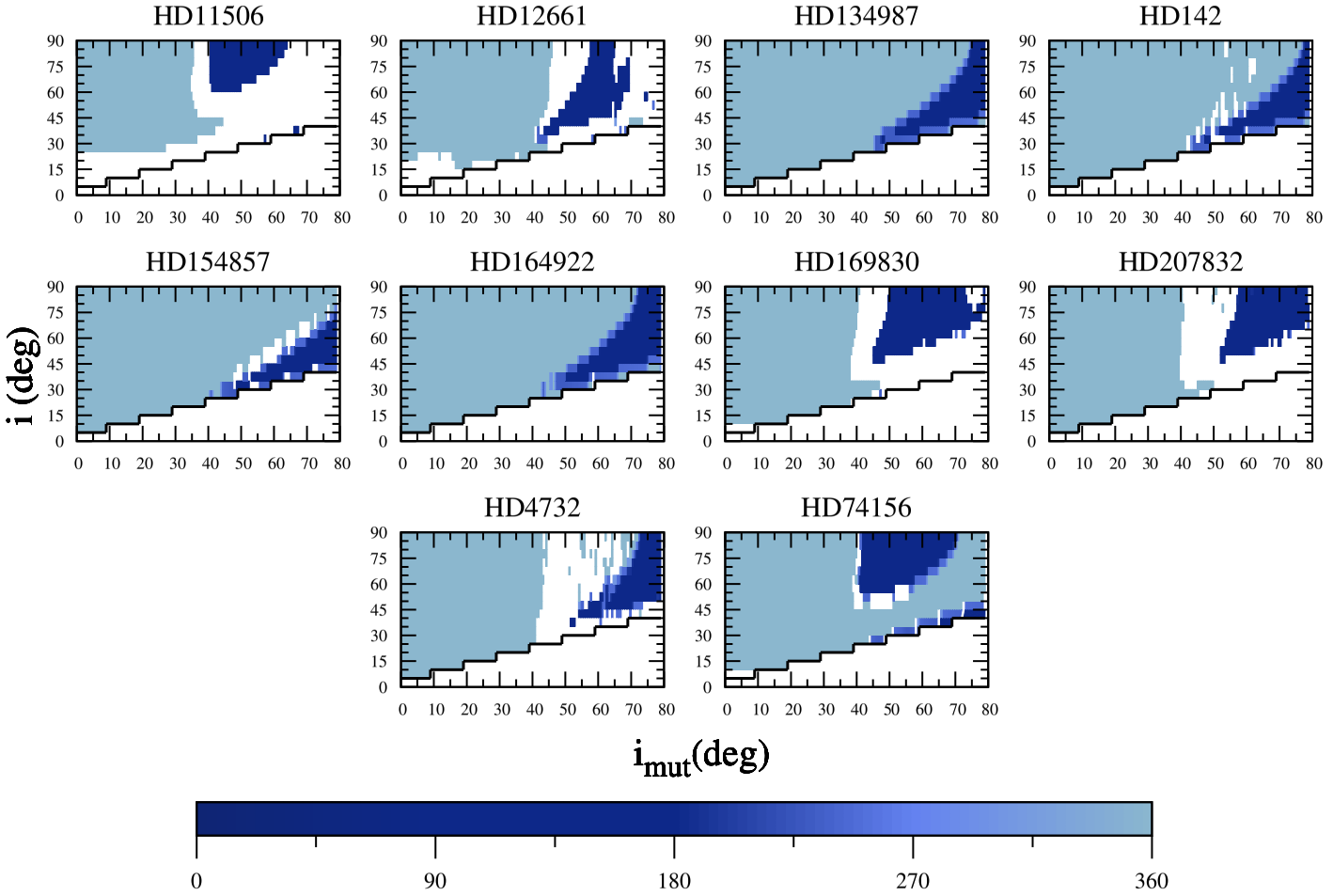

Figure 4.10 – Same as Fig. 4.7, where the initial system parameters leading to chaotic motion (defined by the mean MEGNO value greater than 8) are coloured in white (above the black curve).

4.4 Conclusions

We studied the possibility for ten RV-detected exoplanetary systems to be in a 3D configuration. In particular, we determined ranges of orbital and mutual inclinations for which the system is in a LK-resonant state. Our results were compared with n-body simulations, showing the accuracy of the analytical approach up to very high inclinations ($\sim 70^\circ - 80^\circ$). We showed that all the systems considered here might be in a LK-resonant state for sufficiently mutually inclined orbit. By means of the MEGNO chaos indicator, we revealed the extent of the chaotic zone surrounding the stability islands of the LK resonance. Long-term regular evolutions of the orbits are possible i) at low mutual inclinations and ii) at high mutual inclinations, preferentially in the LK region, due to the significant extent of the chaotic zone in many systems.

It should be noted that we did not consider systems with close-in planets. The reason for this choice is that our model considers only gravitational forces and would not correctly describe the dynamics of planets really close to the host star, for which other short-range forces should be taken into account. In Chap. 5 we extend our study by including in our model the perturbation due to the general relativity, hence considering systems with close-in planets.

Chapter 5

Close-in planetary systems

In this chapter we extend the study described in Chap. 4 to two-planet systems whose inner planet is close to the host star. For such systems, perturbations given by the general relativity have to be taken into account when analysing the long-term stability of the system.

5.1 Motivation

In Chap. 4 we investigated the action of the LK resonance as a protective mechanism for three-dimensional configurations. Regarding the constraints of the selected systems, we restricted our choice amongst the systems with orbital period of the inner planet longer than 45 days.

Nevertheless, we discussed in Chap. 1 how both the transit and RV methods are strongly biased to detect preferentially planets with short orbital period, and the study of such systems would reveal to be particularly relevant. Besides the gravitational interactions, the relativistic effects on the planetary motion have to be considered for these systems.

The major effect induced by the action of the general relativity (hereafter GR) on the motion of a planet concerns the precession of the pericenter. In particular, the GR causes an advance of the pericenter. Given that the LK resonance acts on the pericenter as well, it is relevant to study how the two phenomenons compete on the long-term evolution of the systems.

As in our previous work, the aim here is to find constraints for the values of the orbital inclinations and of the mutual inclination between the orbital planes. Such a parametric study including the GR has previously been performed by Veras and Ford (2010), where they explore the spatial dynamics of five two-

planet systems by means of long-term n-body numerical integrations. The differences with our work are significant. First of all, contrary to our secular approach, they needed to consider more orbital parameters (such as the mean anomaly), while our study restricts the parameter space to study. Secondly, given the purely numerical nature of the method (Monte Carlo simulations), their simulations have a higher computational cost and require longer machine time to be completed.

We should remark that we do not consider in the present work the tidal effects acting on the systems whose inner planet is extremely close to the star ($a \lesssim 0.08$ AU typically), for different reasons. The computation of the tidal effects relies on parameters (such as the radius of the planet and the tidal Love number) that are currently not known for most of the exoplanets. Let us note that in order to include these effects various authors in the past have fixed arbitrary values for the unknown parameters (see for example Migaszewski and Goździewski (2009) and Veras and Ford (2010)), and found that the tidal effects are generally negligible with respect to the relativistic corrections. Moreover, the perturbation due to the dynamical flattening of the star and/or of the inner planet depends on the orbital inclination of the equatorial plane of the star (see Migaszewski and Goździewski (2009)). This implies that the Laplace plane would not be constant reference plane anymore, and it would ask for a new analytical approach to reduce the number of degrees of freedom. For these reasons, for the extremely close-in planets considered here the specific dynamics described by our model does not include the tidal effects.

5.2 Secular Hamiltonian with relativistic corrections

It is common in the secular approximation framework to consider the effects of the GR on the inner planet only (see, e.g., Naoz (2016)), since we are interested in the LK resonance acting on the argument of the pericenter of the inner planet. As we focus on the long-term evolution of the system, we add to the purely gravitational three-body problem described by the Hamiltonian formulation (4.1.1) the secular perturbation caused by the GR, as given in Migaszewski and Goździewski (2009) after an averaging over the fast angles,

$$\langle H_{GR} \rangle = -\frac{3\mu_1^4 \beta_1^5}{c^2 L_1^3 G_1} \tag{5.2.1}$$

where $\mu_1 = m_0 + m_1$, $\beta_1 = \frac{m_0 m_1}{m_0+m_1}$, $L_1 = \beta_1\sqrt{\mu_1 a_1}$ (and therefore, $L_1 = \Lambda_1$ in our coordinates), $G_1 = L_1\sqrt{1-e^2}$ and c is the speed of light[1]. This expression in the modified Delaunay variables is particularly convenient to highlight the relativistic effects on the dynamics of the system, since the coordinate relative to the conjugate momenta G_1 is the argument of the pericenter of the inner planet. Therefore, it is possible to derive the precession of the pericenter of the inner planet explicitly through the Hamiltonian equations:

$$\dot{\omega}_1 = \dot{g}_1 = \frac{\partial\langle H_{GR}\rangle}{\partial G_1} = \frac{3\mu_1^4\beta_1^5}{c^2 L_1^3 G_1^2} = \frac{3\mu_1^4\beta_1^5}{c^2 L_1^5(1-e_1^2)} = \frac{3\mu_1^{3/2}}{c^2 a^{5/2}(1-e_1^2)}\,. \tag{5.2.2}$$

The Hamiltonian term corresponding to the relativistic correction can be written in the heliocentric Poincaré variables (2.2.7):

$$\langle H_{GR}\rangle = -3\mu_1^4\beta_1^5\left[c^2\Lambda_1^3\Big(\Lambda_1 - \frac{\xi_1^2+\eta_1^2}{2}\Big)\right]^{-1}, \tag{5.2.3}$$

and directly added to the former Hamiltonian formulation

$$H(D_2,\boldsymbol{\xi},\boldsymbol{\eta}) = \sum_{j=0}^{ORDECC/2} \mathcal{C}_{j,\boldsymbol{m},\boldsymbol{n}} D_2^j \sum_{\boldsymbol{m}+\boldsymbol{n}=0}^{ORDECC-j} \boldsymbol{\xi}^{\boldsymbol{m}}\boldsymbol{\eta}^{\boldsymbol{n}} + \langle H_{GR}\rangle. \tag{5.2.4}$$

5.3 Methodology

We intend to expand the study described in Chap. 4 to systems with close-in planets. We select systems fulfilling the same criteria listed in Sect. 4.2, except for the lower bound for the orbital period of the inner planet. Therefore, said criteria are: (a) the semi-major axis of the outer planet is smaller than 10 AU (systems with significant planet-planet interactions); (b) the system is not close to a mean-motion resonance; (c) the initial planetary eccentricities are lower than 0.65; (d) the masses of the planets are smaller than $10\,M_J$; (e) the orbital period of the inner planet is shorter than 45 days. The choice of this last limit comes from the following observation. For the systems considered in Chap. 4 (i.e., with inner orbital period longer than 45 days), the inclusion of the GR effects does not modify their dynamics. However, it is not always the case for systems whose inner planet has period shorter than 45 days, as it will be shown in the following. The orbital parameters of all the two-planet systems referenced on `exoplanet.eu` and considered in this chapter, as well as their references, are listed in Tab. 5.1.

For the parametric study, we follow the approach described in Chap. 4. We vary both the inclinations of the orbital planes with respect to the line of sight

[1]It should be noted that the value of the speed of light has to be converted to our units of measure for space and time. We then consider $c \simeq 6.31968914 \times 10^4$ AU/yr.

i (supposing the two planes inclined by the same angle) and the mutual inclination between the orbital planes i_{mut}. The complete set of initial conditions is derived as detailed in Sec. 4.2.1.

We left unchanged the grid for the mutual inclination i_{mut} (from 0° to 80°, with a step of 0.5°) and the orbital inclination i (from 5° to 90°, with a step of 5°). However, for the parameters relative to the numerical integration, it has to be taken into account that some of the selected systems have planets whose orbital period is a few days only. The time step has then to be well adapted. In order to achieve an optimal balance between precision and computational cost, we set the time step as the minimum between 20 times the orbital period of the inner planet and 1 year.

5.4 Results

The goal of the present work is to study how the contribution due to the GR affects the extent or the existence of the LK resonance region. Therefore, we compare the results obtained by numerically integrating the purely gravitational secular Hamiltonian (4.1.1) and the one including the relativistic correction on the argument of the pericenter of the inner planet described by Eq. (5.2.4).

Firstly, we study the convergence of the Hamiltonian (4.1.1) (without the relativistic effects) for the selected systems. In Tab. 5.2 we show the convergence *au sens des astronomes* computed for $i = i_{mut} = 50^\circ$, as described in detail in Sect. 4.2.2. The numerical convergence of the expansion at high mutual inclinations is obvious for most of the systems. In the cases for which the decrease of the expansion is less marked, however, the results obtained for higher values of the mutual inclination should be treated cautiously.

5.4.1 Influence on the extent of the LK region

Let us discuss in detail the evolution of two typical systems we choose as examples. In Fig. 5.1 we show the results obtained for the system HD 147018, whose orbital parameters are listed in Tab. 5.1. The top panels show the evolutions of the system for $i = 50^\circ$ and $i_{mut} = 30^\circ$ without and with relativistic corrections (left and right panels, respectively). Similarly, the bottom panels refer to the evolutions when $i = 50^\circ$ and $i_{mut} = 50^\circ$ without and with relativistic corrections (left and right panels, respectively). For $i_{mut} = 30^\circ$, the argument of the pericenter of the inner planet ω_1 circulates, hence showing that the system is not in a LK resonance. On the contrary, when $i_{mut} = 50^\circ$ we observe the libration of the angle ω_1, as the system is in a LK resonance. When the relativistic corrections are considered (right panels), we do not observe any significant difference, neither concerning the LK resonance nor the general behaviour.

Table 5.1 – Orbital parameters of the selected systems.

System		$m \sin i\,(M_J)$	$M_{\mathrm{Star}}\,(M_\odot)$	a	e	ω	References
GJ 433	b	0.01667	0.48	0.06	0.05	309.4	Tuomi et al. (2014)
	c	0.14		3.6	0.08	337.1	
GJ 649	b	0.33	0.54	1.14	0.2	332	Wittenmyer et al. (2013)
	c	0.03		0.043	0.2	334	
GJ 682	b	0.013845	0.27	0.08	0.08	85.94	Tuomi et al. (2014)
	c	0.027376		0.175	0.1	320.9	
GJ 832	b	0.67967	0.45	3.56	0.08	246	Wittenmyer et al. (2014)
	c	0.01699		0.163	0.18	10	
HD 117618	b	0.21	1.069	1.75	0.0	0	Wittenmyer et al. (2013)
	c	0.2		0.93	0.0	0	
HD 11964	b	0.622	1.125	3.16	0.041	155	Wright et al. (2009)
	c	0.0788		0.229	0.3	102	
HD 147018	b	1.045	0.889	0.2388	0.4686	336	Ségransan, D. et al. (2010)
	c	6.56		1.922	0.133	226.9	
HD 159243	b	1.13	1.125	0.11	0.02	223	Moutou, C. et al. (2014)
	c	1.9		0.8	0.075	69	
HD 187123	b	0.526	1.06	0.0426	0.004	25	Wright et al. (2009)
	c	1.99		4.89	0.252	243	
HD 190360	b	1.49515	1.04	0.392	0.343	14.7	Courcol, B. et al. (2015)
	c	0.06381		0.128	0.343	305.8	
HD 217107	b	1.39	1.02	0.0748	0.1267	24.4	Wright et al. (2009)
	c	2.6		5.32	0.517	198.6	
HD 47186	b	0.07167	0.99	0.05	0.038	59	Bouchy, F. et al. (2009)
	c	0.35061		2.395	0.249	26	
HD 9446	b	0.7	1.0	0.189	0.2	215	Hébrard, G. et al. (2010)
	c	1.82		0.654	0.06	100	

Table 5.2 – Convergence *au sens des astronomes* for the 13 systems. The value H_j corresponds to the sum of the absolute values of the terms of the Hamiltonian (4.1.1) of order j in eccentricities and inclinations (see definition in Eq. (4.2.3)). The values are computed for the initial condition $(i_{mut}, i) = (50°, 50°)$.

System	H_2	H_4	H_6	H_8	H_{10}	H_{12}	H_{12}/H_2
GJ 433	3.03e-11	7.90e-12	1.94e-13	3.119e-15	4.89e-17	1.04e-18	$\mathcal{O}(10^{-8})$
GJ 649	1.40e-08	1.60e-08	3.80e-09	5.21e-10	2.16e-11	3.17e-11	$\mathcal{O}(10^{-3})$
GJ 682	8.39e-08	4.88e-08	1.13e-08	1.33e-09	7.58e-11	1.70e-12	$\mathcal{O}(10^{-5})$
GJ 832	6.94e-10	2.23e-09	1.57e-10	1.20e-11	6.59e-13	1.44e-13	$\mathcal{O}(10^{-4})$
HD 117618	1.49e-07	2.17e-07	1.25e-07	2.16e-07	1.14e-07	2.75e-08	$\mathcal{O}(10^{-1})$
HD 11964	1.26e-08	1.65e-09	1.12e-10	7.93e-12	2.51e-13	7.04e-14	$\mathcal{O}(10^{-6})$
HD 147018	5.34e-05	1.78e-05	3.32e-06	2.53e-06	8.31e-07	2.47e-07	$\mathcal{O}(10^{-3})$
HD 159243	9.03e-07	1.96e-08	2.05e-10	2.53e-12	5.23e-15	8.12e-16	$\mathcal{O}(10^{-10})$
HD 187123	2.53e-08	2.17e-08	2.93e-09	2.51e-10	1.73e-11	1.92e-12	$\mathcal{O}(10^{-4})$
HD 190360	2.92e-06	2.24e-06	1.37e-06	1.52e-06	9.16e-07	2.69e-07	$\mathcal{O}(10^{-2})$
HD 217107	6.75e-07	1.71e-07	1.72e-07	8.67e-08	9.00e-09	2.44e-08	$\mathcal{O}(10^{-2})$
HD 47186	3.81e-09	4.19e-08	5.46e-10	4.90e-11	3.35e-12	9.16e-13	$\mathcal{O}(10^{-4})$
HD 9446	1.49e-05	3.82e-07	9.48e-09	2.14e-09	1.29e-10	5.24e-12	$\mathcal{O}(10^{-7})$

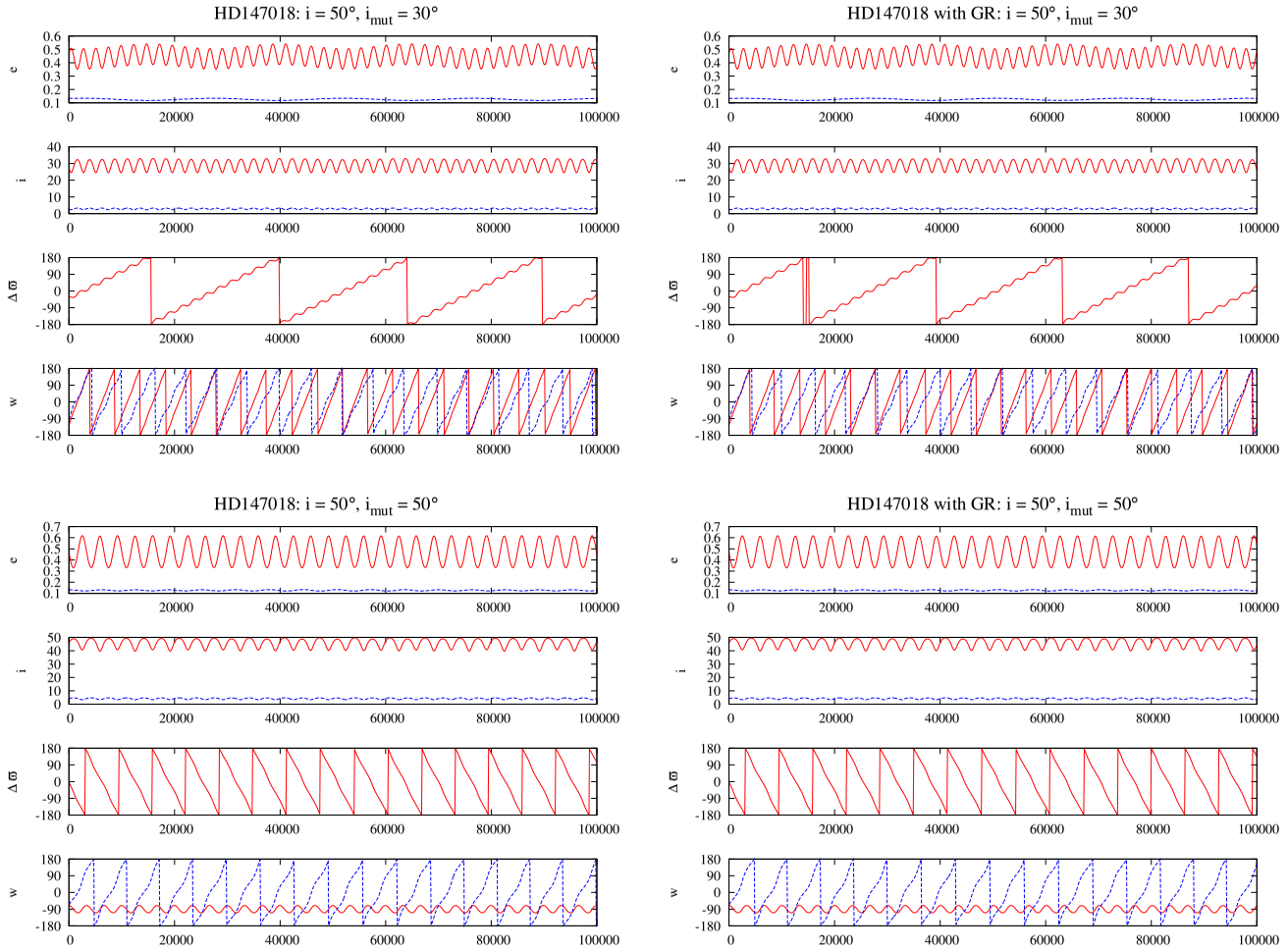

Figure 5.1 – Dynamical evolution of the HD 147018 system. In the left panels, the evolution is given by the secular Hamiltonian (4.1.1) and in the right panels, by the Hamiltonian (5.2.4) including relativistic corrections. The inclination of the orbital plane is fixed to $i = 50°$, the mutual inclination between the planets to $i_{mut} = 30°$ (top panels) and $50°$ (bottom panels).

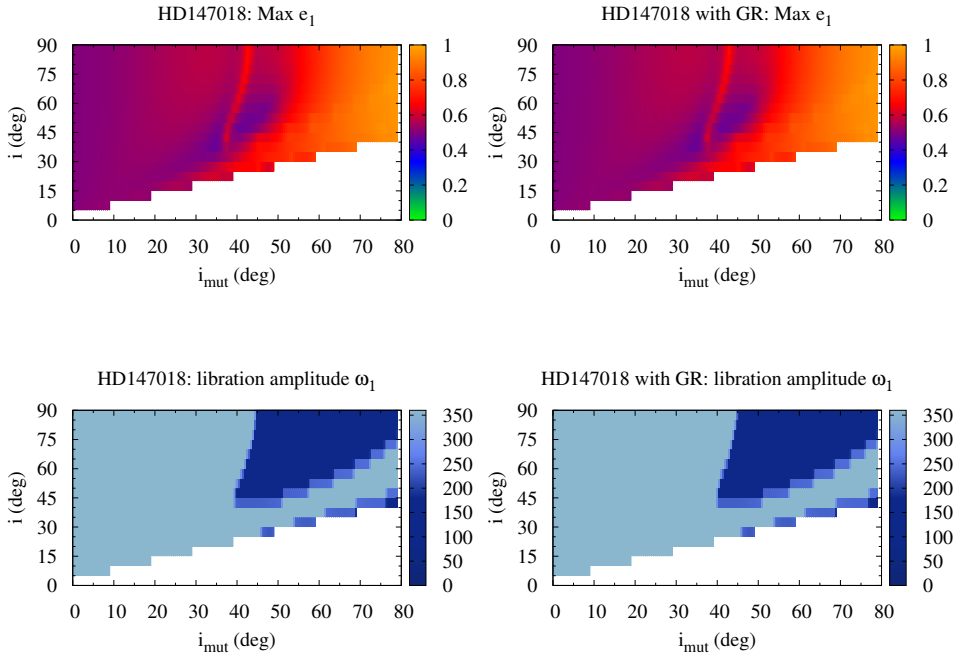

Figure 5.2 – Long-term evolution of the HD 147018 system when varying the mutual inclination i_{mut} (x-axis) and the inclination of the orbital plane i (y-axis), both expressed in degrees. Top panels: the maximal eccentricity of the inner planet, as defined by Eq. (4.3.1), without (left) and with (right) relativistic corrections. Bottom panels: the libration amplitude of the argument of the pericenter ω_1 (in degrees), as defined by Eq. (4.3.2), without (left) and with (right) relativistic corrections.

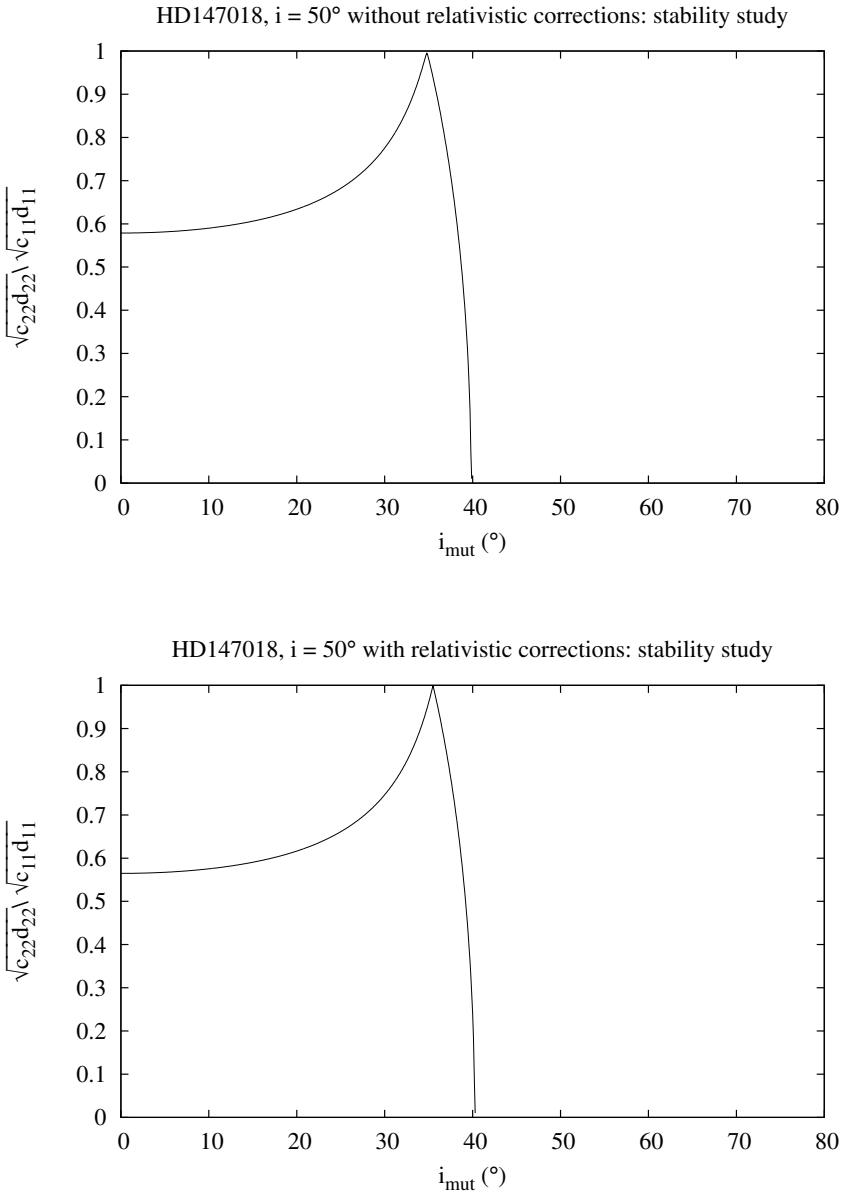

Figure 5.3 – Evolution of the ratio of the linear frequencies $\sqrt{c_{11}d_{11}}$ and $\sqrt{c_{22}d_{22}}$ as defined by Eq. (4.3.7), relative to the central equilibrium point of the system HD 147018, having fixed $i = 50°$. On the top panel, the results obtained when taking into account only gravitational forces. On the bottom panel, those obtained when including relativistic corrections.

In Fig. 5.2 we show, for the whole parameter space, the maximal eccentricity of the inner planet (top panels) and the libration amplitude of the angle ω_1 (bottom panels), as defined by Eq. (4.3.1) and Eq. (4.3.2), respectively. On the left, we show the results obtained by integrating the Hamiltonian equations given by the purely gravitational formulation (4.1.1). We remark the presence of a LK resonance region, appearing from $i_{mut} \simeq 40^\circ$. On the right, we present the plots referring to the system when considering relativistic corrections, as described by Eq. (5.2.4). It is straightforward to note that there is no significant difference between the two cases, in particular the LK resonance region is unperturbed by the additional effect. The negligible effect of the GR can be also observed when studying the linear stability of the central equilibrium point, as previously shown in Sec. 4.3.1. In Fig. 5.3 we show the evolution of the ratio of the linear frequencies $\sqrt{c_{22}d_{22}/c_{11}d_{11}}$, relative to the central equilibrium point having fixed $i = 50^\circ$. In the top panel we display the results when taking into account only gravitational forces, in the bottom panel when including the relativistic corrections. It shows that the critical value of the mutual inclination is not affected by the introduction of the relativistic effects.

Let us now focus on the system GJ 649, whose orbital parameters are listed in Tab. 5.1. In Fig. 5.4 we show the evolution of the system for the same two initial conditions. The top panels refer to $i = 50^\circ$ and $i_{mut} = 30^\circ$, whereas the bottom ones are relative to $i = 50^\circ$ and $i_{mut} = 50^\circ$. Again, on the left panels, we show the results obtained considering only gravitational interactions, and on the right panels, those related to the model including the relativistic corrections. Unlike the previous case, the differences between the left and right plots are noticeable. For $i_{mut} = 30^\circ$, we observe a drastic change in the secular period of the evolution: for example, the secular period of the eccentricity of the inner planet decreases from $\simeq 1.1 \times 10^5$ yr down to $\simeq 1.5 \times 10^4$ yr. Moreover, it can be observed that the eccentricity of the inner planet undergoes smaller variations (see also , e.g., Migaszewski and Goździewski (2009) and Sansottera et al. (2014)). This is due to the dumping of the eccentricity excitation that characterises the GR contribution (see, e.g., Naoz (2016)). For $i_{mut} = 50^\circ$ (bottom panels), we remark an additional consequence: where we could observe the libration of the angle ω_1 (bottom left), when considering relativistic corrections we find that the angle now circulates (bottom right). The introduction of the GR has therefore inhibited the LK resonance.

The effects of the GR are even more obvious when we consider the plots for all the parameter space. In Fig. 5.5 we represent the analogue of Fig. 5.2 for the system GJ 649. On the top panels, we can appreciate a stabilising effect: the maximal eccentricity of the inner planet is much closer to the initial value ($e_1 = 0.2$), as the excitation is dumped by the GR. The LK resonance region does not exist anymore: all the initial conditions show the circulation of the angle ω_1.

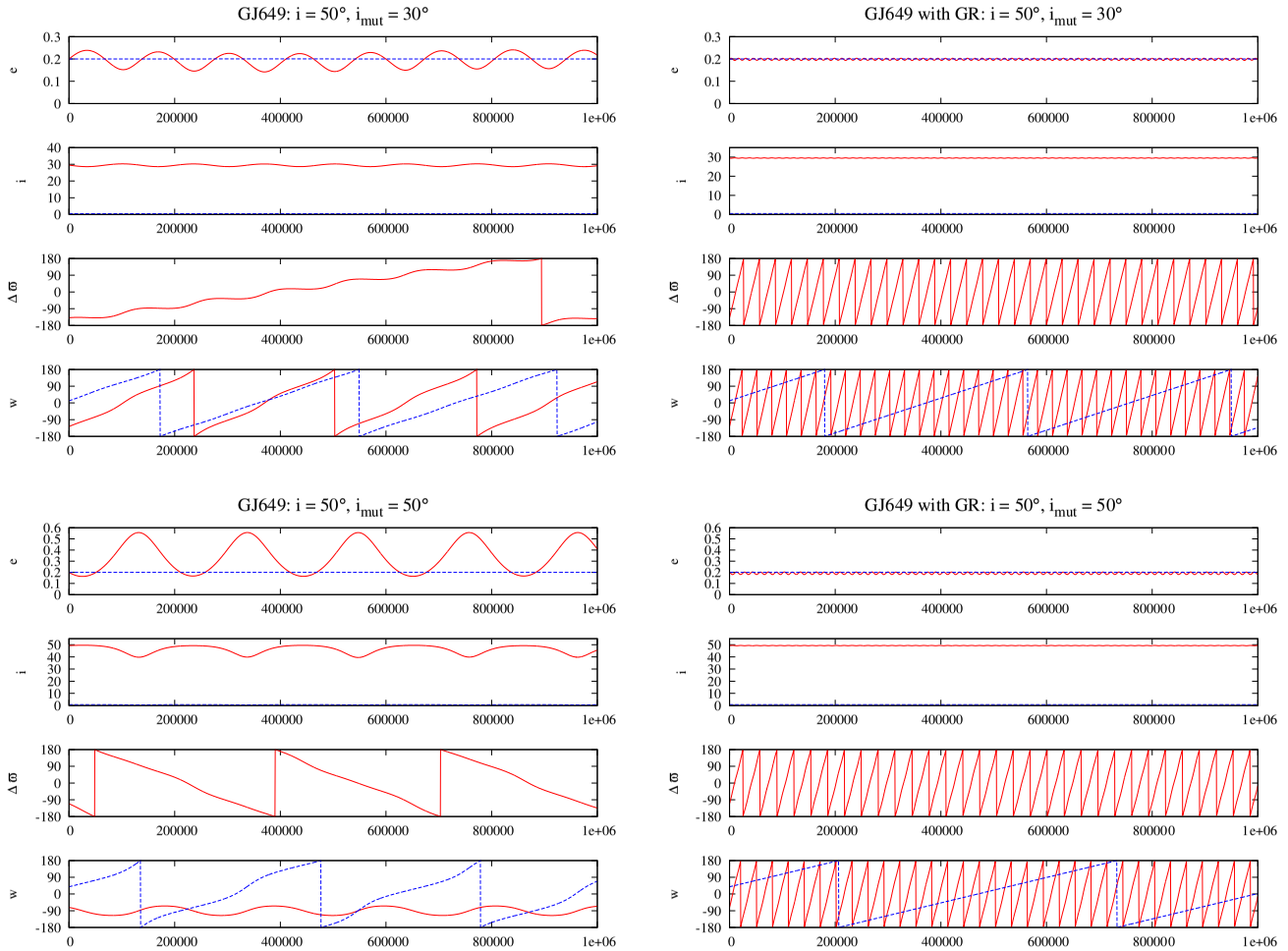

Figure 5.4 – Same as Fig. 5.1 for the system GJ 649.

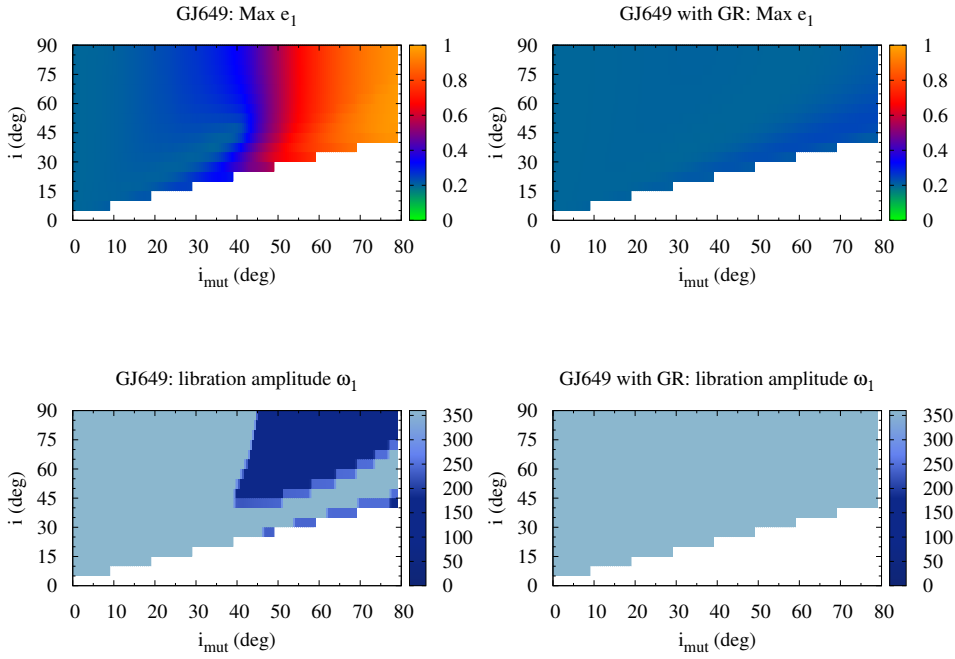

Figure 5.5 – Same as Fig. 5.2 for the system GJ 649.

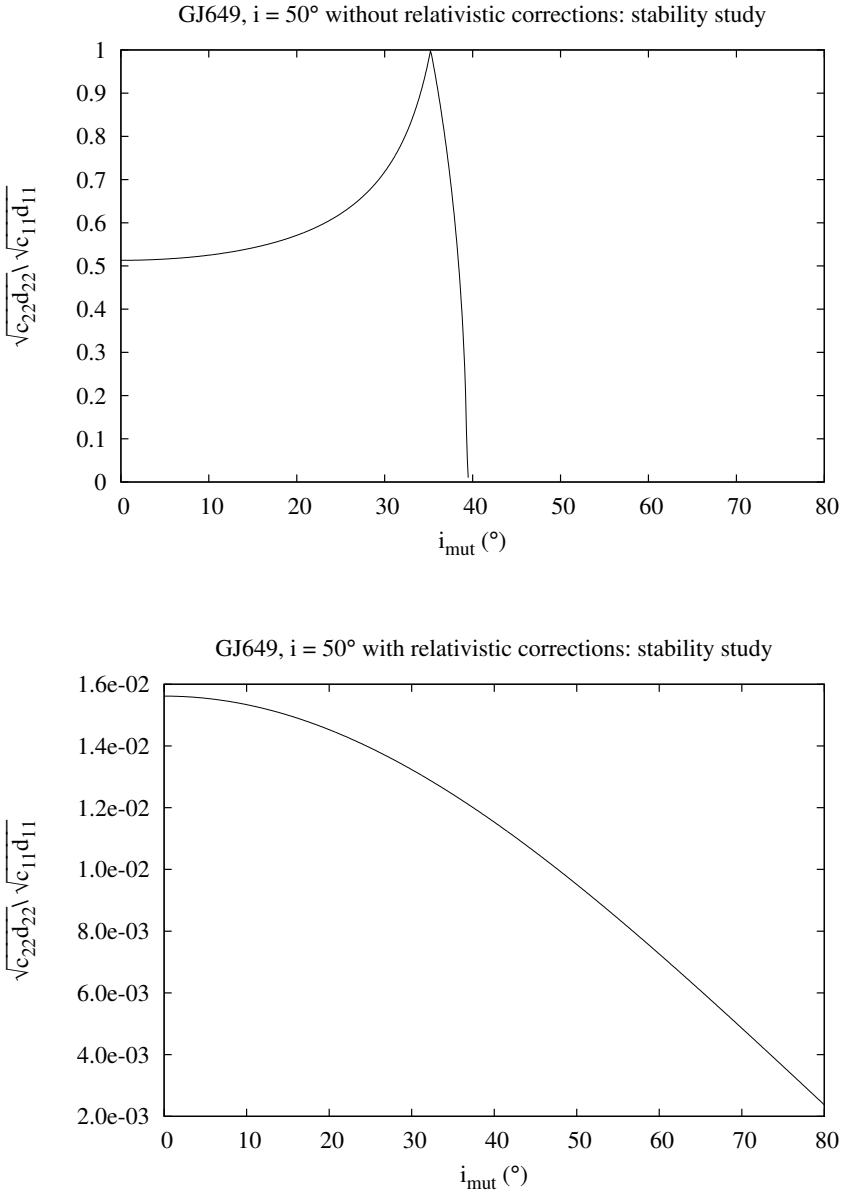

Figure 5.6 – Same as Fig. 5.3 for the system GJ 649, having fixed $i = 50°$.

This can also be observed when studying the linear stability of the central equilibrium point. In Fig. 5.6 we show the evolution of the ratio of the linear frequencies $\sqrt{c_{22}d_{22}/c_{11}d_{11}}$, associated to $i = 50^\circ$, without considering the GR effects (top panel) and including the relativistic corrections (bottom panel). In the last case, we observe no change of the linear stability of the central equilibrium around $i_{mut} = 40^\circ$, but the destabilisation, if any, would take place at very high mutual inclination. This explains that no LK resonance region is observed in the bottom right panel of Fig. 5.5.

In Fig. 5.7 and Fig. 5.8 we show the maximal eccentricity and the libration amplitude of the argument of the pericenter of the inner planet (respectively) for all the 13 systems considered, in the purely gravitational case. In Fig. 5.9 and Fig. 5.10 we report the corresponding results when taking into account the relativistic correction. We observe that almost all the systems experience a dumping of the excitation of the eccentricity, similarly to the system GJ 649. This is in line with the results obtained by Veras and Ford (2010), where they show that the inclusion of the GR in the simulations flattened the evolution of the eccentricities. Our results show that to this flattening corresponds the disappearance of the LK resonance region. As it can be observed from Fig. 5.10, the LK region remains in place for only 4 systems when the relativistic effects are considered.

It should be noted that some of the systems (namely, GJ 433, HD 187123, HD 217107 and HD 147186) present, in the purely gravitational case, extremely long secular periods. In particular, for a large subset of the initial conditions, a closer examination of the evolution of the system shows that the angle ω_1 has not achieved a complete circulation in the total integration time (10^6 yr). In these cases, simulations for an extended integration time are currently running.

5.4.2 Importance of the GR effects

As highlighted in the previous section, the relevance of the GR in the dynamics of the selected systems varies from case to case. We are then interested in evaluating the contributions of the different effects acting on their dynamical evolution, in particular on the pericenter of the inner planet (see also, e.g., Migaszewski and Goździewski (2009) and Sansottera et al. (2014)). To investigate the importance of the GR effects on the secular motion (LK resonance included), we compute the ratios of the precession rates $\frac{\dot{\omega}_{sec}}{\dot{\omega}_{GR}}$ and $\frac{\dot{\omega}_{LK}}{\dot{\omega}_{GR}}$, following Veras and Ford (2010). We recall the expression of the pericenter precession due to the GR derived by Eq. (5.2.1)

$$\dot{\omega}_{GR} = \frac{3\mu_1^{3/2}}{a_1^{5/2}c^2(1-e_1^2)}\,. \tag{5.4.1}$$

The precession caused by the secular interaction with the outer planet can be derived from the Laplace-Lagrange secular theory (approximation to the second order in the eccentricities), as (Zhou and Sun (2003))

$$\dot{\omega}_{sec} \simeq \sqrt{(y_1 - y_2)^2 + 4y_1 y_2 \left(\frac{b_{3/2}^{(2)}(\alpha)}{b_{3/2}^{(1)}(\alpha)} \right)}, \tag{5.4.2}$$

where

$$\begin{aligned} y_1 &= \frac{1}{4} \frac{m_2 a_1^{-3/2}}{\sqrt{m_0 + m_1}} \alpha^2 b_{3/2}^{(1)}(\alpha), \\ y_2 &= \frac{1}{4} \frac{m_1 a_2^{-3/2}}{\sqrt{m_0 + m_2}} \alpha b_{3/2}^{(1)}(\alpha), \end{aligned} \tag{5.4.3}$$

being $b_{3/2}^{(j)}(\alpha)$ Laplace coefficients and α the semi-major axis ratio a_1/a_2. The ratio between these two precession rates,

$$\chi_{sec} = \frac{\dot{\omega}_{sec}}{\dot{\omega}_{GR}}, \tag{5.4.4}$$

gives an estimation of the importance of the GR in the long-term evolution of the system. The smaller the value of χ_{sec}, the more relevant the effect of the GR.

In Tab. 5.3 we list the values of χ_{sec} for the systems considered. The results shown in Fig. 5.8 and Fig. 5.10 are perfectly coherent with the values of χ_{sec}. All the systems for which $\chi_{sec} \ll 1$ are evidently affected by the introduction of the relativistic correction, namely GJ 433, GJ 649, HD 187123, HD 190360, HD 217107 and HD 47186. The importance of the GR corrections for the GJ 649 system was previously shown in Fig. 5.4. For all the other cases, the influence of the relativistic effects are more moderate. No variation in the long-term evolution are reported when $\chi_{sec} \gg 1$, as previously shown in Fig. 5.1 for the HD 147018 system.

Regarding the highly mutually inclined systems, we can also estimate the relevance of the relativistic effect on the LK resonance. The period of the LK oscillations is given by (Kiseleva et al. (1998))

$$P_{LK} = \frac{2P_2^2}{3\pi P_1} \frac{m_0 + m_1 + m_2}{m_2} (1 - e_1^2)^{3/2}. \tag{5.4.5}$$

Consequently, the ratio of the two precession rates writes

$$\chi_{LK} = \frac{\dot{\omega}_{LK}}{\dot{\omega}_{GR}} = \frac{2\pi}{P_{LK} \dot{\omega}_{GR}}. \tag{5.4.6}$$

The smaller the value of the χ_{LK}, the more relevant the effects of the GR on the long-term evolution. In Tab. 5.3 are reported the values of χ_{LK} for the different

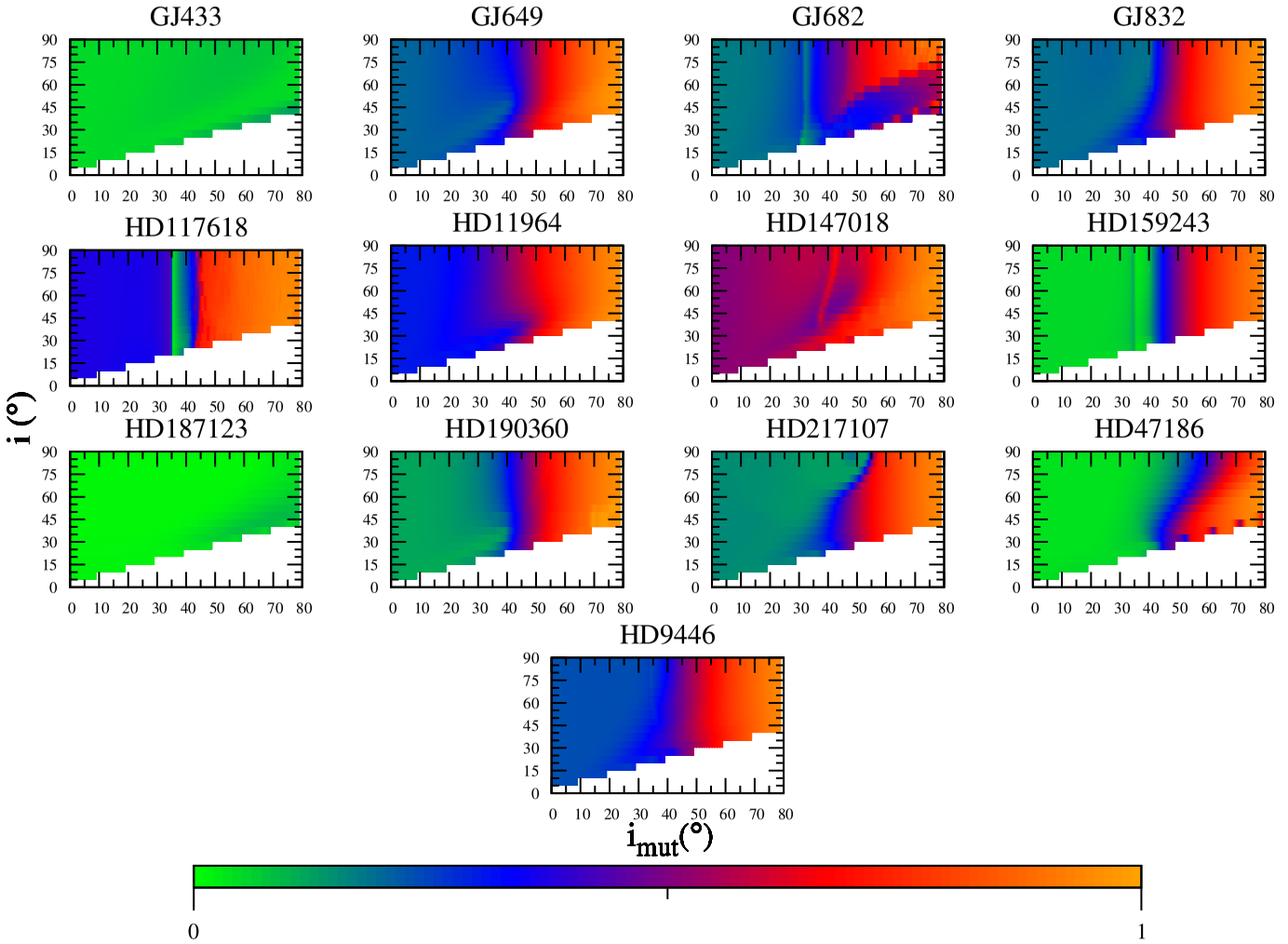

Figure 5.7 – Maximal eccentricity of the inner planet for the 13 systems listed in Tab. 5.1, when no relativistic corrections are taken into account.

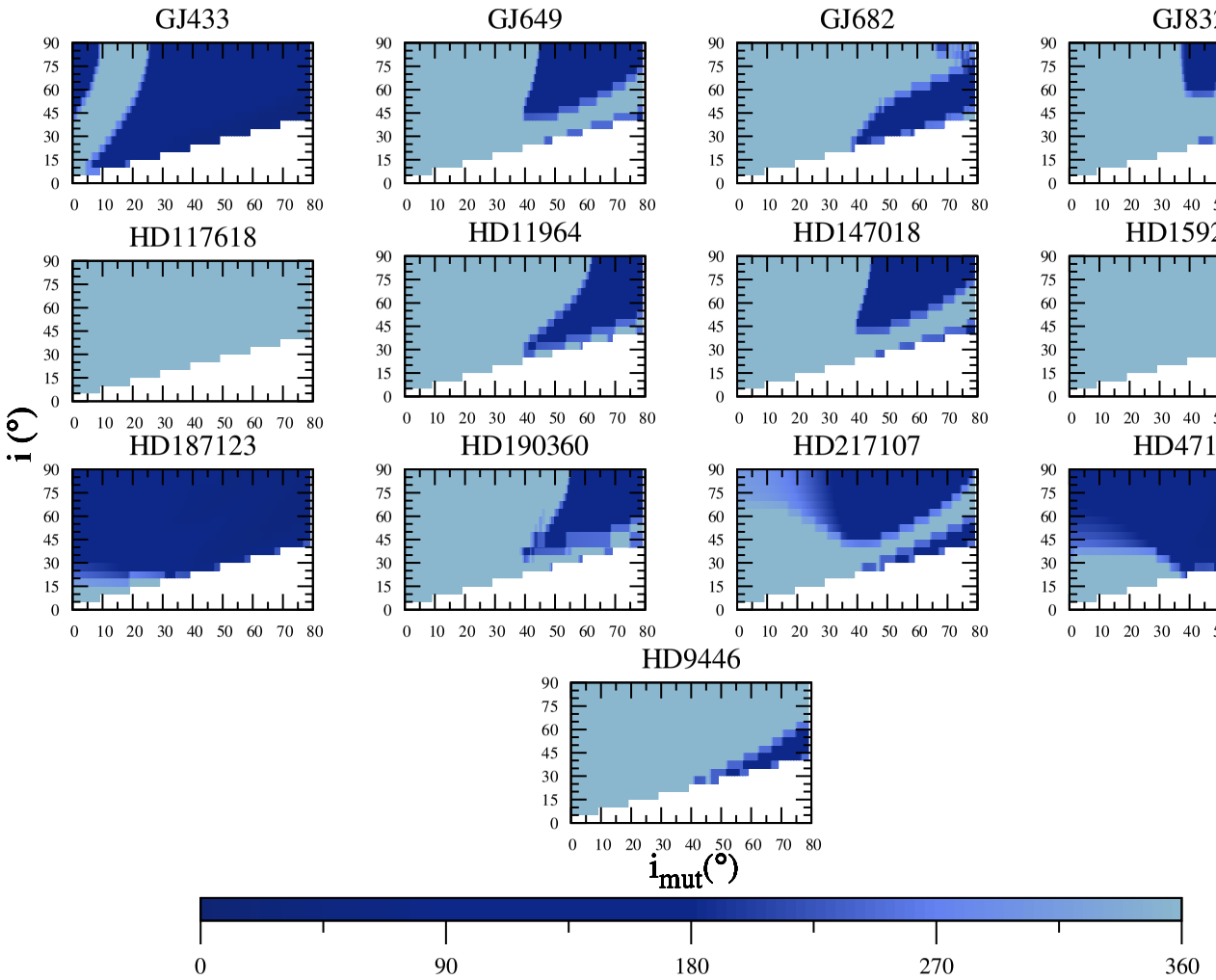

Figure 5.8 – Libration amplitude of ω_1 for the 13 systems listed in Tab. 5.1, where no relativistic corrections are taken into account.

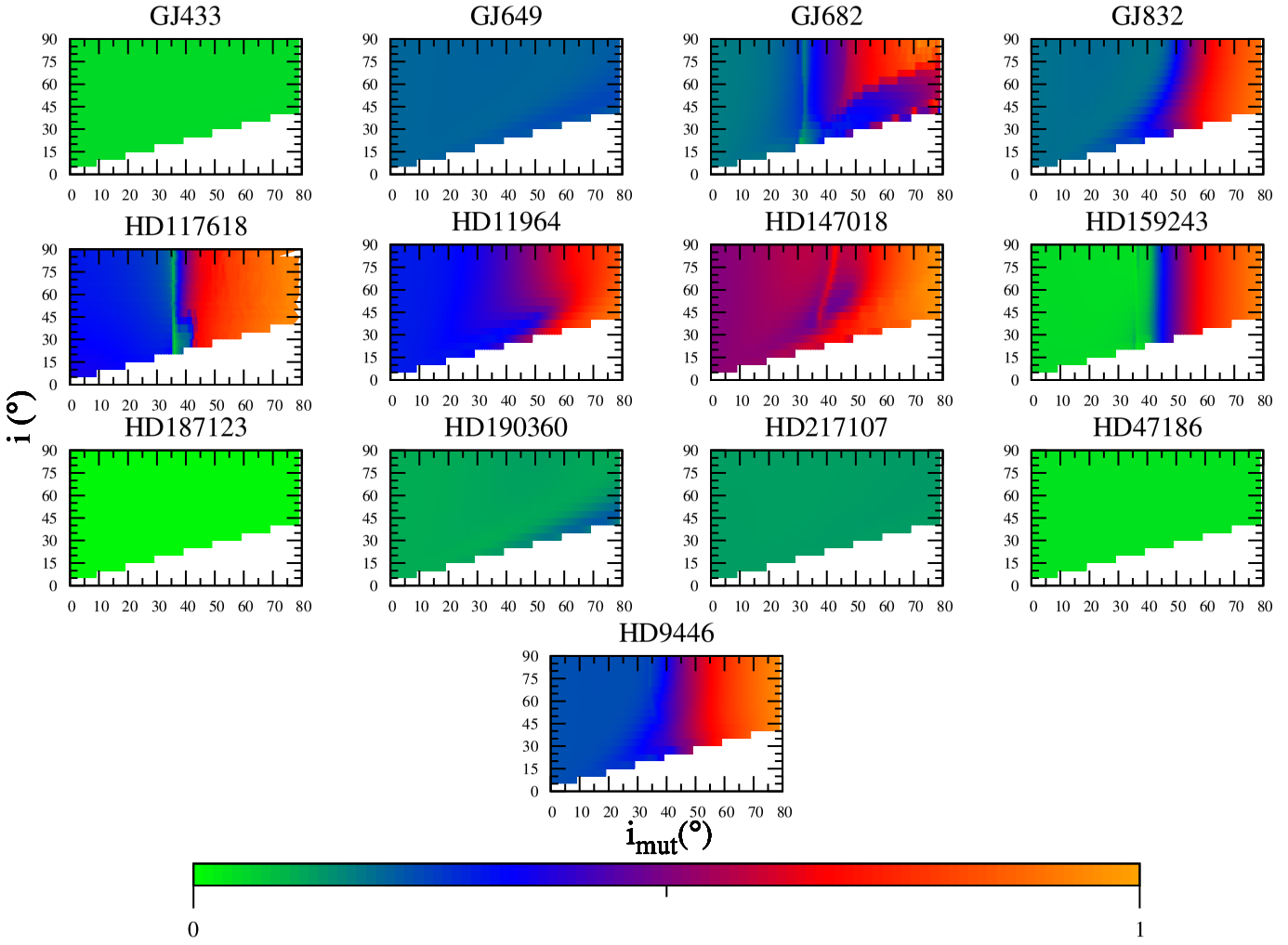

Figure 5.9 – Same as Fig. 5.7, where relativistic corrections therefore included.

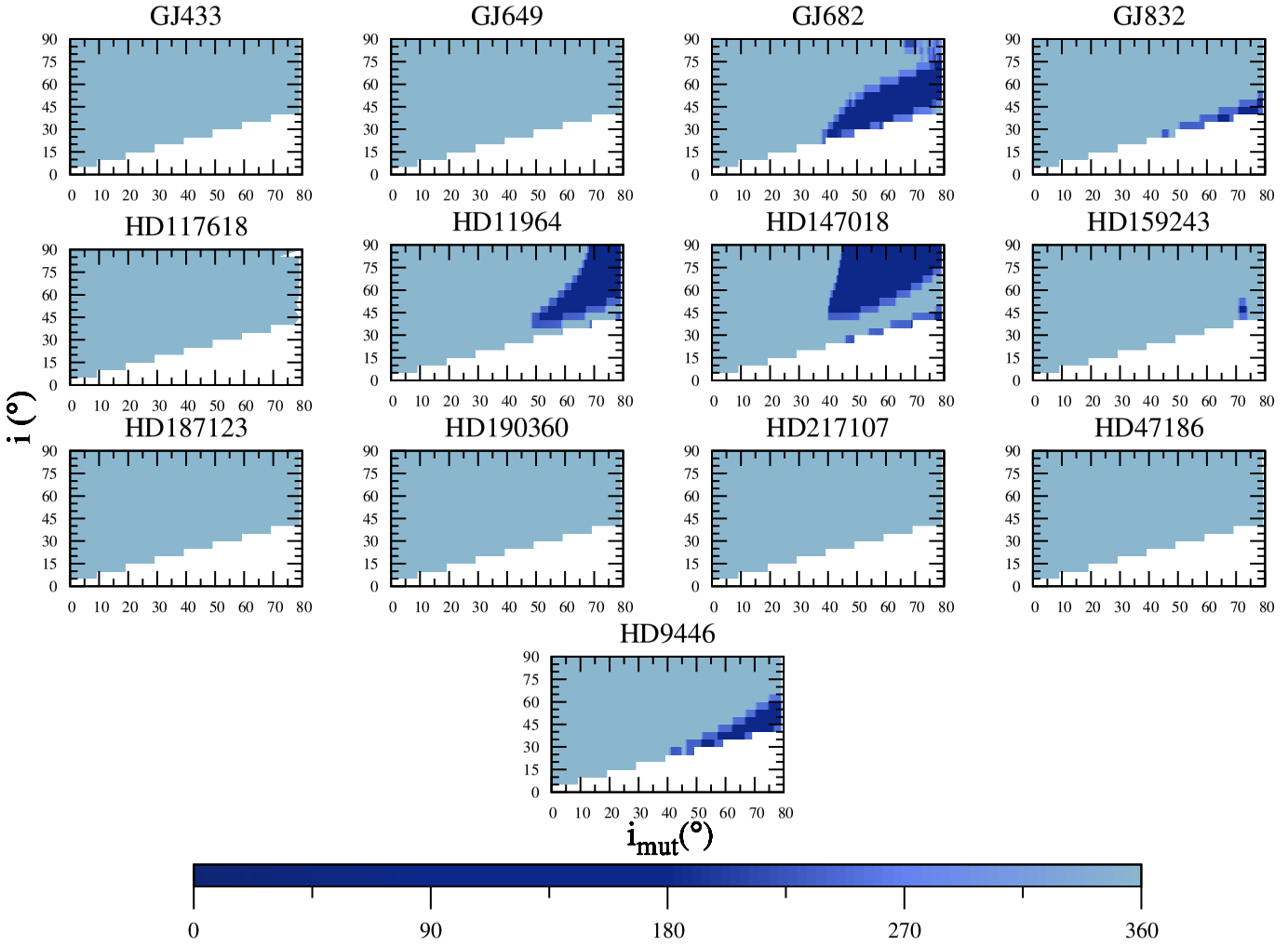

Figure 5.10 – Same as Fig. 5.8, when relativistic corrections are included.

Table 5.3 – Parameters χ_{sec} and χ_{LK} for the selected systems.

System	i	χ_{sec}	χ_{LK}
GJ 433	90	4.25e–04	2.75e–02
GJ 649	90	6.33e–03	4.14e–01
	70	6.74e–03	4.41e–01
	50	8.27e–03	5.41e–01
	30	1.27e–03	8.28e–01
	10	3.64e–02	2.38e+00
GJ 682	90	2.02e+01	3.89e+02
GJ 832	90	1.30e–01	7.75e+00
HD 117618	90	5.95e–01	2.88e+01
HD 11964	90	9.77e–02	5.90e+00
HD 147018	90	6.70e+00	4.22e+02
	70	7.12e+00	4.49e+02
	50	8.73e+00	5.49e+02
	30	1.33e+01	8.34e+02
	10	3.78e+01	2.30e+03
HD 159243	90	1.05e+00	6.47e+01
HD 187123	90	1.25e–04	8.39e–03
HD 190360	90	1.55e–02	1.09e+00
HD 217107	90	1.23e–03	1.28e–01
HD 47186	90	4.04e–04	2.73e–02
HD 9446	90	2.93e+01	1.22e+03

systems. The systems for which the LK region is maintained in Fig. 5.10, namely GJ 682, HD 11964, HD 147018 and HD 9446, correspond well to the high values of χ_{LK}.

It should be noted that both χ_{sec} and χ_{LK} depend on the masses of the three bodies. Therefore, they should be computed for each value of the orbital plane inclination i, as its variation determines a change in the masses of the planets as well. In Tab. 5.3 we have listed the precession ratios corresponding to different i values, for the GJ 649 system which is highly influenced by the GR and HD 147018 which is not significantly affected by the GR. We see that the change on the precession ratios in minor. For the systems here considered, we observe that the balance between the effects is independent of the value of the inclination of the orbital plane i.

5.5 Conclusions

We studied the possibility for 13 RV-detected exoplanetary systems with close-in planets to be in a 3D configuration. Given the proximity of the planets to the host star, we considered the relativistic corrections for the innermost planet. We determined the influence of this effect on the purely gravitational evolution. We found that most of the considered systems do show LK resonance regions when we only take into account the gravitational interactions between the bodies, in line with our previous results (see Sect. 4.3). However, in the majority of the cases the LK resonance region disappears as we introduce the relativistic corrections. This was expected, as the LK resonance and the general relativity both influence the evolution of the argument of the pericenter of the inner planet. The behaviour predicted by the approximations for the pericenter precession ratios match with the dynamical evolutions given by our secular Hamiltonian approach, highlighting their validity.

The work carried on so far is open to many future developments. Firstly, it would be appropriate to achieve a study of the stability of the systems, as done in Chap. 4 by means of the MEGNO chaos indicator. It would provide a more complete panoramic view of the stability of the systems, since it was previously shown that the initial conditions for which the LK resonance appears are not the only ones that guarantee the long-term stability (as discussed in Sect. 4.3.3). Secondly, we have already mentioned that tidal effects were not considered here. Taking into account this additional effect would provide a more precise description of the dynamics of the systems. However, as it was previously noted (see Sect. 5.1), its implementation is not straightforward, and would require a far more general approach that is beyond the scope of this work.

Conclusions and perspectives

In the thesis we studied the stability of non-coplanar exoplanetary systems. We focused on two-planet systems far from mean-motion resonances, therefore dealing with the non resonant three-body problem. Our aim was to provide constraints on the observational data coming from radial velocity detections, which lack information on the inclinations of the system. The incompleteness of the data implies a scarce knowledge of the exact value of the masses of the planets and of the potential three-dimensional architecture of the exoplanetary systems. Our goal was to determine boundaries for the unknown parameters that ensure the long-term stability of non-coplanar configurations of the observed systems.

Our work consists in two main parts, each one considering a different definition of the stability for a planetary system. In the first part, we exploited the nearly-integrable nature of the problem at hand, granted by the small ratio between the mass of the host star and the masses of the planets. Thus, we could apply the theoretical and computational tools that belong to the perturbation theory. We considered the minimal value of the masses of the planets provided by the observations and performed a parametric study on the mutual inclination between the orbital planes. We studied the stability of the system in the KAM sense, applying a reverse KAM approach. Broadly speaking, the KAM theory states that if the size of the perturbation of an integrable problem is small enough, it is possible to apply a convergent algorithm. This algorithm determines a new set of variables such that the evolution of the system expressed in these variables lies on an invariant tori. We reverted the procedure: we applied the constructing algorithm and used its convergence (or lack of convergence) to classify the initial conditions compatible with the KAM stability. We provided a synthetic coverage of the initial conditions by implementing an automatic procedure using interval arithmetic. The procedure spanned the

whole range of initial conditions excluding non-acceptable values by creating a tree-like subdivision in smaller intervals. Following this first approach, we studied three exoplanetary systems and proved their stability for configurations with mutual inclination up to $\sim 18^\circ$ (with the exact maximal value depending on the specific system). The downside of this strategy is that it is highly demanding in terms of computational cost and in terms or requirements that the initial conditions have to satisfy. Nevertheless, it is the first application to extrasolar planetary systems of an explicit algorithm constructing KAM tori and improvements can be achieved.

In the second part of this thesis, we focused on the concept of stability in the sense of proximity to the secular equilibria of the three-body-problem, as well as regularity of the orbits. We performed a parametric study not only on the mutual inclination between the orbital planes, but also on the inclination of these planes with respect to the line of sight. This implies varying the masses of the planets as well. In the framework of three-dimensional planetary systems, particular relevance is attributed to the Lidov-Kozai resonance. It is a protection mechanism appearing for highly-mutually inclined systems (with mutual inclination usually above 40°) that ensures the long-term stability of the system. When choosing the invariant Laplace plane as a reference plane, the action of the Lidov-Kozai resonance is indicated by the libration of the argument of the pericenter of the inner planet, easily detectable in the long-term numerical simulations. We found that all the selected systems presented, in the parameter space of the initial conditions, regions at high mutual inclinations displaying the action of the Lidov-Kozai resonance. Consequently, all the systems could be in a clear three-dimensional configuration and be stable in the long-term. We pursued this parametric study with a chaos indicator that classifies the initial conditions based on the regularity of the orbit. We found that three-dimensional configurations are stable in two cases: for low values of the mutual inclination or for high values inside of the Lidov-Kozai resonance. Otherwise, 3D configurations of the planetary system are chaotic. Indeed, a rapid destabilisation of highly mutually inclined orbits is commonly observed, due to the significant chaos that develops around the stability islands of the Lidov-Kozai resonance.

In the last chapter, we expanded this approach relying on the Lidov-Kozai resonance to systems with close-in planets. Thus, we had to take into account the additional perturbation due to the general relativity, causing and advance of the inner pericenter. Our aim was to study how the inclusion of this additional effect would have impact on the existence and extent of the Lidov-Kozai resonance region in the parameter space. For the majority of the systems, we did observe the disappearance of the Lidov-Kozai region, combined with a dumping of the eccentricity variations for the inner planet.

In conclusion, the present work highlights, by means of two different approaches, the possibility for an exoplanetary system to be in a long-term stable three-dimensional configuration. Both the strategies described here are open to further developments. Concerning the reverse KAM approach, we imposed strict requirements to the initial conditions of the systems, in particular on the initial eccentricity values. A perspective would be to weaken such demands in order to determine a wider application field. For the Lidov-Kozai approach, a natural extension, for the close-in planet systems, would be to include in the model the tidal effects that have been neglected. Another development could be the adoption of different orbital inclinations for each planet (also meaning different scaling factors of the masses of planets). This would increase the size of the parameter space and ask for a careful managing of the initial conditions.

Bibliography

Almenara, J.M., et al. (2015). Absolute masses and radii determination in multiplanetary systems without stellar models. *Monthly Notices of the Royal Astronomycal Society*, 453:2644–2652.

Arnol'd, V.I. (1963). Proof of a Theorem of A. N. KOLMOGOROV on the Invariance of Quasi-Periodic Motions Under Small Perturbations of the Hamiltonian. *Russian Mathematical Surveys*, 18:9–36.

Baluev, R.V. (2011). Orbital structure of the GJ876 extrasolar planetary system based on the latest Keck and HARPS radial velocity data. *Celestial Mechanics and Dynamical Astronomy*, 111:235–266.

Batalha, N.M., et al. (2011). Kepler's First Rocky Planet: Kepler-10b. *Astrophysical Journal*, 729:27.

Beaugé, C., Ferraz-Mello, S., and Michtchenko, T.A. (2012). Multi-planet extrasolar systems — detection and dynamics. *Research in Astronomy and Astrophysics*, 12:1044–1080.

Benettin, G., et al. (1984). A proof of Kolmogorov's theorem on invariant tori using canonical transformations defined by the Lie method. *Nuovo Cimento B Serie*, 79:201–223.

Biasco, L., Chierchia, L., and Valdinoci, E. (2006). Corrigendum to: Elliptic Two-Dimensional Invariant Tori for the Planetary Three-Body Problem. *Archive for Rational Mechanics and Analysis*, 180:507–509.

Bond, I.A., et al. (2001). Real-time difference imaging analysis of MOA Galactic bulge observations during 2000. *Monthly Notices of the Royal Astronomycal Society*, 327:868–880.

Bond, I.A., et al. (2004). OGLE 2003-BLG-235/MOA 2003-BLG-53: A Planetary Microlensing Event. *Astrophysical Journal*, 606:L155–L158.

Bouchy, F., et al. (2009). The harps search for southern extra-solar planets *** - xvii. super-earth and neptune-mass planets in multiple planet systems hd and hd. *Astronomy & Astrophysics*, 496(2):527–531.

Butler, R.P., et al. (1999). Evidence for Multiple Companions to υ Andromedae. *Astrophysical Journal*, 526:916–927.

Butler, R.P., et al. (2006). Catalog of Nearby Exoplanets. *Astrophysical Journal*, 646:505–522.

Campbell, B., Walker, G.A.H., and Yang, S. (1988). A search for substellar companions to solar-type stars. *Astrophysical Journal*, 331:902–921.

Celletti, A. (1994). Construction of librational invariant tori in the spin-orbit problem. *Zeitschrift Angewandte Mathematik und Physik*, 45:61–80.

Celletti, A. and Chierchia, L. (2007). *KAM Stability and Celestial Mechanics*. American Mathematical Society.

Celletti, A., Giorgilli, A., and Locatelli, U. (2000). Improved estimates on the existence of invariant tori for Hamiltonian systems. *Nonlinearity*, 13:397–412.

Chierchia, L. (2008). Kolmogorov's 1954 paper on nearly-integrable Hamiltonian systems. *Regular and Chaotic Dynamics*, 13:130–139.

Cincotta, P.M. and Simo, C. (2000). Simple tools to study global dynamics in non-axisymmetric galactic potentials - I. *Astronomy and Astrophysics, Supplement*, 147(2):205–228. ISSN 0365-0138.

Courcol, B., et al. (2015). The sophie search for northern extrasolar planets - vii. a warm neptune orbiting hd595. *Astronomy & Astrophysics*, 581:A38.

Cumming, A., et al. (2008). The Keck Planet Search: Detectability and the Minimum Mass and Orbital Period Distribution of Extrasolar Planets. *Publications of the Astronomical Society of the Pacific*, 120:531.

Dawson, R.I., et al. (2014). Large Eccentricity, Low Mutual Inclination: The Three-dimensional Architecture of a Hierarchical System of Giant Planets. *Astrophysical Journal*, 791:89.

Fabrycky, D.C., et al. (2014). Architecture of Kepler's Multi-transiting Systems. II. New Investigations with Twice as Many Candidates. *Astrophysical Journal*, 790:146.

Feng, Y.K., et al. (2015). The California Planet Survey IV: A Planet Orbiting the Giant Star HD 145934 and Updates to Seven Systems with Long-period Planets. *Astrophysical Journal*, 800:22.

Ferraz-Mello, S. (1994). The convergence domain of the Laplacian expansion of the disturbing function. *Celestial Mechanics and Dynamical Astronomy*, 58:37–52.

Fulton, B.J., et al. (2016). Three Temperate Neptunes Orbiting Nearby Stars. *Astrophysical Journal*, 830:46.

Funk, B., et al. (2011). On the influence of the Kozai mechanism in habitable zones of extrasolar planetary systems. *Astronomy & Astrophysics*, 526:A98.

Gabern, F., Jorba, À., and Locatelli, U. (2005). On the construction of the Kolmogorov normal form for the Trojan asteroids. *Nonlinearity*, 18:1705–1734.

Gaudi, B.S. and Winn, J.N. (2007). Prospects for the Characterization and Confirmation of Transiting Exoplanets via the Rossiter-McLaughlin Effect. *Astrophysical Journal*, 655:550–563.

Giorgilli, A. (2015). Notes on Hamiltonian systems. `http://www.mat.unimi.it/users/antonio/hamsys/hamsys.html`.

Giorgilli, A., Locatelli, U., and Sansottera, M. (2014). On the convergence of an algorithm constructing the normal form for elliptic lower dimensional tori in planetary systems. *Celestial Mechanics and Dynamical Astronomy*, 119:397–424.

Giorgilli, A., Locatelli, U., and Sansottera, M. (2017). Secular dynamics of a planar model of the Sun-Jupiter-Saturn-Uranus system; effective stability in the light of Kolmogorov and Nekhoroshev theories. *Regular and Chaotic Dynamics*, 22:54–77.

Gröbner, W. and Knapp, H. (1967). *Contributions to the Method of Lie-Series*. Bibliographisches Institut.

Haghighipour, N., et al. (2012). The Lick-Carnegie Survey: A New Two-planet System around the Star HD 207832. *Astrophysical Journal*, 756:91.

Han, E., et al. (2014). Exoplanet Orbit Database. II. Updates to Exoplanets.org. *Publications of the Astronomical Society of the Pacific*, 126:827.

Hatzes, A.P., et al. (2003). A Planetary Companion to γ Cephei A. *Astrophysical Journal*, 599:1383–1394.

Hébrard, G., et al. (2010). The sophie search for northern extrasolar planets* - ii. a multiple planet system around hd6. *Astronomy & Astrophysics*, 513:A69.

Henrard, J. and Lemaître, A. (2005). The Untangling Transformation. *Astronomical Journal*, 130:2415–2417.

Henry, G.W., et al. (1999). HD 209458. *International Astronomical Union Circular*, 7307.

Henry, G.W., et al. (2000). A Transiting "51 Peg-like" Planet. *Astrophysical Journal*, 529:L41–L44.

Holman, M.J., et al. (2010). Kepler-9: A System of Multiple Planets Transiting a Sun-Like Star, Confirmed by Timing Variations. *Science*, 330:51.

Huber, D., et al. (2013). Stellar Spin-Orbit Misalignment in a Multiplanet System. *Science*, 342:331–334.

Jones, H.R.A., et al. (2010). A long-period planet orbiting a nearby Sun-like star. *Monthly Notices of the Royal Astronomycal Society*, 403:1703–1713.

Kiseleva, L.G., Eggleton, P.P., and Mikkola, S. (1998). Tidal friction in triple stars. *Monthly Notices of the Royal Astronomycal Society*, 300:292–302.

Kolmogorov, A.N. (1954). On preservation of conditionally periodic motions under a small change in the Hamiltonian function. *Dokl. Akad. Nauk SSSR*, 98(4):527–530.

Kozai, Y. (1962). Secular perturbations of asteroids with high inclination and eccentricity. *Astronomical Journal*, 67:591.

Laskar, J. (1989a). A numerical experiment on the chaotic behaviour of the solar system. *Nature*, 338:237.

Laskar, J. (1989b). Systèmes de variables et éléments. In D. Benest and F. C., editors, *Les Méthodes modernes de la Mécanique Céleste*, pages 63–87. Editions Frontières.

Laskar, J. (1990). The chaotic motion of the solar system - A numerical estimate of the size of the chaotic zones. *Icaurs*, 88:266–291.

Laskar, J. (1996). Large Scale Chaos and Marginal Stability in the Solar System. *Celestial Mechanics and Dynamical Astronomy*, 64:115–162.

Laskar, J. (1997). Large scale chaos and the spacing of the inner planets. *Astronomy & Astrophysics*, 317:L75–L78.

Laskar, J. (2003). Frequency Map analysis and quasi periodic decompositions. In C. Benest D..Froeschlé and L. E., editors, *Hamiltonian systems and Fourier analysis*. Taylor and Francis.

Laskar, J. (2012). Is the Solar System Stable? *arXiv e-prints*, arXiv:1209.5996.

Laskar, J. and Correia, A.C.M. (2009). Hd 60532, a planetary system in a 3:1 mean motion resonance. *Astronomy & Astrophysics*, 496:L5–L8.

Laskar, J. and Gastineau, M. (2009). Existence of collisional trajectories of Mercury, Mars and Venus with the Earth. *Nature*, 459:817–819.

Laskar, J. and Petit, A.C. (2017). AMD-stability and the classification of planetary systems. *Astronomy & Astrophysics*, 605:A72.

Levison, H.F. and Duncan, M.J. (1994). The long-term dynamical behavior of short-period comets. *Icaurs*, 108:18–36.

Libert, A.S. and Henrard, J. (2005). Analytical Approach to the Secular Behaviour of Exoplanetary Systems. *Celestial Mechanics and Dynamical Astronomy*, 93:187–200.

Libert, A.S. and Henrard, J. (2007). Exoplanetary systems: The role of an equilibrium at high mutual inclination in shaping the global behavior of the 3-D secular planetary three-body problem. *Icaurs*, 191:469–485.

Libert, A.S. and Henrard, J. (2008). Secular frequencies of 3-D exoplanetary systems. *Celestial Mechanics and Dynamical Astronomy*, 100:209–229.

Libert, A.S. and Sansottera, M. (2013). On the extension of the Laplace-Lagrange secular theory to order two in the masses for extrasolar systems. *Celestial Mechanics and Dynamical Astronomy*, 117:149–168.

Libert, A.S. and Tsiganis, K. (2009). Kozai resonance in extrasolar systems. *Astronomy & Astrophysics*, 493:677–686. ISSN 0004-6361.

Lidov, M.L. (1962). The evolution of orbits of artificial satellites of planets under the action of gravitational perturbations of external bodies. *Planetary Space Science*, 9:719–759.

Limbach, M.A. and Turner, E.L. (2015). Exoplanet orbital eccentricity: Multiplicity relation and the Solar System. *Proceedings of the National Academy of Science*, 112:20–24.

Lissauer, J.J. (1999). Chaotic motion in the Solar System. *Review of Modern Physics*, 71:835–845.

Lissauer, J.J., et al. (2011). A closely packed system of low-mass, low-density planets transiting Kepler-11. *Nature*, 470:53–58.

Locatelli, U. and Giorgilli, A. (2000). Invariant tori in the secular motions of the three-body planetary systems. *Celestial Mechanics and Dynamical Astronomy*, 78(1-4). ISSN 09232958.

Maffione, N.P., Giordano, C.M., and Cincotta, P.M. (2011). Testing a fast dynamical indicator: The MEGNO. *International Journal of Non-Linear Mechanics*, 46(1):23–34. ISSN 00207462.

Mayor, M. and Queloz, D. (1995). A Jupiter-mass companion to a solar-type star. *Nature*, 378:355–359.

Mayor, M., et al. (2004). The CORALIE survey for southern extra-solar planets. XII. Orbital solutions for 16 extra-solar planets discovered with CORALIE. *Astronomy & Astrophysics*, 415:391–402.

McArthur, B.E., et al. (2010). New Observational Constraints on the υ Andromedae System with Data from the Hubble Space Telescope and Hobby-Eberly Telescope. *Astrophysical Journal*, 715:1203–1220.

McLaughlin, D.B. (1924). Some results of a spectrographic study of the Algol system. *Astrophysical Journal*, 60.

Michtchenko, T.A., Ferraz-Mello, S., and Beaugé, C. (2006). Modeling the 3-D secular planetary three-body problem. Discussion on the outer υ Andromedae planetary system. *Icarus*, 181(2):555–571. ISSN 00191035.

Migaszewski, C. and Goździewski, K. (2009). Secular dynamics of a coplanar, non-resonant planetary system under the general relativity and quadrupole moment perturbations. *Monthly Notices of the Royal Astronomycal Society*, 392:2–18.

Mills, S.M. and Fabrycky, D.C. (2017). Kepler-108: A Mutually Inclined Giant Planet System. *Astronomical Journal*, 153:45.

Morbidelli, A. and Giorgilli, A. (1995). Superexponential stability of KAM tori. *Journal of Statistical Physics*, 78:1607–1617.

Moser, J. (1962). On invariant curves of area-preserving mapping of an annulus. *Matematika*, 6(5):51–68.

Moser, J. (1968). *Lectures on Hamiltonian systems*. Memoirs of the American Mathematical Society. American Mathematical Society.

Moutou, C., et al. (2014). The sophie search for northern extrasolar planets - vi. three new hot jupiters in multi-planet extrasolar systems. *Astronomy & Astrophysics*, 563:A22.

Muterspaugh, M.W., et al. (2010). The Phases Differential Astrometry Data Archive. V. Candidate Substellar Companions to Binary Systems. *The Astronomical Journal*, 140(6):1657–1671.

Naoz, S. (2016). The Eccentric Kozai-Lidov Effect and Its Applications. *Annual Review of Astronomy & Astrophysics*, 54:441–489.

O'Toole, S.J., et al. (2009). Selection functions in doppler planet searches. *Monthly Notices of the Royal Astronomycal Society*, 392:641–654.

Páez, R.I. and Locatelli, U. (2015). Trojan dynamics well approximated by a new Hamiltonian normal form. *Monthly Notices of the Royal Astronomycal Society*, 453:2177–2188.

Páez, R.I., Locatelli, U., and Efthymiopoulos, C. (2016). New Hamiltonian expansions adapted to the Trojan problem. *Celestial Mechanics and Dynamical Astronomy*, 12,6:519–541.

Perryman, M. (2018). *The Exoplanet Handbook*. Cambridge University Press. ISBN 9781108419772.

Petit, A.C., Laskar, J., and Boué, G. (2017). AMD-stability in the presence of first-order mean motion resonances. *Astronomy & Astrophysics*, 607:A35.

Poincaré, H. (1893). *Les méthodes nouvelles de la mécanique céleste: Méthodes de MM. Newcomb, Glydén, Lindstedt et Bohlin. 1893*. Les méthodes nouvelles de la mécanique céleste. Gauthier-Villars et fils.

Robutel, P. (1995). Stability of the planetary three-body problem. *Celestial Mechanics & Dynamical Astronomy*, 62(3):219–261. ISSN 0923-2958.

Rodigas, T.J. and Hinz, P.M. (2009). Which Radial Velocity Exoplanets Have Undetected Outer Companions? *Astrophysical Journal*, 702:716–723.

Rodriguez, J.E., et al. (2018). A Compact Multi-planet System with a Significantly Misaligned Ultra Short Period Planet. *Astronomical Journal*, 156:245.

Rossiter, R.A. (1924). On the detection of an effect of rotation during eclipse in the velocity of the brigher component of beta Lyrae, and on the constancy of velocity of this system. *Astrophysical Journal*, 60.

Sanchis-Ojeda, R., et al. (2012). Alignment of the stellar spin with the orbits of a three-planet system. *Nature*, 487:449–453.

Sansottera, M., Grassi, L., and Giorgilli, A. (2014). On the relativistic Lagrange-Laplace secular dynamics for extrasolar systems. In *Complex Planetary Systems, Proceedings of the International Astronomical Union*, volume 310 of *IAU Symposium*, pages 74–77.

Sansottera, M., Locatelli, U., and Giorgilli, A. (2013). On the stability of the secular evolution of the planar sun-jupiter-saturn-uranus system. *Mathematics and Computers in Simulation*, 88.

Sato, B., et al. (2013). A Double Planetary System around the Evolved Intermediate-mass Star HD 4732. *Astrophysical Journal*, 762:9.

Schneider, J., et al. (2011). Defining and cataloging exoplanets: The exoplanet.eu database. *Astronomy & Astrophysics*, 532.

Ségransan, D., et al. (2010). The CORALIE survey for southern extrasolar planets*** - XVI. Discovery of a planetary system around HD 147018 and of two long period and massive planets orbiting HD 171238 and HD 204313. *Astronomy & Astrophysics*, 511:A45.

Sussman, G. and Wisdom, J. (1992). Chaotic Evolution of the Solar System. *Science*, 257:56–62.

Tuomi, M. and Kotiranta, S. (2009). Bayesian analysis of the radial velocities of HD 11506 reveals another planetary companion. *Astronomy & Astrophysics*, 496:L13–L16.

Tuomi, M., et al. (2014). Bayesian search for low-mass planets around nearby M dwarfs – estimates for occurrence rate based on global detectability statistics. *Monthly Notices of the Royal Astronomical Society*, 441(2):1545–1569. ISSN 0035-8711.

Udalski, A. (2003). The Optical Gravitational Lensing Experiment: Is Interstellar Extinction toward the Galactic Center Anomalous? *Astrophysical Journal*, 590:284–290.

Veras, D. and Ford, E.B. (2010). Secular Orbital Dynamics of Hierarchical Two-planet Systems. *Astrophysical Journal*, 715:803–822.

Volpi, M., Locatelli, U., and Sansottera, M. (2018). A reverse KAM method to estimate unknown mutual inclinations in exoplanetary systems. *Celestial Mechanics and Dynamical Astronomy*, 130:36.

Volpi, M., Roisin, A., and Libert, A.S. (2019). The 3D secular dynamics of radial-velocity-detected planetary systems. *Astronomy & Astrophysics*, 626:A74.

Wittenmyer, R.A., et al. (2012). The Anglo-Australian Planet Search. XXII. Two New Multi-planet Systems. *Astrophysical Journal*, 753:169.

Wittenmyer, R.A., et al. (2013). Forever Alone? Testing Single Eccentric Planetary Systems for Multiple Companions. *Astrophysical Journal*, 208:2.

Wittenmyer, R.A., et al. (2014). GJ 832c: A Super-Earth in the Habitable Zone. *The Astrophysical Journal*, 791(2):114.

Wittenmyer, R.A., et al. (2014). The Anglo-Australian Planet Search. XXIII. Two New Jupiter Analogs. *Astrophysical Journal*, 783:103.

Wolszczan, A. and Frail, D.A. (1992). A planetary system around the millisecond pulsar PSR1257 + 12. *Nature*, 355:145–147.

Wright, J.T., et al. (2009). Ten New and Updated Multiplanet Systems and a Survey of Exoplanetary Systems. *Astrophysical Journal*, 693:1084–1099.

Zhou, J.L. and Sun, Y.S. (2003). Occurrence and Stability of Apsidal Resonance in Multiple Planetary Systems. *The Astrophysical Journal*, 598(2):1290–1300.

Zinzi, A. and Turrini, D. (2017). Anti-correlation between multiplicity and orbital properties in exoplanetary systems as a possible record of their dynamical histories. *Astronomy & Astrophysics*, 605:L4.